Environmentally Sensitive Hyaluronan Hydrogel Adjustable by Physical and Chemical Cross-links for Biomedical Applications

Referees:

PD. Dr. Heike Boehm

Prof. Dr. Dahint

Zeka, insanın kullandığı bir malzemedir.

Insan gönüldür, gönül!

Prof. Dr. Haydar Baş

-Für meine Familie-

Eidesstattliche Versicherung

gemäß § 8 der Promotionsordnung für die Naturwissenschaftlich-Mathematische Gesamtfakultät der Universität Heidelberg

1. Bei der eingereichten Dissertation zu dem Thema "**Environmentally Sensitive Hyaluronan Hydrogel Adjustable by Physical and Chemical Cross-links for Biomedical Applications**" handelt es sich um meine eigenständig erbrachte Leistung.

2. Ich habe nur die angegebenen Quellen und Hilfsmittel benutzt und mich keiner unzulässigen Hilfe Dritter bedient. Insbesondere habe ich wörtlich oder sinngemäß aus anderen Werken übernommene Inhalte als solche kenntlich gemacht.

3. Die Arbeit oder Teile davon habe ich bislang nicht an einer Hochschule des In- oder Auslands als Bestandteil einer Prüfungs- oder Qualifikationsleistung vorgelegt.

4. Die Richtigkeit der vorstehenden Erklärungen bestätige ich.

5. Die Bedeutung der eidesstattlichen Versicherung und die strafrechtlichen Folgen einer unrichtigen oder unvollständigen eidesstattlichen Versicherung sind mir bekannt.

Ich versichere an Eides statt, dass ich nach bestem Wissen die reine Wahrheit erklärt und nichts verschwiegen habe.

Heidelberg, den 24. Juni 2020

Saliha Erikci

Contents

Danksagung/Acknowledgements

An erster Stelle ein sehr großes Dankeschön an meine Betreuerin PD. Dr. Heike Boehm. Liebe Heike, du kannst wahrscheinlich nicht ermessen, wie viel es mir bedeutet hat, damals die Zusage von dir bekommen zu haben. In einer Welt voller Vorurteile habe ich durch dich wieder ein Stück Glauben an die Menschheit gewonnen und bin in meiner Überzeugung bestärkt worden, dass man durch Fleiß und Ehrgeiz viel erreichen kann. Ich danke dir, dass du mich so selbstständig hast arbeiten lassen und ich mich dadurch sowohl persönlich als auch im wissenschaftlichen Arbeiten so sehr weiterentwickelt habe.

Des Weiteren möchte ich bei Herrn Prof. Reiner Dahint für die Bereitschaft bedanken, die Aufgabe des Zweitgutachters zu übernehmen.

Ich möchte mich auch bei Herrn Prof. Joachim Spatz bedanken, dafür das ich an so einem interessanten Projekt arbeiten durfte und für die vielen technischen Möglichkeiten am Institut.

Ich bedanke mich bei all meinen Kollegen aus der Spatz Gruppe für das tolle Arbeitsklima. Besonderer Dank gilt meinen Kolleginnen aus der AG Böhm Gruppe, hier vor allem Dr. Patricia Hegger, die eine super Vertretung und Unterstützung war. Vielen Dank auch an unsere technischen Mitarbeiter, ohne sie würden die Labore nicht so in Schuss bleiben, Bestellungen nicht rechtzeitig ankommen und vieles mehr! Danke Sabine Grünewald, Cornelia Weber, Anette Fautsch und Raimund Jung.

Ebenfalls bedanke ich mich auch bei meinen Praktikanten Matthias Brandenstein, Felix Landwehr, Ambika Singh, Johanna Mörs und Patrick Gemessy, die während ihrer Praktikumszeit erfolgreich an dem Projekt mitgewirkt haben.

Bei meinen Kunigunden, Carmen Sahm und Lutz Neuhäuser möchte ich mich für die vielen lustigen als auch tiefgründigen Kaffeepausen bedanken. Ohne unsere gemeinsame Mittagscola und unsere Treffen hätte ich wahrscheinlich die Tage nicht so leicht überstanden. Ich schätze mich glücklich, dass ich euch habe!!!

Ich möchte mich auch ganz herzlich bei Dr. Rebecca Medda bedanken! Du hast es immer geschafft genau die Rolle zu übernehmen, die ich gerade gebraucht habe. Ob als Mentorin, als Psychotherapeutin, Lebensberaterin und Stütze während den Experimenten, ich wusste ich kann immer zu dir kommen! Du hast es immer wieder geschafft mich zu motivieren und aufzubauen, dafür danke ich dir!

Was wäre ich ohne meinen Goldhamster, meiner Freundin und besten Kollegin, Franziska Dietrich. Liebe Franzi, ich glaube daran und bin dankbar dafür, dass uns das Schicksal zusammengeführt hat. Du warst mir in den letzten drei Jahren, die beste Unterstützerin, die man sich vorstellen kann. Es schien immer wie, wir zwei gegen den Rest der Welt. Ich danke dir für die tolle Zeit und, dass du immer wieder meine Launen ertragen hast und mir trotzdem nie böse warst! Es gibt noch so vieles mehr, was ich dir sagen möchte aber das wichtigste an dieser Stelle ist: DANKE!

Großer Dank gilt auch meiner Familie! Ich danke ihnen allen für ihre Unterstützung und ihren Glauben in mich. Ganz besonders meinem Onkel Adem und meiner Tante Habibe Özhan, und meinem Onkel Hüseyin und meiner Tante Gülfariz Özhan. Ich möchte mich auch bei meiner Cousine Emine Özhan bedanken, die mich immer bestärkt hat indem was ich tue! Durch unsere vielen gemeinsamen Reisen, hast du immer einen Teil des Stresses abbekommen, deswegen danke ich dir für deine Geduld mit mir! Ich danke meinen drei Brüdern, Salih, Hakan und Mikail Erikci für ihre Liebe und Freude. Auf euch ist immer Verlass und ich hätte mir keine anderen Brüder gewünscht!

Mein größter Dank gilt meinen Eltern! Meinem Vater danke ich dafür, dass er immer für mich da war und versucht hat mir immer jeden Wunsch zu erfüllen. Vielen Dank für die tägliche Snack Versorgung, auf dich ist immer Verlass!

Ganz besonderer Dank gilt meiner Mama! Sie ist und bleibt mein größter Fan und meine beste Freundin. Ohne deine Unterstützung und Motivation, wüsste ich nicht, ob ich so weit gekommen wäre. Du bist meine Heldin, meine beste Zuhörerin, meine beste Köchin, meine beste Motivatorin und die beste Seelsorge, die man sich wünschen kann. Mama- Ich liebe dich!

Abstract

In recent years, hydrogels developed to promising tools for biomedical and industrial applications. For biomedical approaches hydrogels, possess the capacity to immobilize and release cells, they offer the desired 3D environment to induce cell specific behaviour or serves as a drug delivery system. Moreover, they can be used for tissue engineering approaches by mimicking the ECM.

In this thesis, a novel hybrid double cross-linked hydrogel is presented and designed based on the bottom-up approach of synthetic biology. It consists of simultaneously formed chemical and physical cross-links and made out of two components: (1) thiol functionalized HA (74 kDa) (**HA-DTPH**) and (2) ionic crosslinker (**Cl^+**). **HA-DTPH** provides the chemical cross-link by forming disulphide bonds and the ionic cross-linker forms physical cross-links, such as hydrogen bonds and salt bridges. Three different ionic cross-linker were used: (1) deacetylated disaccharide unit of HA (**dHA^+**) (2) charged glucosamine (**$GluA^+$**) and (3) ammonium chloride (**NH_4^+**). These ionic cross-linker were chosen due to their biocompatibility and ability to form physical cross-links, such as hydrogen bonds and salt bridges. The increasing capacity to form hydrogen bonds from **NH_4^+** to **dHA^+** enabled us to study the influence of the physical cross-link on the hydrogel properties. I could show that the disulphide bond formation was enhanced, by adding an ionic cross-linker and led to the formation of stable hydrogels. Under the same reaction conditions, **HA-DTPH** without an ionic cross-linker, needed further oxidation with hydrogen peroxide to result in a stable hydrogel (**HA-DTPH-Ox.**). By varying the degree of thiolation on HA and additionally by varying the type and concentrations of the used ionic cross-linker, the mechanical stiffness, swelling properties and response to external stimuli were tuneable. Varying the degree of modification and used ionic cross-linker enables a specific adjustment of the hydrogels specifically the hydrogel suitable for cell studies with mechanical range of 0.1 Pa to 8 kPa. Furthermore, swelling ratios of **HA-DTPH-Cl^+** hydrogels are highly influenced by the ionic strength and pH. Remarkably **HA- DTPH- dHA^+** hydrogels upon incubation in a solution of pH 7 showed a feedback loop swelling behaviour. At the swollen state of the hydrogel, the ionic cross-linker **dHA^+**, leaked out of the hydrogel network, acidified the solution, which resulted in shrinking of the hydrogel. Biological properties like

enzymatic degradability showed that the half-live of **HA-DTPH-Cl$^+$** hydrogels are increasing with increasing capacity of the ionic cross-linker to form hydrogen bonds. Moreover, due to the absence of any toxic agent during the hydrogel formation the hydrogel system was used for live cell applications such as cell encapsulation or cell adhesion studies. To conclude, a hybrid double cross-linked hydrogel system could be presented, mimicking the ECM, in a minimal model and a critical influence of physical cross-links is observed from results obtained by characterizing the physical and biochemical properties by investigating the gels' swelling capability, response to environmental changes and sensitivity to hyaluronidases. Depending on the desired biomedical application, these hydrogel systems can be tuned in regards to their stiffness, swelling behavior and degradability enabling applications in 3D tissue engineering, drug delivery and regenerative medicine.

Zusammenfassung

Hydrogele spielen in der heutigen Zeit eine wichtige Rolle sowohl in der biomedizinischen als auch in der industriellen Forschung. Sie eigenen sich besonders gut für biomedizinische Anwendungen, hinsichtlich ihrer Fähigkeiten Zellen zu immobilisieren und freizusetzen, die 3D *in vivo* Umgebung *in vitro* nachzuahmen, um Zell-spezifisches Verhalten auszulösen und dienen als Wirkstoff Carrier im Körper. Außerdem, werden sie in der Gewebezüchtung benutzt, da sie die hydratisierte EZM wiederspiegeln können. In dieser Arbeit wurde ein Hybrid Hydrogel System präsentiert und entworfen, welches basierend auf der „bottom up“ Anwendung der Synthetischen Biologie aufgebaut wurde. Es besteht aus gleichzeitig ausgebildeten chemischen und physikalischen Verknüpfungen und beinhaltet zwei Komponenten: (1) eine thiol funktionalisierte HA (74kDa) (**HA- DTPH**) und einen ionischen Vernetzer (**Cl^+**). **HA-DTPH** bildet hierbei die chemischen Verknüpfungspunkte im Hydrogel, basierend auf der Reaktion von freien Thiolgruppen zu Disulfidbrücken. Der Ionische Vernetzer, bildet die physikalischen Vernetzungspunkte aus, bestehend aus Wasserstoffbrückenbindungen und elektrostatischen Wechselwirkungen. Es wurden insgesamt drei verschiedene Vernetzer benutzt, die sich in ihrer Fähigkeit Wasserstoffbrückenbindungen auszubilden unterscheiden. Benutzt wurden: (1) deacetylierte Disaccharid Einheit von HA (**dHA^+**), (2) positiv geladenes Glukosamin (**$GluA^+$**) und (3) Ammoniumchlorid (**NH_4^+**). Diese Vernetzer wurde vor allem aufgrund ihrer Biokompatibiliät und der Fähigkeit physikalische Verknüpfungen auszubilden ausgewählt. Die Zunahme der Fähigkeit Wasserstoffbrücken auszubilden von **NH_4^+** zu **dHA^+** ermöglichte es uns den Einfluss von physikalischen Verknüpfungen auf die Eigenschaften des Hydrogeles zu untersuchen. Ich konnte zeigen, dass durch Zugabe des ionischen Vernetzers die Reaktion der Thiolgruppen zu Disulfidbrücken beschleunigt wurde und zu einem stabilen Hydrogel geführt hat. Ohne einen ionischen Vernetzer mussten die Thiolgruppen des **HA-DTPH** mit Wasserstoffperoxid oxidiert werden, um ein stabiles Hydrogel zu erhalten (**HA-DTPH-Ox.**). Durch die Veränderung der chemischen Modifikation an HA und durch die Veränderung in Art und Konzentration des Ionischen Vernetzers, konnte die mechanische Steifheit, die Schwellrate und die Reaktion auf externe Stimuli variiert werden. Die Veränderung der chemischen Modifikation und des

Ionischen Vernetzers ermöglicht es das Hydrogel so zu variieren, dass es für verschiedene Zell-Untersuchungen anhand der mechanischen Steifheit von 0.1 Pa bis 8 kPa verwendbar ist. Außerdem ist die Schwellrate der **HA-DTPH-Cl**$^{+}$ stark durch den pH und der ionischen Konzentration aus der Umgebung beeinflusst. Besonders auffällig, ist das Schwellverhalten von **HA- DTPH- dHA**$^{+}$, während der Inkubation des Hydrogeles in einer Lösung mit pH 7. Hier findet ein Rückkopplungseffekt auf das Schwellverhalten statt. Im geschwollenen Stadium des Hydrogeles diffundiert ionischer Vernetzer in die Inkubationslösung und säuert die Lösung an, was im Umkehrschluss wieder zum Schrumpfen des Hydrogeles führt. Auch wurde festgestellt das **HA- DTPH-Cl**$^{+}$ Hydrogele eine höhere Halbwertszeit, beim enzymatischen Verdau, mit steigender Anzahl an gebildeten Wasserstoffbrückenbindungen haben. Durch die Abwesenheit von toxischen Verknüpfungsreagenzien während der Hydrogel Synthese wurde das etablierte Hydrogel System auch für Zelluntersuchungen, wie zum Beispiel Zell Adhesion und Zell Verkapselung verwendet. Abschließend lässt sich sagen, dass ein Hybrid-Hydrogel System erfolgreich etabliert wurde und ein starker Einfluss von physikalischen Verknüpfungen, auf die mechanische Steifheit, Schwellrate und Hydrogel Abbau festgestellt wurde. Dieses etablierte Hydrogel System ist durch seine Variabilität in Steifheit, Schwellrate und Abbaurate besonders gut geeignet für die Nutzung in der 3D Gewebezüchtung, als Wirkstoff Carrier und in der Regenerativen Medizin.

Abbreviations

2D	two dimensional
3D	three dimensional
A_{420}	absorbance of the samples at 420 nm
BSA	Bovine Albumin Serum
CD44	cell-surface glycoprotein involved in cell-HA interactions
Cl^+	positively charged ionic cross-linker
ddH_2O	double distilled water
dHA^+	charged disaccharide unit of HA
DTNB	5,5'-dithiobis(2-nitrobenzoic-acid)
DTP	3,3'-dithiopropionic-hydrazide
DTPH	3,3'-dithiopropionic acid
DTT	dithiothreitol
E-Modul	Elastizitätsmodul
ECM	extracellular matrix
EZM	Extrazelulläre Matrix
FGM2	Fibroblast growth basal medium
GAG	glycosaminoglycan
$GluA^+$	charged glucosamine
HA	hyaluronic acid/hyaluronan
dHA^+	charged disaccharide unit of HA
HA-$DTPH^x$	HA functionalized with DTPH and degree of thiolation x
HA-$DTPH^x$-Cl^+	HA functionalized with DTPH and degree of thiolation x cross-linked with any positively charged ionic cross-linker
HA-$DTPH^x$-dHA^+	HA functionalized with DTPH and degree of thiolation x cross-linked with disaccharide unit based positively charged HA
HA-$DTPH^x$-$GluA^+$	HA functionalized with DTPH and degree of thiolation x cross-linked with positively charged glucosamine

HA-DTPH^{x}-NH_4^+	HA functionalized with DTPH and degree of thiolation x cross-linked with amoinumchloride
HYAL	hyaluronidase
Q_M	swelling ratio
m_d	dry weight of hydrogels
m_s	weight of hydrogels swollen to equilibrium in different solutions
NHDF	primary normal human dermal fibroblast
NMR	nuclear magnetic resonance spectroscopy
PBS	phosphate buffered saline
RGD	tripeptide Arg-Gly-Asp
RHAMM	receptor for HA mediated motility

1 Introduction

1.1 The Idea of Developing a Novel Biomimetic Hydrogel System

Since the 1960s researchers started to design and build novel biologically based parts, devices and systems, as well as re-built existing natural biological systems. Since then, the emerging field of synthetic biology gained a lot of popularity. Two main scopes can be distinguished: "bottom-up" and "top-down". "Bottom-up" approaches aim to create artificial life *de novo* by assembling single biological building blocks. "Top-down" approaches design systems based on known biological modules to perform a specific task. The "bottom-up" approach is prominent in the field of extracellular matrix (ECM) engineering, aiming to mimic the extracellular environment *in vitro*. By this a better understanding of the influence of single components of the ECM or defined multi components on cell behavior and function is pursued. One possible technique to mimic the ECM is the development of a three-dimensional (3D) network of cross-linked polymer chains, namely hydrogels. In this thesis, I aim to develop a novel biomimetic hybrid double cross-linked hydrogel system, based on the bottom up approach of synthetic biology with special emphasis on the influence of chemical and physical cross-linking on the chemical and physical properties of the hydrogel system. Therefore, hydrogels are designed based on thiol functionalized hyaluronic acid (HA), a natural component of the ECM, which is able to form disulphide bonds, resembling the chemically cross-links, and a charged ionic cross-linker, providing the physical cross-links. The precise ratio of HA to ionic cross-linker and the degree of thiol functionalization enables us to study the influence of chemical and physical cross-links on the physicochemical properties of the presented ECM model. The design itself of the double cross-linked hydrogel system also allows studies for further plausible biomedical applications.

1.2 The Bottom-Up Approach in Synthetic and Engineering Biology

Exploring nature, gaining knowledge about complex living systems and the desire to understand is what motivates researchers and drives scientific discoveries forward. However,

the guiding question still is: How do these complex systems work? To get the right answer for this question one approach is to create and redesign the living system by ourselves. However, to rebuild such complex system is not that easy since the function of single building units still remains unclear. One way to overcome the challenge to assign specific functions to single components is, to first reduce the complexity of the system to a minimal number of components and after increase it in a stepwise manner. Moreover, in order to synthetically re-design an existing biological system one has to first identify its functional units (Majumder and Liu, 2018). This approach is used in several scientific fields, like the "dimension reduction" in data science (Wirsch, Cisl and Wirsch, 2014) or the "bottom-up" approach in synthetic biology (Andrianantoandro *et al.*, 2006).

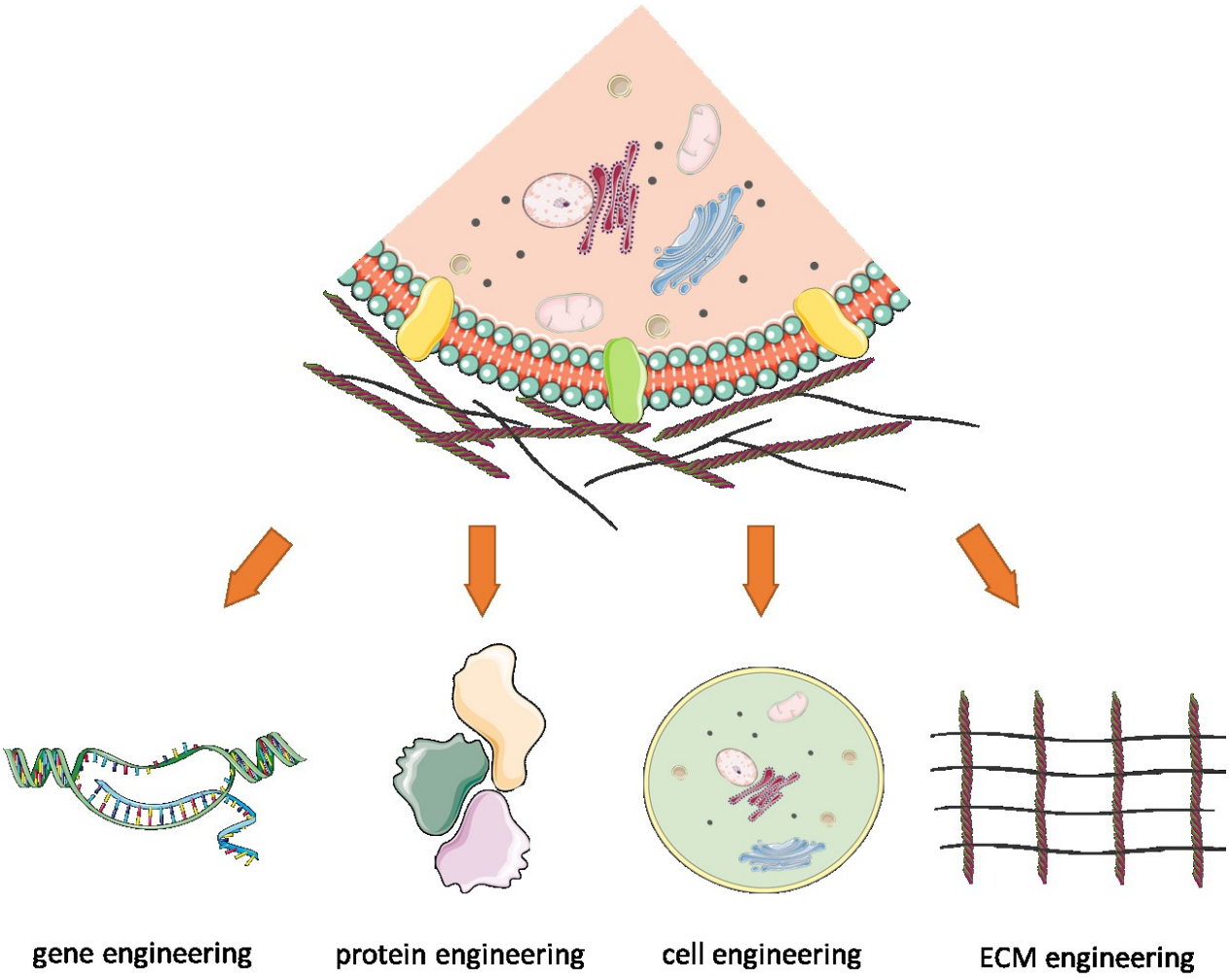

Figure 1 Applications of the bottom-up approach in synthetic and engineering biology

The field of synthetic biology encompasses a broad range of engineering fields, including protein, gene, cell and ECM engineering (Fig.1). Each field makes use of the bottom-up approach, to get a better understanding of the smallest functional unit of the complex system of interest. These functional units are the smallest biological building blocks like base pairs (A-T or C-G) (gene engineering), amino acids (protein engineering), the cell membrane (cell engineering) or single components of the extracellular matrix (ECM) (ECM engineering). In the following I will take a closer look on ECM engineering in general and the best way to design and mimic the ECM.

1.3 The ECM

In native tissue, the ECM is a mixture of mainly three classes of macromolecules: polysaccarides, proteoglycans and fiber-forming proteins. Polysaccharides are mostly linked to proteoglycan and fiber-forming proteins like collagen, elastin, fibronectin and laminin and are thus called glycosaminoglycans (GAG). In general, GAGs provide structural support and anchor points for cells (Fig.2 Theocharis et al., 2016).

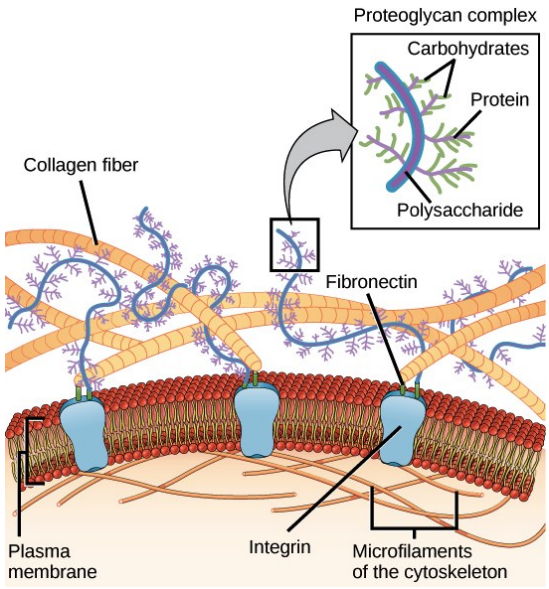

Figure 2 Composition of the ECM and anchoring points of cells1

[1] Theocharis et al., 2016

The network of collagen fibers and other molecules such as HA, an important glycosaminoglycan, are also mainly responsible for the diffusion of metabolites, hormones and signalling molecules within the ECM (Theocharis *et al.*, 2016). Thereby the ECM regulates various cell functions such as cell survival, proliferation, differentiation, morphogenesis and migration (Yue et al., 2014). The precise regulation of cellular function is controlled by the optimized composition of the ECM in each tissue and furthermore, by the interaction of specific ECM components with each other (Dicker et al., 2014). Dysregulation of the ECM composition and structure often results in the development and progression of several physiological and pathological conditions, such as cancer or chronic wounds (Cox and Erler, 2011). It is known that an aberrant ECM composition supports cancer progression by directly promoting cellular transformation and metastasis (Lu, Weaver and Werb, 2012). In wound healing the ECM composition plays a key role. The process itself consists of a series of physiological events including coagulation, granulation tissue formation, re-epithelialization and most important ECM remodelling (Bennett and Schultz, 1993). Each phase of the wound healing process is controlled and regulated e.g. the ECM-mediated migration of cells into the wound site as well as the ECM-induced expression of growth factors and their subsequent retaining in the ECM network. Acute wound healing in adult results in a formation of a scar, whereas, healing of fetal wounds occurs scarless (Larson et al., 2014). Several studies showed that the composition of the ECM could be responsible for these different outcomes (Chen and Thibeault, 2010). One main difference in the ECM composition in fetal skin, is the amount of collagen III and HA during the remodelling phase of the wound healing process. It comprises ∼30–60% of the total collagen compared to 10–20% in adult skin (Middelkoop and Ulrich, 2010) and contains 4-5 pg/mL HA in adult wound fluid and 15-25 pg/mL in fetal wound fluid (West *et al.*, 1997). This is one process amongst other processes and mechanisms in the human body, that makes it crucial to get a better understanding of how ECM composition and topography are maintained and how their deregulation influences physiological and pathological conditions (Cox and Erler, 2011). However, it is still challenging to develop a comprehensive understanding of the impact of ECM on cell specific functions because of the number of players (a great multitude of ECM proteins) involved in those processes. Making the situation even more complex, the exact composition of the ECM varies not only between different types of tissue but has been proved to be very heterogeneous even within one

specific type of tissue (Hinderer, Lee and Schenke-layland, 2016). Furthermore, each component of the ECM can have a different function depending on the surrounding matrix and the respective cell type (Chen and Thibeault, 2010). Therefore, identification of a minimal combination of ECM components allowing to reproduce *in vitro* the cell behaviour and response observed *in vivo* remains a challenge. One way to tackle this challenge is the development of an ECM mimicking system, which will be presented in the upcoming chapter.

1.4 Designing a ECM mimetic

The following parameters have to be considered in order to design an ECM mimicking system: type of biomaterial; biocompatibility; biodegradability, incorporation of variants of ECM, and mechanical properties (Ma & Zang 2001). However, the design of a suitable ECM mimetic raises the question “How simple is complex enough?” (Kyburz et al., 2015). What minimal biological signals are necessary to guide desired cellular functions, and how might temporal addition and/or removal of ECM components influence these? In an attempt to answer this question several ECM mimicking models have been established.

1.4.1 2D vs. 3D ECM Mimicking System

At the beginning two dimensional (2D) systems were used in order to mimic the ECM. For this either cell culture plastic or glass surfaces were coated with ECM proteins such as collagen or other biomaterials, like agarose (Fig. 3 a-b).

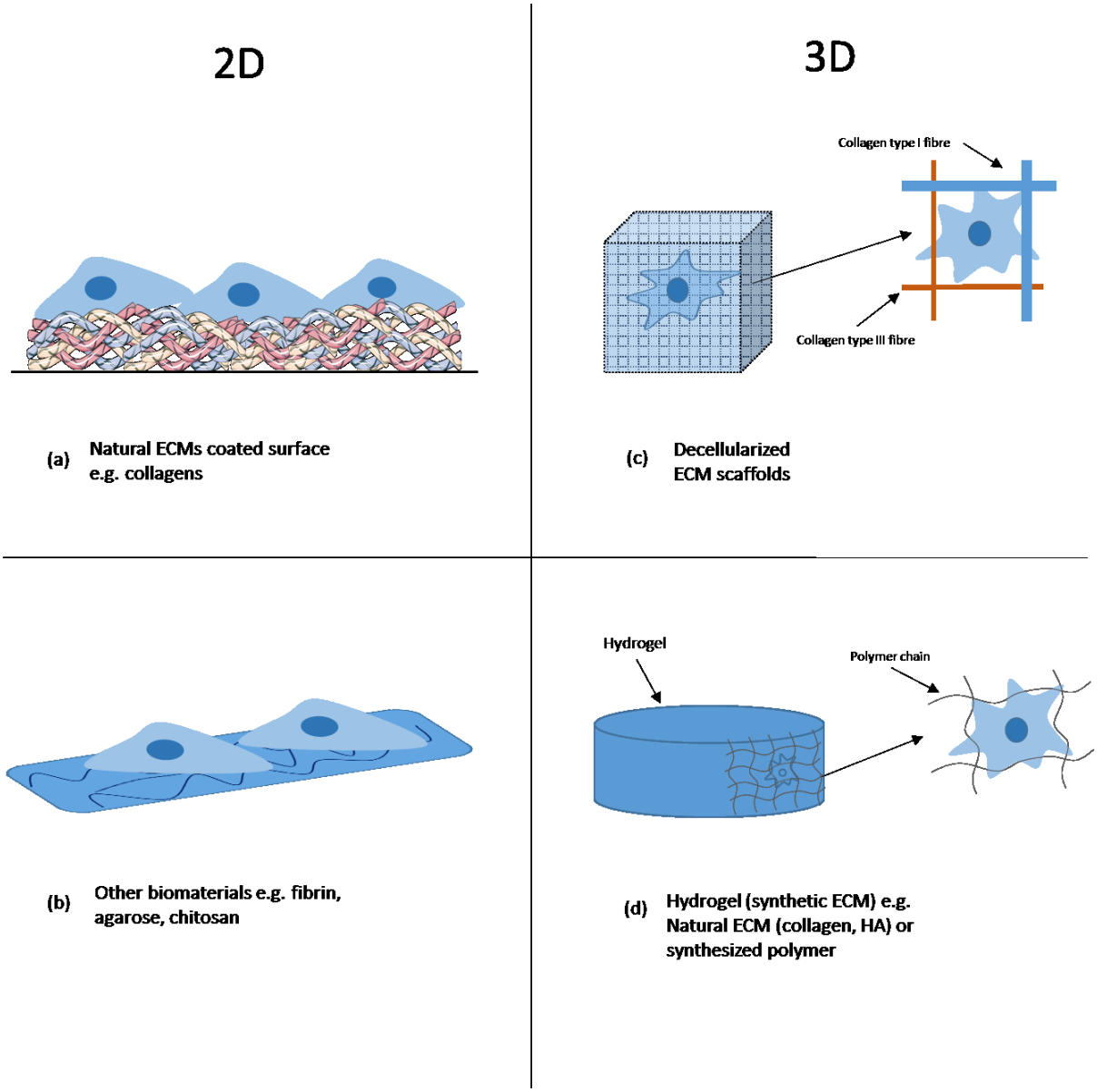

Figure 3 ECM mimicking models. Natural ECM or other biomaterial coated surfaces represent 2D model (a-b) and decellularized ECM scaffolds and hydrogels represent 3D model of an ECM mimicking system (adapted from Hinderer et al., 2016).

However, Klaus von der Mark *et al.,* showed already in 1977 that 2D mimicking systems have many limitations to study the interplay between cell behavior and the surrounding ECM. For example, cells cultured on a 2D matrix normally grow as a monolayer attached to the surface. Whereas cells in 3D grow in a 3D manner. Thus 2D and 3D ECM systems evidently induce changes in the cell morphology and polarity (Weaver *et al.*, 2009) (Mseka, Bamburg and Cramer, 2007). Since the shape of the cell is synergistic with its function (Gospodarowicz,

Greenburg and Birdwell, 1978), changes in the morphology affect cell response and behavior (Highley, Prestwich and Burdick, 2016). It has been shown that cells cultured on a 2D substrate failed to express certain tissue-specific genes and proteins at levels comparable to those found in tissue (Chen and Thibeault, 2010). In order to resemble the *in vivo* microenvironment of cells, the 2D systems were extended to three dimensional (3D) systems. The main two impact factors for the suitability of a 3D mimicking system are: (1) the physical resistance to cell movement by the surrounding microenvironment, which also exists *in vivo* and (2) the ability of cells to remodel their surroundings by proteolytic catabolism. For this purpose, scientists developed either decellularized ECM scaffolds, mimicking the whole microenvironment in a 3D manner or hydrogels, made out of either natural ECM components or synthesized polymers (Fig.3 c- d).

Decellularized ECM scaffolds are obtained in the process of decellularization of existing tissues or organs in which all of the cellular components are enzymatically removed until only the ECM scaffold and organ specific ECM remain. After the decellularization process, cells of this specific organ or tissues are seeded back and induced a re-cellularization (Gupta, Mishra and Dhasmana, 2018). Even though the process of decellularization is a promising method to study cell behaviour and function in a 3D system, it brings several draw-backs. Besides the lack of tissue source and possible inevitable changes within ECM composition due to the decellularization procedure (Fernández-pérez, 2019), the main problem remains which is the assignment of single components of the ECM to cell behaviour and function (Chaicharoenaudomrung, Kunhorm and Noisa, 2019). Moreover, isolation procedure derived changes in the ECM might also affect the stiffness scaffold. As these produced ECM scaffolds differ from *in vivo* and as it has been reported that substrate stiffness has an influence on specific cell behaviour, aberrant cell behaviour might be observed (Hoshiba et al., 2019). Naturally the tunability of biomechanical properties of decellularized ECM scaffolds is limited. To overcome these challenges hydrogels can be employed. Describe hydrogels here Ideally, the engineered hydrogels combine the precision and control of the used natural or synthetic biomaterial, together with the advantage to specifically incorporate defined bioactive proteins. By applying such highly controlled hydrogels single biomaterials can be assigned to

certain cell behaviours. Additionally, the use of hydrogels can promote desired cell response, behaviour and function in situ. given the benefit.

1.5 Hydrogels – a Promising Biomaterial?

1.5.1 Hydrogel – ECM Mimicking Properties

In recent decades, hydrogels have been developed to serve a variety of biomedical and industrial applications such as visual correction through contact lenses, as biosensor or as a supercapacitor hydrogel in the development of electronic equipments (Ahmed, 2015). Further, hydrogels possess the capacity to immobilize and release cells, drugs, proteins due to their porosity. Therefore, hydrogels are also an attractive material as a delivery system, (Mero and Campisi, 2014). Different natural polymers can serve as building blocks for the 3D network of a hydrogel (Drury and Mooney, 2003). The use of natural polymers is in general advantageous due to their known biocompatibility and biodegradability (Alesa *et al.*, 2017). By tuning different parameters such as the molecular weight, sequence, and structures of the used polymers, hydrogel can widely vary within their mechanical properties where viscoelasticity is combined with material stiffness (Ahmed, 2015). This provides the opportunity to mimic different extracellular matrices throughout the human body. For example, the very soft and viscoelastic brain with a shear modulus of 0.1 kPa to 0.7 kPa (Budday *et al.*, 2016), compared to a rigid and stiff bone with an elastic modulus of 15000 kPa to 20000 kPa (Barnes, Przybyla and Weaver, 2017). However, hydrogels are not only tuneable by the choice of polymer but also by the way of cross-linking.

1.5.2 Hydrogel classification via Polymer Cross-linking

Hydrogels, formed by a polymer chain can be either held together by chemical or physical cross-links. In chemically cross-linked networks, the polymer backbones are linked via a covalent chemical bond required often assistance of a catalyst (Liu, Shu and Prestwich, 2005). In contrast, physically cross-linked hydrogels, called reversible networks are held together by

physical interactions such as ionic interactions, hydrogen bonding or hydrophobic interactions (Berger *et al.*, 2004).

1.1.1.1 Chemical cross-link – Taking a Closer Look on Disulfide Bond Formation

Chemically cross-linked hydrogels display relatively high mechanical strength owing to the covalent bonds within the cross-linked network. Chemical cross-linking can be achieved by a variety of different reactions, depending on the polymer backbone. A commonly used method utilizes a click-reaction as introduced by Sharpless et al. (2001). Due to its mild reaction conditions and applicability to a wide range of reactant (Xu and Bratlie, 2018), it represents the most important technique in biomaterial chemistry to from covalent bonds (Wang et al., 2011). Another widely used method is the radical polymerization of polymers derivatized with polymerizable groups such as vinyl groups (Maitra and Shukla, 2014). Other cross-linking methods such as condensation reactions between hydroxyl or amine groups with carboxylic acids have been reported and were used efficiently for the cross-linking of water soluble polymers such as polysaccharides (Parhi, 2017). The established hydrogel system in this thesis consists partly of disulfide bonds, which also represents an important type of chemical cross-link. The disulfide bond formation is mainly controlled by two reaction conditions: (1) the environmental pH and (2) the oxidizing agent (Thorpe et al., 2002). The key reaction is the deprotonation of the thiol compound, which is induced by an alkaline pH, resulting in the thiolate anion (I) (Gyarmati, Némethy and Szilágyi, 2013). Subsequently, after deprotonation the thiolate anion can get oxidized by air or by an oxidizing agent, such as hydrogen peroxide (Shu *et al.*, 2002). The key step of the oxidation is the formation of thyil radical (II), which reacts further to the desired disulfide bond (III) (Fig.4) (Gyarmati, Némethy and Szilágyi, 2013).

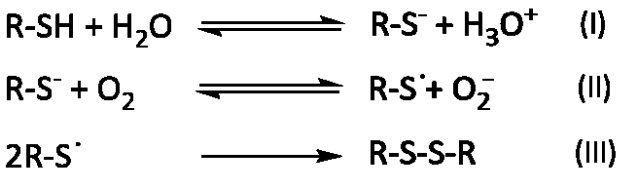

Figure 4 Reaction Scheme of disulfide bond formation. Deprotonation of thiol compound (I), Oxidation thiolate anion (II) and reaction of two thyil radicals to disulfide (III) (adapted from Bergen, Roos, & Proft, 2014).

Disulfide bonds are known as the weak link among other covalent bonds. S-S bonds reach only 40% of the strength of e.g. C-C and C-H bonds (Khoo and Norton, 2012). However, the dissociation energy of disulfide bonds is 60 kcal/mol (251 kJ mol^{-1}), which is stronger than physical cross-links such as hydrogen bonds or electrostatic interaction (Haworth, George and Wouters, 2010). Disulfide bonds play a key role in stabilizing protein structures, their disruption is typically connected with the loss of protein function and activity (Wedemeyer *et al.*, 2000). Disulfide bonds fulfill also a catalytic role in enzymes such as thioredoxin, which acts as a cellular redox sensor based on the oxidation status of its thiol groups (Nakamoto and Bardwell, 2004). *In vivo* thiols are oxidized to disulfide bonds via reactive oxygen species (Baba et al., 2019) resulting from hydrogen peroxide, which is also the main oxygen agent *in vitro* (Paoli *et al.*, 2001) (Bergen, Roos and Proft, 2014) (Shu *et al.*, 2002). In both cases, oxidation with hydrogen peroxide leads to the formation of several thiol derivatives, including the irreversible formed oxidation states: sulfinic - and sulfonic acid (Fig. 5) (Zeida et al, 2013).

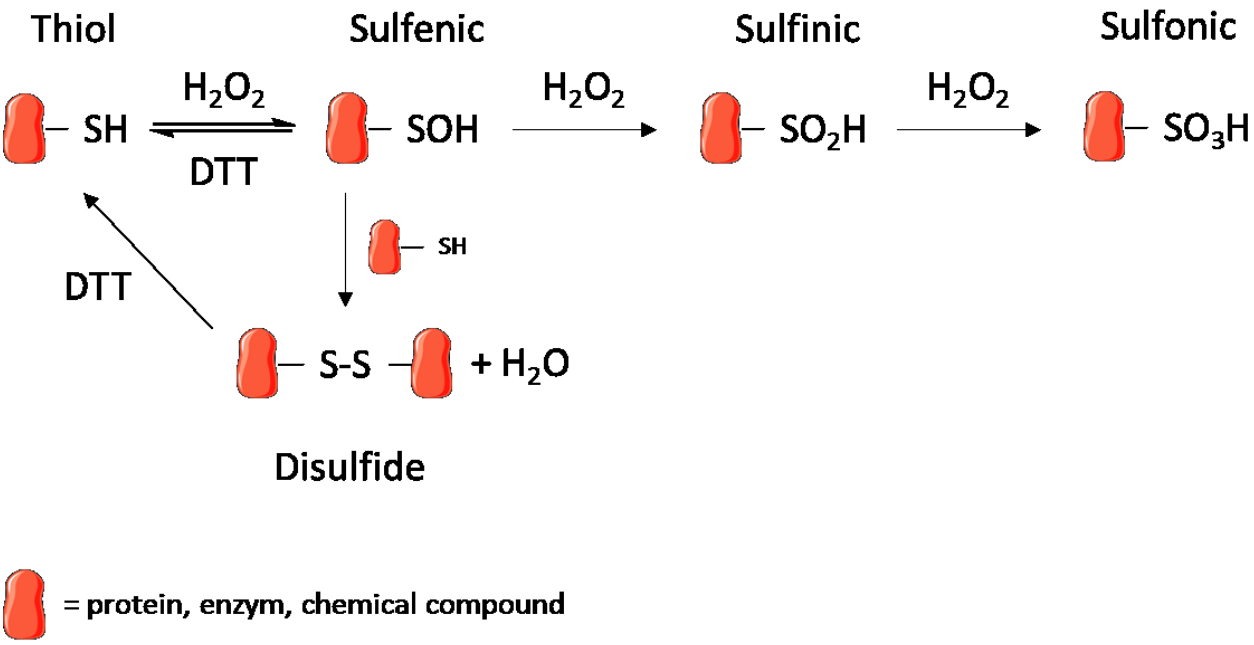

Figure 5 Oxidation states of thiol groups by H_2O_2 and reduction by DTT.

In vivo the formation of sulfinic and sulonic acid results in irreversible oxidative damage and in the course to cell death (Allen and Mieyal, 2012). To avoid this, cells perform a protecting mechanism, the so called S-glutathionylation. Hereby gluthathion reacts in a reversible way

with cysteine residues and forms disulfide bonds. Due to this mechanism thiol groups are shielded and not available for oxidation processes (Mao and Mooney, 2015). However, *in vitro* hydrogen peroxide induced disulfide bond formation is hard to control. In respect of hydrogels the formation of sulfenic -, sulfinic, and sulfonic acid results in destabilization of the network. Taken all together, the most important disadvantage of chemically cross-linked hydrogels is the need for additional reactants for the cross-linking reaction like hydrogen peroxide. Depending on the application, this creates the necessity of additional purification steps, especially when used for biomedical application.

1.1.1.2 Physical cross-link – Hydrogen Bond Formation and Salt Bridges

Compared to covalently cross-linked hydrogels, physical cross-linking is eliminating the need for additional cross-linking agents and enables *in-situ* gel formation. Electrostatic interaction, such as the coordination of cations like calcium with anionic side groups such as carboxyl groups for example in alginate hydrogels (Zhang, Zhang and Wu, 2013) and hydrogen bond formation are the most commonly used techniques for physical cross-linking (Ren *et al.*, 2015). Physical-cross-linking also includes hydrophobic interactions, dipol-dipol interaction and Van-der Waals forces. Utilizing physical cross-links, included hydrogen bonds and salt bridges, resulted in the established hydrogel system of this thesis. Therefore, I will discuss the formation of hydrogen bonds and salt bridges in detail.

Hydrogen bonding is a special type of dipole-dipole attraction between molecules. It results from the attractive force between a hydrogen atom covalently bonded to a very electronegative atom such as a N, O, or F atom and another very electronegative atom (Daniel, 2013). Hydrogen bond strengths range from 4 kJ to 50 kJ per mole of hydrogen bond (Desiraju, 2011). This type of physical cross-link is ubiquitous in many biological system, such as the participation in the DNA helix formation or the folding processes of proteins (Coulocheri *et al.*, 2007). However, hydrogen bonds are not only crucial in biological systems but have been used in the development of biomaterials and chemical components (Hu *et al.*, 2015). Figure 6 highlights the versatile use of hydrogen bonds.

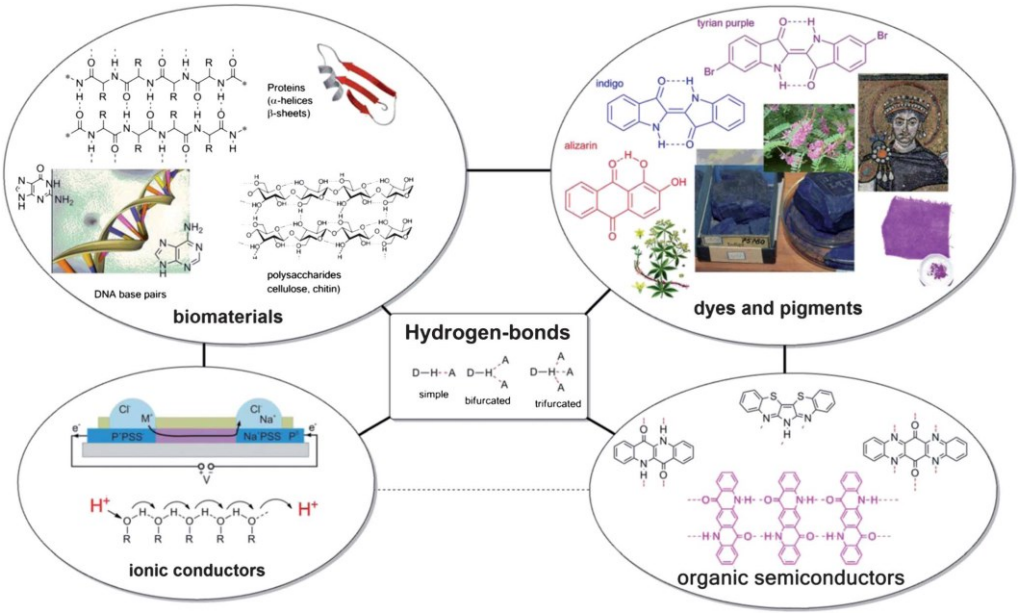

Figure 6 Overview of the role of hydrogen-bonding in biomaterials, dyes and pigments, ionic conductors, and organic semiconductors[2].

The second participant of the physical cross-link in the established hydrogel, are salt bridges. Salt bridges are mainly known to occur between amino acids (Pylaeva, Brehm and Sebastiani, 2018). It consists of the simultaneous formation of a hydrogen bond and an electrostatic interaction, between a carboxyl group and a protonated amine group (Fig.7) (Donald, Kulp and Degrado, 2012).

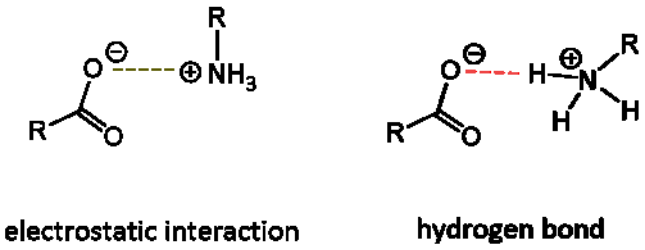

Figure 7 Formation of salt bridges.

Salt bridges are known to occur between amino acids and contribute to the stabilization of proteins (Jelesarov & Karshikoff, 2009). On the one hand the main drawback of the physical cross-linking, is the weak interaction. Physical cross-linked hydrogels are generally weak and

[2] Daniel, 2013

they tend to break under certain physical stimuli or when stress is applied due to the non-covalent and reversible nature of the junctions in the network. (Ghobril and Grinstaff, 2015). On the other the most important advantage of physically cross-linked hydrogels, are the sensitivity to external chemical stimuli, the self-healing property and the injectability under room temperature (Hu, Wang and Xiao, 2019).

1.1.1.3 Simultaneous Chemical and Physical Cross-link – Hybrid Double Cross-linked Hydrogel

With the aim to get the best of both worlds, chemically and physically cross-linked hydrogels, a new type of hydrogel was developed, the so called hybrid double cross-linked hydrogels (Martini et al., 2016). Hybrid double cross-linked hydrogels contain both, chemical cross-linking points formed by covalent bonding and physical cross-linking points formed by physical interaction (Mondal, Das and Nandi, 2020). The advantage of a hybrid hydrogel is the maintenance of the integrity of the hydrogel network in aqueous solution caused by the chemical cross-linking and the reforming capability maintained by the physical cross-linked. One hybrid double cross-linked system was developed and established by Fajardo et al. (2013). Here they combined a glycidyl methacrylate functionalized chitosan (CSH-gel) hydrogel, in which methacrylates form the chemical cross-links, while the polyanionic polymer chondroitin sulfate, forms the physical cross-links inside the CSH-gel (Fajardo *et al.*, 2013). This hybrid hydrogel showed different liquid uptake capacities than the chemical hydrogels (CSH-gel) and additionally exhibited a great sensitivity towards changes in the pH, which can be attributed to the additional physical cross-link inside the network (Fajardo *et al.*, 2013). This developed hybrid double cross-linked hydrogel system is an example for a prominent hydrogel category, namely “smart”.

1.5.3 “SMART” Hydrogels and Biomedical Applications

Kuhn *et al*. introduced the word “smart” in 1949 in order to describe a specific type of hydrogels. Smart hydrogels were hydrogel systems which held the capability to respond to environmental stimuli, which in turn induced subsequently changes in the hydrogel’s structure and function (Kuhn, 1949). Environmental changes include changes within physical parameter

such as pressure, light and temperature, as well as chemical or biochemical parameters including ionic strength, pH and ions (N. N. Ferreira et al., 2018). One of the first smart hydrogel was a hydrogel consisting of methacrylic acid, which showed a swelling and shrinking behavior depending on the pH of the surrounding solution (Katalachsky et al.,1994). Besides the response of swelling and shrinking, hydrogels are also capable to react upon external stimuli via sol-gel transition (Lele, 2017). Sol-gel transition describes the process when xxx which is often an important characteristic of injectable hydrogels (Takata *et al.*, 2017). Since, I will characterize the swelling behavior of the hydrogel, the swelling behavior in water and upon external stimuli, the swelling process itself and external stimuli including temperature, pH, and ionic strength will be explored in more detail.

1.1.1.4 Swelling Process of Hydrogels

In general the swelling process of hydrogels involves three steps: (1) diffusion of water into the hydrogel network, (2) reduced entanglement of the polymer chains upon hydration and (3) expansion of the hydrogel network (Ferreira, Vidal and Gil, 2000). The diffusion of water into the hydrogel network is induced by the attraction and later adsorption of water molecules to hydrophilic and polar groups, such as - OH, - COOH, $–COO^-$, - C=O and - $CHNH_2$. This results in the so called primary bound water. Due to this primary bound water hydrogels swell and the exposed hydrophobic moieties interact with more water molecules, the secondary bound water (Gun, Savina and Mikhalovsky, 2017). Following an osmotic driving force additional water molecules will move into the hydrogel, which is controlled by the elastic retractive force of the cross-linking density. Owing to this additionally imbibed “free water”, hydrogels reach their equilibrium swelling (Gritsch, Motta and Natta, 2015).

1.1.1.5 Temperature-Sensitive Hydrogel

Temperature sensitive hydrogels are changing the swelling behavior in response to the changing temperature. Either, the hydrogel swells or shrinks with increasing temperature, the first called a positive temperature response and the latter negative temperature response. The swelling behavior is not the only reaction towards temperature changes but also a sol-gel

transition can occur upon temperature change. This sol – gel transition is especially used for injectable hydrogels, which are fluid at room temperature and form with increasing temperature (typically up to physiological 37°C) a gel. For example, Tsao *et al*. (2016) used a drug loaded chitosan-PEG hydrogel as an injection into an irregularly-shaped tissue defect caused by tumor resection. The hydrogel experienced a sol - gel transition at physiological temperature and thus filled the defected tissue. This proved to be a method for implantation of tissue-like structures with minimal invasiveness.

1.1.1.6 pH-Sensitive Hydrogel

In general, pH sensitive hydrogels are distinguished by the charge of the applied polymer. For example, hydrogels made out of chitosan or poly (ethylene imine) (Xu and Matysiak, 2017), as a polycation polymer, swell at acidic pH due to the protonation of amino or imine groups (Rizwan et al., 2017). The protonated and thus positively charged moieties on the polymer chains cause repulsion and hence are responsible for swelling. Consequently poylanion polymers, such as HA, with a negatively charged moiety swell at basic pH (Ourjavadi, Urdtabar and Hasemzadeh, 2008). The key factors for controlling the swelling properties of pH sensitive hydrogels are a charged moiety and the pH of the surrounding medium. pH sensitive hydrogels are often used as drug delivery systems. Since they have the benefit to respond to different pH values in the human body and they subsequently release the drug at the desired location of the body for example in the stomach at acidic pH or in the intestine at basic pH (Fig.8) (Karimi *et al.*, 2018).

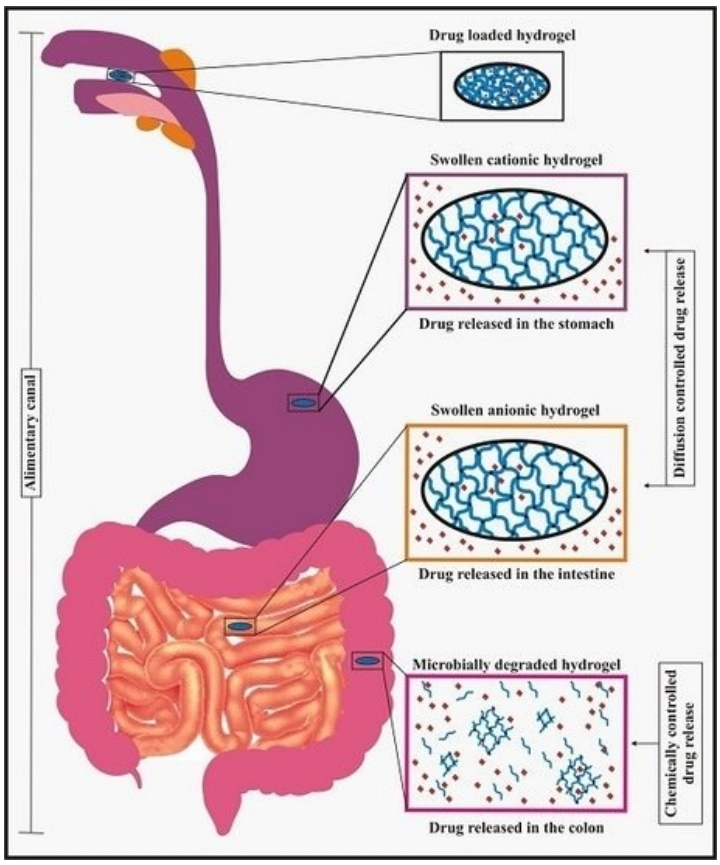

Figure 8 Drug release upon hydrogel swelling. *Swollen cationic hydrogel releases drug at acidic pH in the stomach, whereas swollen anionic hydrogel at basic pH in the intestine. 3*

1.1.1.7 Ionic Strength Sensitive Hydrogel

Changing salt concentrations of the environment leads to structural changes of some hydrogels, resulting in ionic strength sensitive hydrogels (Buenger, Topuz and Groll, 2012). The response of the hydrogel can be either induced by changing the salt species or by changing the salt concentration of the surrounding medium (Kato, Yamanobe and Takahashi, 1997). The underlying mechanism is explained by the increased hydrophobic interactions induced by salt concentrations, resulting in a reduction of electrostatic repulsion between the polymers, enabling network precipitation (Gil and Hudson, 2004). Such ionic strength sensitive hydrogels are important for cellular processes like nerve excitation and muscle contraction which involves ionic strength modifications (Horkay, Tasaki and Basser, 2000). Hydrogels can also be

[3] J. Liu et al., 2012

used as a chelation tool for ions in case of increasing concentration. For example, a great application would be the absorption of sodium salt in the blood by a hydrogel as increasing ionic concentrations are linked to tumor malignancy in human brain (Onitilo, 2007).

1.6 Which Biomaterial to use?

Taken all together, to fulfil certain requirements, such as the ECM mimicking ability, biocompatibility, ability to form physical cross-links and sensitivity to environmental changes, the used biomaterial to develop a ECM mimicking hybrid double cross-linked hydrogel system based on the bottom up approach of synthetic biology has to be chosen carefully. Possible candidate is the negatively charged GAG, hyaluronic acid. It is one of the most important natural polymers in the ECM and due to this provides the necessary biocompatibility for future biomedical applications. Furthermore, it consists of repeating saccharide units, providing a polyanion backbone, which is able to form physical cross-link with positively charged molecules, which I am interested in studying in our synthetic matrix model. Moreover, it is degradable (Xu et al., 2012), which is a further important property for my hydrogel system. The known ability of HA to bind to certain, receptors such as CD44 and RHAMM, makes it further suitable for non-integrin mediated cell adhesion and motility studies. (Kim and Kumar, 2014) Due to this HA is defined as the best choice of polymer to establish a hybrid double cross-linked ECM mimetic. Therefore, an even closer look at its properties, which are important for my hydrogel system, will be taken.

1.7 Hyaluronic acid – A rising star

HA was first discovered and isolated 1934 by Karl Meyer and John Palmer from the vitreous of a bovine eye. They described HA as an unusual polysaccharide with an extremely high molecular weight but recognized the structural similarity to already known GAGs, such as chondroitin sulfate and keratin sulfate (Pomin and Mulloy, 2018). What distinguished HA from already known GAGs was that the newly discovered polymer had no sulfate group. Over the next 10 years HA was found in and extracted from almost all vertebrate tissues. One important

finding was the existence of HA in the capsules of *streptococci* bacteria. This is nowadays the main source of synthetic HA and brings the advantage of avoiding animal sources and can be produced *in vitro* in high amounts (Liu *et al.*, 2011). 1943 was the first time that reduced amounts of HA in synovial fluid had been connected to damaged joints. This finding already indicated a possible role for HA as a lubricant and thus hinted to a high viscosity for HA (Selyanin, Boykov and Khabarov, 1934). A later discovery where a HA solution lost its viscosity upon radiation showed the dependency of viscosity on HA polymer size, since it was known from previous studies that radiation led to degradation of HA (Huang *et al.*, 2019). The first medical use of HA occurred in 1943 during the Second World War. Since it was observed before that HA might have an effect on cell growth, N.F. Gamaleya developed bandages based on extracts of human umbilical cord and called this bandages “factor of regeneration” (Selyanin, Boykov and Khabarov, 1934). Given that HA is one of the main components in the umbilical cord, HA was apparently responsible for the known healing effect of the used bandage. Ever since, HA has been and still is studied to utilize it as a biomaterial for wound healing, drug delivery or tissue engineering purposes.

1.7.1 Structure and Properties of HA

HA is a linear, unbranched negatively charged polysaccharide consisting of D-Glucuronic acid and N-Acetylglucosamine, which are linked together through alternating β -1,4 and β -1,3 glycosidic bonds (Papakonstantinou, Roth and Karakiulakis, 2012). HA can reach a length of 2000 to 25000 disaccharides, corresponding to 2 µm to 25 µm (Fallacara, 2018) and thus a molecular mass of 10^6 Da to 10^7 Da. The bulky substituents, such as the hydroxyl-, carboxyl- and acetamide group and a glycosidic bond occupy an equatorial and sterically more favourable position. These groups are responsible for the hydrophilic backbone. Additionally, these moieties represent sites for possible chemical modification of HA. The hydrogen atoms, are in the axial, less sterically favourable position giving the molecules a hydrophobic character (Fig.9).

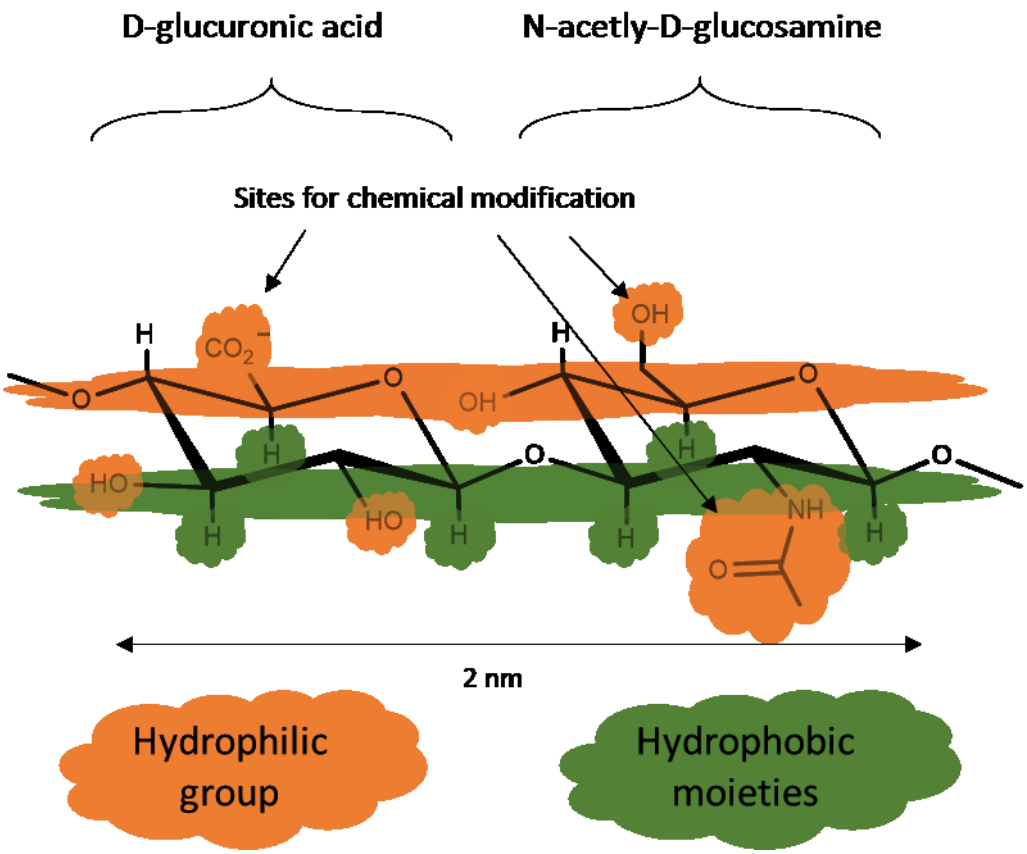

Figure 9 Chemical structure of hyaluronic acid (HA), composed of D-glucuronic acid N-acetyl glucosamine. Monomers are linked via β -1,3-glycosidic bonds and disaccharide units themselves are connected through β-1,4-glycosidic bonds. HA consists hydrophilic backbone (orange) and hydrophobic moieties (green). The average length of one disaccharide unit is estimated to be 2 nm.

Due to this hydrophilic and hydrophobic parts, HA can be found in various conformations, like elongated chains, non-condensed helixes, condensed rod shaped structures, helixes as well as structures similar to pearl necklaces and clips (Chase, 1999). In physiological solutions, the backbone of a HA is stiffened through the formation of internal hydrogen bonds, which also contributes to the stability of the taken conformation. Stabilization of the conformation also depends on the solvent and the presence of salts (Cowman *et al.*, 2005). HA with divalent cations, like Ca^{2+} are insoluble in water and form intermolecular cross-links, leading also to a gel like structure (Napier and Hadler, 1978). The network formation of HA in solution depends also on the concentration and molecular weight. It is reported by Beloded, A.B. (2008), that HA in concentrations of 1-4 weight % can form pseudo- gels with magnesium and ammonium chloride. High molecular weight HA forms networks independently from the concentration

and low molecular weight HA has been reformed to island-type structures at low concentrations (Kujawa *et al.*, 2005). The network structure determines the diffusion of small molecules, such as water, electrolytes and nutrients. Larger molecules, like proteins dwell because of their hydrodynamic size. As a consequence HA also provides a polymer mesh which protects from penetration of high molecular weight toxins and microbiological invasions (Selyanin, Boykov and Khabarov, 1934). Furthermore, the pK_a value of the carboxyl groups is 3-4, which results in complete deprotonation and a negative charge at physiological pH (Kim *et al.*, 2012). The high negative charge together with the hydrophilic groups of HA causes its affinity to water molecules and represents a crucial function of HA, namely water binding and retention (Panagopoulou, Molina and Kyritsis, 2013). The large amount of bound water serves among others as a resisting parameter to compression force, which is used for example in joints as a shock absorber and lubricant (Wu *et al.*, 2015). However, the structure of HA depends also on the pH of the surrounding solution. Maleki et al. (2008) showed that HA chains contract and thus have shorter persistence lengths in solutions with high ionic strength or low pH. Two additional effects affect HA's structure and thus its impact within a cellular environment: (1) its molecular size and (2) HA-receptor interactions.

1.7.2 HA - Synthesis and Degradation

The synthesis of HA takes place on the cytosolic side of the plasma membrane by three hyaluronan synthase (HAS): HAS1, HAS2 and HAS3. HAS enzymes are integral membrane proteins with 4–6 transmembrane domains in addition to 1–2 membrane-associated domains (Weigel, Hascall and Tammi, 1997). These enzymes add Mg^{2+} or Mn^{2+}dependent monosaccharides of uridine diphosphate (UDP) in a together (Weigel and Deangelis, 2007). While the synthesising process is ongoing, the polymer chain is transferred to the extracellular space through a trans-membrane pore. By this mechanism it is possible to form extremely long polymer chains. HAS1, HAS2 and HAS3 are responsible for the synthesis of specific molecular sizes of HA. HAS3 is known to synthesizes the shortest HA polymer sizes (1×10^5 to 1×10^6 Da), while HAS1 and HAS2 synthesizes larger polymers (2×10^5 to 2×10^6 Da) (Itano *et al.*, 1999) (Itano, 2002). As the synthases are only known to produce relatively high molecular weight HA smaller polymers are most likely the result of different degradation mechanisms.

Three independent mechanisms for HA degradation are known: (1) Degradation by specialized hyaluronan degrading enzymes, known as hyaluronidases. In humans six hyaluronidases are known to date HYAL1-4, HYALP and HYAL-PH20, all of them acting as hydrolases, belonging to the endoglucosaminidases digesting HA at the beta 1,4 glycosidic bond (Buhren *et al.*, 2016). This degradation process requires the release of HA from the tissue matrix into the vasculature or lymphatic system and occurs inside specific liver, kidney or spleen cells (Göranson et. al, 2004). (2) In the human body, degradation of HA occurs upon the formation of reactive oxygen species, like nitric oxide and superoxide, which destruct the tertiary structure of HA (Mendichi *et al.*, 2006).(3) HA can also be cleaved at an acidic pH < 4 or alkaline pH > 11 (Tokita and Okamoto, 1995). Interestingly, degradation of HA is linked to pathophysiological incidences. Many cellular functions and signaling pathways are shown to be induced by different molecular sizes of HA, thus it is important while designing a ECM mimicking system to choose the molecular size of HA carefully to get the desired cell behavior, function and signaling. A HA based hydrogel system delivers the advantage of specific degradation by local secreted hyaluronidases from cells or unspecific by reactive oxygen species, which can be used in the biomedical applications for wound dressing and drug delivery (Zhang *et al.*, 2012). Further it has the benefit to be used in tissue engineering studies since encapsulated cells are able to remodel the surrounding ECM mimetic (Tan *et al.*, 2009).

1.7.3 Non Integrin Mediated Cell Adhesion via HA

Typically, cells interact with the surrounding ECM via integrins, transmembrane structures which recognize specific motifs within extracellular proteins. Adhesion and spreading of the cells upon binding to an integrin receptor, is known as the integrin mediated adhesion (Bro, Friedl and Za, 1998). HA has been reported to be either adhesive or non-adhesive. Two main HA receptors are known to play a critical role in non-integrin mediated cell attachment and motility (1) cluster designation 44 (CD44) and (2) receptor for hyaluronic acid-mediated motility (RHAMM) (Misra and Ghatak, 2015). Both, the CD44 and RHAMM receptor belong to the family of HA-binding proteins, known as hyaladherins. CD44 contains a Link module, which has been identified to be a general motif for HA binding (Cyphert, Trempus and Garantziotis, 2015). Link module containing proteins bind to the carboxylate group of the glucuronic acid

moiety by the formation of physical cross-links, such as electrostatic interactions and hydrogen bonds. Regarding the effect of the HA receptors on cell adhesion, Kouvidi *et al*. (2011) reported an increasing adhesion capacity of fibrosarcoma cells upon binding of HA to the RHAMM receptor. HA binding to CD44 and subsequent cell signaling or cell behavior has been shown to be HA size dependent. Low molecular weight HA (< 10 kDa) binds in a reversible way to CD44, whereas high molecular weight HA is bound stronger (Wolny *et al.*, 2010). Depending on the HA size different signals are transmitted and different effects are transduced into the cell (Tavianatou *et al.*, 2019). Further, it has been demonstrated by Y. Kim *et al.* (2014), that by blocking CD44 the adhesion of glioblastoma multiforme cells is reduced for a short time scale, even if an integrin binding motif is presented. This led to the assumption that CD44 enhances integrin function upon HA binding. Therefore, ECM mimicking systems hold the potential to unravel the effects of HA on CD44-mediated cell adhesion by designing a minimal extracellular environment based on HA building blocks.

1.7.4 Existing Hydrogel Systems

HA-based hydrogels with their above described properties fulfill several requirements as a biomedical tool or to analyze specific cell behavior. To illustrate this, the following section describes several existing hydrogel systems based on HA and other ECM proteins. A special focus will lay on current drawbacks and limitations, in order to emphasize the need for a novel HA based hydrogel. For example, using fibrin-based hydrogels, it is required to treat the hydrogel system with a protease inhibitor throughout the experiment, as fibrin can be degraded within 2 days. Thus, these hydrogels are not suitable for long term cell studies *in vitro* (Hunt and Grover, 2010). Hydrogels based on collagen, are reported to be limited within the range of gel stiffness. A range of only 1 to 100 Pa shear modulus G', makes it less attractive for research questions, such as bone engineering where a higher shear modulus is needed (Velegol and Lanni, 2001).

Extracell4, an already developed HA based hydrogel system, is a chemically cross-linked hydrogel. It is based on thiol-modified HA and thiol-modified gelatin, which are cross-linked by poly(ethylene glycol) diacrylate (Zheng *et al.*, 2003). Main drawback of this system is the possible leakage of unreacted cytotoxic acrylates or their release upon hydrogel degradation. Another developed hydrogel based on HA is, Corgel BioHydrogel[5]. It is formed by the conjugation of tyramine to the carboxyl groups of HA and subsequent cross-linking catalyzed by hydrogen peroxide (Loebel *et al.*, 2015). As it has been shown that hydrogen peroxide is cytotoxic, the usage of this hydrogel as a biomaterial is limited and thus experiments requiring e.g. cell encapsulation are not possible (Symons *et al.*, 2001). Another HA-based hydrogel is manufactured by combining HA with a polycation. For this, chitosan, which occurs naturally as a poylcation, is combined with HA and chitosan-HA fibers are formed via self-assembling. However, this formulation based only on electrostatic interaction between the positively charged chitosan and negatively charged HA has the disadvantage of thermal instability (Maitra and Shukla, 2014). The aim of this thesis was to tackle these challenges. For this, a novel hybrid double cross-linked hydrogel system, which is biodegradable and tunable in stiffness has been established. This hydrogel system is based only on HA building blocks and is therefore biocompatible and thus highly suited to study HA-induced cell behavior and holds the capacity to be applied in a wide range of biomedical applications.

.

[4] Glykosan BioSystems, Inc., Salt Lake City, UT

[5] Lifecore Biomedical, Chaska, MN

2 Materials and Methods

2.1 Synthesis of Hydrogel Compounds

2.1.1 Synthesis of HA-DTPH

Material

Material	Company	Cat.- No.
Sodium hyaluronate (HA_m) (LOT: 025828)	Lifecore-Biomedical, Chaska, USA	-
DTPH	Self-made 2.1.2	-
1-Ethyl-3-(3-dimethylaminopropyl)-carbodiimidhydrochloride (EDC*HCl)	Merck, Darmstadt, Germany	E7750
Sodium hydroxide (NaOH)	Merck, Darmstadt, Germany	S8045
Dithiotreithol (DTT)	Merck, Darmstadt, Germany	D0632
Hydrochloric acid (HCl)	Merck, Darmstadt, Germany	H1758
Dialysis tubing	VWR, Pennsylvania, USA	25218-016

Procedure

For the functionalization procedure 500 mg of sodium hyaluronate (HA) (1.20 mmol of disaccharide repeating units) are dissolved in 50 mL MilliQ water. 285.6 mg of synthesized DTPH (1.20 mmol) are added and the pH is adjusted to 4.75 with 1 M HCl. 285.6 mg EDCl (1.20 mmol) are added to the reaction mixture, to activate the carboxylic group on the HA. The solution is then stirred for a definite time to yield various thiolation degrees. By adding 1M NaOH the reaction is stopped and the pH is adjusted to 8.5. 1.85 g DTT (12 mmol) is added and the reaction mixture is stirred for another 5h under pH monitoring at 8.5. After 5 h stirring 1M HCl is added to prevent the formation of dithiol bonds. The reaction mixture is dialyzed against 0.1 M HCl at pH 3.5 overnight and against. MilliQ water pH 3.5 while exchanging the dialysis solution every 2h, until no free thiols of unreacted DTP or DTT could be detected in the dialysis water anymore. The thiolated HA is purified through freeze drying for 2 d (Shu *et al.*, 2002).

2.1.2 Synthesis of HD-HPH

Material

Material	Company	Cat.- No.
Sodium hyaluronate (HAm) (LOT: 025828)	Lifecore-Biomedical, Chaska, USA	-
3-hydroxypropanehydrazide (HPH)	AKos, Steinen, Germany	-
1-Ethyl-3-(3-dimethylaminopropyl)-carbodiimidhydrochloride (EDC*HCl)	Merck, Darmstadt, Germany	E7750
Sodium hydroxide (NaOH)	Merck, Darmstadt, Germany	S8045
Hydrochloric acid (HCl)	Merck, Darmstadt, Germany	H1758
Dialysis tubing	VWR, Pennsylvania, USA	25218-016

Procedure

For the functionalization procedure 500 mg of sodium hyaluronate (HA) (1.20 mmol of disaccharide repeating units) are dissolved in 50 mL MilliQ water. 285.6 mg of synthesized HPH (1.20 mmol) are added and the pH is adjusted to 4.75 with 1 M HCl. 285.6 mg EDCl (1.20 mmol) are added to the reaction mixture, to activate the carboxylic group on the HA. The solution is then stirred for a 60 min. to yield 60% functionalization degree. By adding 1M NaOH the reaction is stopped and the pH is adjusted to 8.5. The reaction mixture is dialyzed against MilliQ water while exchanging the dialysis solution every 2h.

2.1.3 Synthesis of 3,3 - Dithiopropionic-Hydrazide (DTPH)

Material

Material	Company	Cat.- No.
3,3´ -dithiopropionic acid (DTPA)	Merck, Darmstadt, Germany	109010
Abs. ethanol (EtOH)	Carl-Roth, Karlsruhe, Germany	9065.1
Sulfuric acid (H_2SO_4)	Merck, Darmstadt, Germany	339741
Ethyl acetate (EtOAc)	Merck, Darmstadt, Germany	270989
Magnesium sulfate (MgSO4)	Merck, Darmstadt, Germany	M7506
hydrazine monohydrate	Merck, Darmstadt, Germany	207942

Procedure

3,3 - dithiopropionic acid (DTPA) is converted to DTPH according to the protocol described by Vercruysse et al. (1997). 10 g of DTPA (47,62 mmol) are dissolved in 100 mL abs. EtOH and 3 drops of concentrated H_2SO_4 are added to the solution. The reaction mixture is stirred under reflux for 1h and subsequently is concentrated to a volume less than 20 mL under reduced pressure. The product is extracted with EtOAc, washed with MilliQ water and dried over $MgSO_4$. The Ester is then concentrated under reduced pressure again to yield a yellow oily product, which is directly dissolved in 30 ml abs. ethanol. This solution is added dropwise to another stirring solution of 30 mL hydrazine-monohydrate in 10 mL abs. Ethanol. After stirring for 2h under reflux the reaction mixture is allowed to cool down slowly (Fig. 10).

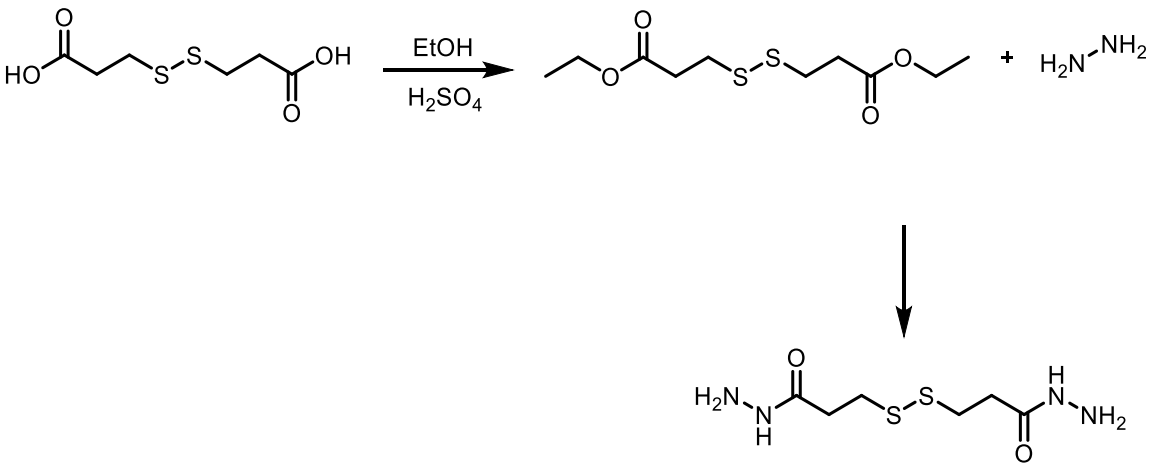

Figure 10 Synthesis of DTPH. *Thiol Linker for HA functionalization.*

2.1.4 Synthesis of Charged Disaccharide Unit of HA (dHA^+)

Material

Material	Company	Cat.- No.
Chondroitin sulfate A	Sigma-Aldrich, Deisenhofen, Germany	C9819
Amberlite®IR120 Hydrogen form	Merck, Darmstadt, Germany	06428
Sulfuric acid (H_2SO_4)	Merck, Darmstadt, Germany	339741
Abs. ethanol (EtOH)	Carl-Roth, Karlsruhe, Germany	9065.1
Bariumhydroxid octahydrat, $Ba(OH)_2$ x 8 H_2O	Carl-Roth, Karlsruhe, Germany	HN75.2
Silica gel	Carl-Roth, Karlsruhe, Germany	0712.3
Acetic acid (CH_3COOH)	Carl-Roth, Karlsruhe, Germany	7332.4
Hydrochloric acid (HCl)	Merck, Darmstadt, Germany	H1758
Ninhydrin	Sigma-Aldrich, Deisenhofen, Germany	BCBT4744

Procedure

In the first step 1 g Chondroitin Sulfate A is dissolved in 10 ml MilliQ water. Amberlite is added under pH monitoring to adjust the pH to 1,6. The mixture is filtered and washed four times with 20 ml MilliQ water. Concentrated H_2SO_4 is added to the solution to get an endconcentration of 0,5 M. The reaction mixture is stirred for 6h at 100 °C. After cooling to RT, $Ba(OH)_2$ x 8 H_2O is added under pH monitoring and vigorous stirring to adjust the pH to 3.5.

After adjusting the pH, the reaction is allowed to settle down over night. The reaction mixture is filtrated over silica gel and the yellow filtrate is concentrated under reduced pressure to approximately 10 ml and applied afterwards slowly to an amberlite column. The column is washed with 250 ml MilliQ water, AcOH/H_2O 3:1 (250 ml) and then with 1M HCl (500 ml). The Ninhydrine positive fractions are collected and are concentrated under reduced pressure to get the wanted product (Vibert, Lopin-Bon and Jacquinet, 2009). The reaction scheme can be seen in Fig. 11.

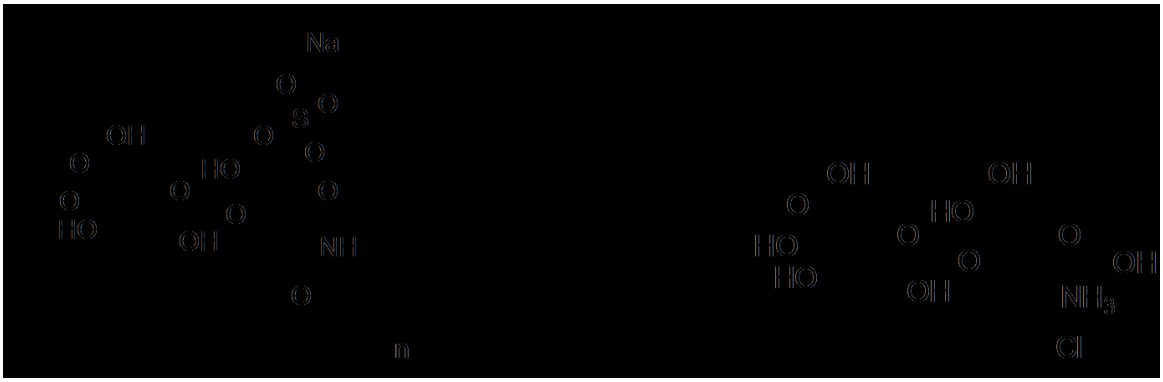

Figure 11 Synthesis of deacetylated and degraded disaccharide unit of HA (dHA^+).

2.2 Nuclear Magnetic Resonance Spectroscopy (NMR)

Material

Material	Company	Cat.- No.
HA-DTPH	Self-made (2.1.1)	-
HA-HPH	Self-made (2.1.2)	-
Charged Disaccharide Unit of HA (dHA+)	Self-made (2.1.3)	-
DTPH	Self-made (2.1.4)	-
Deuterated water (D2O)	Carl-Roth, Karlsruhe, Germany	6672.1
Deuterated chloroform (CDCl3)	Merck, Darmstadt, Germany	611778

Procedure

Samples are dissolved in deuterated solvents (D_2O or $CDCl_3$) at a concentration of 3 mg/mL and filled in an NMR tube. NMR spectra are measured by the NMR-department at the University of Heidelberg. Institute of Inorganic Chemistry. Measurements are done at room temperature with the Avance III (^1H: 600 MHz) from *Bruker*. Calibration of the spectra is carried out in relation to the residual signal of the perspective solvent used (^1H: D_2O = 4.79ppm, $CDCl_3$ = 7.26 ppm). The software MestReNova was used for analysis.

2.3 Determining the Degree of Thiolation

Material

Material	Company	Cat.- No.
HA-DTPH (74 kDa)	Self-made (2.1.1)	-
Tris(hydroxymethyl) aminomethane (TRIS)	Sigma-Aldrich, Deisenhof, Germany	T6791
5,5 - dithiobis-2-nitrobenzoic acid (DTNB)	Sigma-Aldrich, Deisenhof, Germany	D8130
Sodium-acetate (NaAc)	Sigma-Aldrich, Deisenhof, Germany	W302406
Cysteamine Hydrochloride	Sigma-Aldrich, Deisenhof, Germany	C8707

Procedure

The degree of thiolation is analyzed by an adapted Ellman´s assay. Herein, 5,5 - dithiobis-2-nitrobenzoic acid (DTNB) is converted to 2-nitro-5-thiobenzoate (TNB^{2-}), upon reaction with a thiol, see Fig. 12. The reaction is quantitative and can be detected by the yellow color of TNB^{2-}, with an absorption maximum at 412 nm.

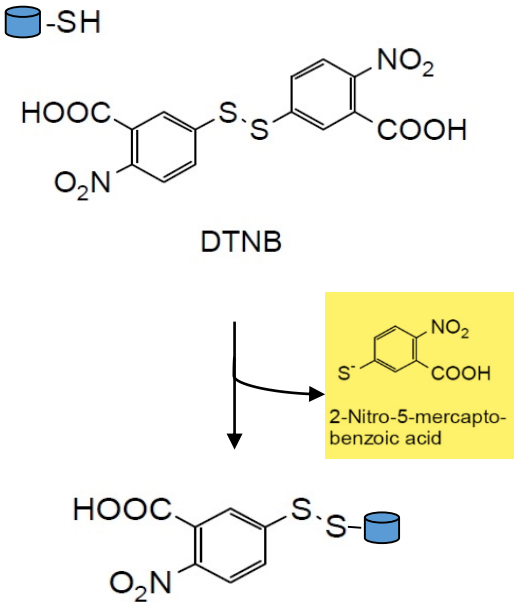

Figure 12 Mechanism of the Ellman´s assay.

For the assay, a 2 mM cysteamine hydrochloride solution in ddH_2O and a DTNB solution (50 mM NaAc and 2 mM DTNB in ddH_2O) are prepared from scratch. The HA-DTPH is dissolved in ddH_2O at a concentration of 1 mg/mL. Subsequently a concentration range is prepared in ddH_2O with 0 µM to 100 µM thiols using the 2 mM cysteamine hydrochloride solution for a calibration curve. **HA- DTPH** solutions are diluted to yield three differently concentrated samples for the measurements (0,02 mg/mL, 0,05 mg/mL and 0,08 mg/mL). To all samples and solutions for the calibration curve 100 µL 1 M TRIS, pH = 8 and 50 µL of DTNB solutions are added. All samples are thoroughly mixed and 300 µL each are pipetted in a 96 well plate, before the absorbance of each sample is measured at 420 nm (A_{420}) in a plate reader TECAN Spark (Männedorf, Switzerland). Data evaluation is preformed using GraphPad Prism7. Values for the concentration range of cysteamine hydrochloride are fitted linearly, following Eq. (1.1) (with c_{thiol} = concentration of thiols in the sample):

$$A_{420} = (a\ x\ c_{thiol}) + b \tag{1.1}$$

Since b represents the y-intercept and a the slope of the linear fit, thiol concentrations of the samples can be calculated from the measured absorbance (A_{420}) (see Eq. (1.2)) and the molecular mass of the thiol linker (M_{linker}):

$$c_{thiol} = \frac{A_{420}-b}{a}\ x\ M_{linker} \tag{1.2}$$

With the volume of the solution (V_{sample}), mass of thiol in the samples (m_{thiol}) can be calculated with Eq. (1.3):

$$m_{thiol} = c_{thiol}\ x\ V_{sample} \tag{1.3}$$

Since the mass of HA-DTPH initially weighted is known ($m_{Ham\text{-}SHn}$), the pure mass of HA in the samples can be calculated, by subtracting the thiol mass following Eq. (1.4):

$$c_{HA} = m_{HA-DTPH} - m_{thiol} \tag{1.4}$$

The molar concentration of HA (c_{HA}) in the samples (m_{HA}) can now easily by calculated, with the molecular mass of one hyaluronic acid repeating unit (M) and the volume of the samples (V_{sample}) with Eq. (1.5):

$$c_{HA} = {}^{\frac{m_{HA}}{M}}\Big/_{V_{sample}} \tag{1.5}$$

From this, the degree of thiolation can be determined as the ratio of thiol and HA concentration following Eq. (1.6):

$$degree\ of\ thiolation = {}^{c_{thiol}}\Big/_{c_{HA}}\ x\ 100 \tag{1.6}$$

2.4 Hydrogel formation

2.4.1 Synthesis of HA-DTPH-Ox. Hydrogel

Material

Material	Company	Cat.- No.
HA-DTPH (29%, 42%, 58%)	Self-made (2.1.1)	-
DPBS (- $CaCl_2$, - $MgCl_2$)	Thermo Scientific	14190250
Sodium hydroxide (NaOH)	Merck, Darmstadt, Germany	S8045

Procedure

HA-DTPH-Ox. is dissolved at 3% (w/v) in DPBS (- $CaCl_2$, - $MgCl_2$) and poured in a petri dish with 3 cm diameter. It is then incubated for 3 days under stirring at 300 rpm. After 3 days of incubation hydrogels are incubated in 0.3% H_2O_2 for 1 hours and incubated afterwards for 24 hours in MilliQ water.

2.4.2 Synthesis of HA-DTPH-Cl^+ Hydrogel

Material

Material	Company	Cat.- No.
HA-DTPH (74 kDa)	Self-made (2.1.1)	-
Charged disaccharide unit of HA (dHA^+)	Self-made (2.1.4)	-
Glucosamine hydrochloride ($GluA^+$)	Merck, Darmstadt, Germany	Y0001406
Ammonium chloride (NH_4^+)	Sigma-Aldrich, Deisenhof, Germany	A9434
Boric acid (H_3BO_3)	Sigma-Aldrich, Deisenhof, Germany	B6768
Ethanol (EtOH)	Merck, Darmstadt, Germany	1009831000
Cylindric teflon mold r = 3mm, h = 5mm	Mechanical workshop MPI for intelligent systems	-
Sonicator	Bandelin Sonorex	-
Parafilm "M"	Bemis	-

Procedure

HA-DTPH-Cl^+ are formed based on an adapted protocol of Hegger et al. (2018). For preparing hydrogels an equimolar ratio of ionic crosslinker to remaining negative groups was used. **HA- DTPH** 4% (w/v) is dissolved in borate buffer (150 mM, pH 8.5) by sonication for 15 min. Ionic crosslinker is dissolved also in borate buffer (150 mM, pH 8.5) in an equimolar ratio to negative groups on the **HA-DTPH** (table 1). The solutions of HA-DTPH and ionic crosslinker are mixed in a 3:7 ratio, yielding a final concentration of 2.8% (w/v) **HA-DTPH**. After sonication the solutions were centrifuged at 1.5 rpm for 2 min and then the ionic crosslinker solution was

added to the **HA-DTPH** solution and mixed by slowly pipetting to get a homogenous mixture. The gelation solution was poured into a cylindrical Teflon-mold and covered with a glass slide. For gelation of hydrogels with **dHA$^+$**, hydrogels are incubated over night at RT. For gelation of hydrogels with **GluA$^+$** and **NH_4^+** the pH is adjusted to 7.4 and are incubated over night at RT.

Table 1 HA (74 kDa) with three different thiolation degrees and ionic crosslinker concentration.

Thiolation degree %	remaining neg. groups on HA %	Concentration Crosslinker [g/L]	Crosslinker Equivalence to free neg. groups
58	42	35,12	0,42
42	58	44,67	0,58
29	71	58,55	0,71

2.4.3 HA-DTPH-dHA$^+$- RGD Hydrogel for Cell Adhesion Assay

Material

Material	Company	Cat.- No.
HA-DTPH (74 kDa)	Self-made (2.1.1)	-
dHA$^+$	Self-made (2.1.4)	-
Peptid GRDGSPK(Acrylamide)-amide	PSL, Heidelberg, Germany	Custom made
Boric acid (H_3BO_3)	Sigma-Aldrich, Deisenhof, Germany	B6768
Ethanol (EtOH)	Merck, Darmstadt, Germany	1009831000
Fibroblast Growth Medium (FGM2)	Promocell, Heidelberg. Germany	C-12012
Syringes Tuberkulin	Braun	15N14C8
Parafilm "M"	Bemis	-

Procedure

For preparing **HA-DTPH-dHA$^+$-RGD** hydrogels an equimolar ratio of **dHA$^+$** to remaining negative groups was used. After UV sterilization of **HA-DTPH** and the **dHA$^+$** under the hood, **HA-DTPH** 4% (w/v) is dissolved in sterile borate buffer (150 mM, pH 8.5) under sterile condition and subsequently sonicated for 15 min. **dHA$^+$** is dissolved also in sterile borate buffer (150 mM, pH 8.5) in an equimolar ratio to negative groups on the **HA-DTPH** (table 1). 5% of linear RGD to free thiol groups of **HA-DTPH** was dissolved in FGM2 and subsequently added to the **HA-DTPH** solution and incubated for 1 hour. The solutions of **HA- DTPH- RGD** and **dHA$^+$** are mixed and poured in a cut syringe. For gelation hydrogels are incubate under sterile conditions over night.

2.5 Physico-Chemical Characterization of HA Hydrogels

2.5.1 Determination of thiol groups in HA Hydrogel

To detect free thiol groups within the hydrogel an Ellman`s assay (Ellman, 1958) is used on the polymerized Hydrogel. HA Hydrogels either prepared as described above in a petri dish or in Eppendorf tubes and cut after gelation mechanically into small pieces. To these pieces 784 µL 1M TRIS buffer (pH 8) are added. After adding 784 µL DTNB solution (50 mM NaAc and 2 mM DTNB in MilliQ water) the reaction mixture is incubated at room temperature under shaking for 20 min. 100 µL of the supernatants are pipetted in a 96 well plate and absorbance is measured at 420 nm in the plate reader. As a reference, containing 100% free thiols, one gelation mixture without crosslinker is also analyzed. The ratio of free thiols in the hydrogels can then be calculated from the ratio of A_{420} of the sample and the reference, see eq.2.

$$\text{free thiols} = \frac{A_{420}\ \text{sample}}{A_{420}\ (\text{reference})}\ \text{x}\ 100\% \qquad (2)$$

2.5.2 Mechanical Properties

Rheological measurements of viscoelastic materials can be used to determine mechanical properties of 3D biomaterials, especially hydrogels which resembles the ECM *in vitro*. Rheology studies the deformation and flow of soft matter. Since soft materials show characteristics of both solids (elasticity) and fluids (viscosity), they are referred to as viscoelastic materials.

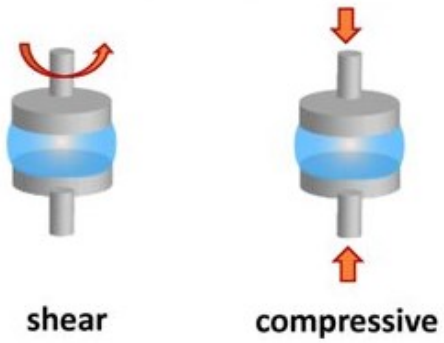

Figure 13 Schematic representation of shear and compressive force applied to a hydrogel [6]

Fig. 13 shows a schematic representation of two types of forces typically used in rheological measurements: shear forces and compression forces. Most commonly, these forces are applied uniformly to the sample and stress-strain models can be used to identify material properties. The two important parameters measured in rheology are stress σ (Eq.3) and strain λ (Eq.4). They respectively describe the forces exerted on the material and the deformation of the material due to these forces. Material properties are defined by the ratio of stress and strain.

$$\sigma = \frac{F}{A} \tag{3}$$

$$\lambda = \frac{\Delta l}{l} \tag{4}$$

[6] Cotts et al., 2016

For compression rheology, a linear correlation between stress and strain can be observed at low stresses. This is called the viscoelastic region. The ratio of stress and strain gives the materials elasticity or Young's modulus E (Eq.5, for compression rheology).

$$E = \frac{\sigma}{\lambda} \tag{5}$$

In the viscoelastic region, material deformation is reversible, meaning that the material will retain its original shape and size if stress is released. When utilizing shear forces (shear rheology), the complex shear modulus G' is obtained instead of E. While G' can be converted into E, this requires material dependent constants not readily available for novel materials.

2.5.2.1 Determination of Storage and Loss Modulus via Shear Rheology

Material

Material	Company	Cat.- No.
Kinexus pro **Shear rheometer**	Malvern	-
HA-DTPH-Cl$^+$ hydrogel solution	Self-made (2.4.2)	-

Procedure

The hydrogel formation was monitored with a rotational rheology (Kinexus pro, Malvern). Therefore, a parallel plate geometry was used with a set gap of 0.5 mm and the prepared gel mixture (80µL) was placed between these plates. An oscillation frequency of 1Hz and an amplitude of 0.2% are applied and measurements are carried out for 24h at RT. In this time the storage modulus G' and the loss modulus G'' are continuously monitored with one data point taken every 5 min.

2.5.2.2 Determination of Young´s Modulus via Compression Rheology

Material

Material	Company	Cat.- No.
NanoBionix Compression rheometer	MTS Systems	-
HA-DTPH-Ox./HA-DTPH-Cl$^+$	Self-made (2.4.1/2.4.2)	-

Procedure

Mechanical characterization of the hydrogels was carried out with a NanoBionix Universal Testing System in compression mode with a parallel plate geometry. Cylindrical hydrogels were measured utilizing a tension trigger of 200 mN at a frequency of 0.001 Hz up to a deformation of 10% while monitoring the applied strain and the resulting stress.

2.5.3 Determination of the Swelling Ratio

Material

Material	Company	Cat.- No.
HA-DTPH-Ox./HA-DTPH-Cl$^+$	Self-made (2.4.1/2.4.2)	-
pH solution 3-10 with NaOH and HCl	Self-made	-
Ionic solution 50 mM, 150 mM, 300 mM ($NaCl$, $CaCl_2$, $MgCl_2$)	Self-made	-
24-well plate	Corning, Kaiserslautern, Germany	3526

Procedure

The prepared hydrogels were used for equilibrium swelling studies. The swelling behavior of these hydrogels were investigated as functions of effect of pH, ionic strength and temperature. Swelling studies were performed in pH solutions of varying pH 3 -10, varying ionic strength solution 50 mM, 150 mM, 300 mM of NaCl, $CaCl_2$ and $MgCl_2$ and ddH_2O at RT and 37 °C. Prepared HA hydrogels were incubated on a shaker in different solutions (1 mL) see above until reaching the equilibrium in a 24-well plate. After incubation the swollen weight was measured and the hydrogel was freeze dried for 48 h. The swelling ratio was determined by weighing the swollen gel and the dried hydrogel using eq. 6.

$$Q_V = {Gel_s}/{Gel_d} \tag{6}$$

2.5.4 Acidifying Effect of HA-DTPH-dHA$^+$

Material

Material	Company	Cat.- No.
HA-DTPH-dHA$^+$	Self-made (2.4.2)	-
aqueous solution (pH = 7)	Self-made	-
24-well plate	Corning, Kaiserslautern, Germany	3526
pH electrode	Sigma-Aldrich Deisenhofen, Germany	-

Procedure

HA-DTPH-dHA$^+$ hydrogels were prepared like described in chapter 2.4.2. Each hydrogel was placed in a well of a 24 - well plate and covered with aqueous pH solution of 7. The pH was

measured at following time points 0 h, 1 h, 3 h, 6 h, 12 h, 24 h. HA hydrogels were placed after 24 h with fresh pH solution of pH of 7.

2.5.5 Osmolarity measurements of HA-DTPH-dHA$^+$/HA-DTPH-Ox.

Material

Material	Company	Cat.- No.
HA-DTPH-Ox./HA-DTPH-dHA$^+$	Self-made (2.4.1/2.4.2)	-
aqueous solution (pH = 7)	Self-made	-
24-well plate	Corning, Kaiserslautern, Germany	3526
Osmomat-030 D	Gonotec, Berlin, Germany	-

Procedure

HA-DTPH-dHA$^+$/HA-DTPH-Ox. hydrogels were prepared like described in chapter 2.4.1/2.4.2. Each hydrogel was placed in a well of a 24 - well plate and covered with pH solution of pH 7. The osmolarity was measured at following time points 0 h, 1 h, 3 h, 6 h, 12 h, 24 h. HA hydrogels were placed after 24 h with fresh pH solution of pH of 7.

2.5.6 Calculation of Mesh size

To estimate the mesh size we used the determined swelling ratio and the measured weight of the hydrogel directly after polymerization. The calculation has been done according to eq. 7 with the method established by Peppas and Merril (Peppas *et al.*, 2000)

$$\xi\ (mesh\ size) = (v_{2,s})^{-1/3} - \sqrt{\frac{2C_n M_c}{M_r}\ x\ l} \qquad (7)$$

M_c = molecular weight between two adjacent crosslinks

M_r = molecular weight of the HA repeating (disaccharide) unit = 415 g/mol

ν = specific volume of bulk HA = 0,764 cm^3/g

C_n = characteristic ratio of HA = 28

2.6 Biological Characterization of HA Hydrogels

2.6.1 Enzymatic degradation of HA-DTPH-dHA$^+$/HA-DTPH-Ox.

Material

Material	Company	Cat.- No.
HA-DTPH-Ox./HA-DTPH-Cl$^+$	Self-made (2.4.1/2.4.2)	-
Phosphate buffered saline (PBS)	Sigma-Aldrich, Deisenhofen, Germany	D8537
Hyaluronidase from bovine testes	Sigma-Aldrich, Deisenhofen, Germany	H3506
Hyaluronidase from *Streptomyces hyalurolyticus*	Sigma-Aldrich, Deisenhofen, Germany	H1136
24-well plate	Corning, Kaiserslautern, Germany	3526

Procedure

In order to gain information about the degradability of the hydrogels by different enzymes, the hydrogels are prepared as described above (see 2.4.1/2.4.2). Hydrogels are put into 24 well plate in solutions of hyaluronic acid degrading enzymes and PBS as a negative control, where the hydrogels shouldn't get degraded. All enzymes are used at a concentration of 100 U with a volume of 1 mL for each hydrogel. Hydrogels are incubated with these enzymes at 37°C and soft shaking 100 rpm, while enzyme and buffer solutions are exchanged every 48 h. For calculating the rate of degradation, the weights of the hydrogels are measured at different time points; after 1 h, 2 h, 4 h, 6 h, 9 h, 12 h, 36 h, 48 h, 72 h, 5 d and 7 d of degradation. The weight measurements at different time points are plotted against weight loss and fitted to an

exponential decay phase. From this data, the half-life ($t_{1/2}$) of each hydrogel is determined, corresponding to the time frame in which the hydrogel lost half of its initial weight.

2.6.2 Long-Term Stability of HA-DTPH-dHA$^+$

Material

Material	Company	Cat.- No.
HA-DTPH-dHA$^+$	Self-made (2.4.2)	-
Phosphate buffered saline (PBS)	Sigma-Aldrich, Deisenhofen, Germany	D8537
24-well plate	Corning, Kaiserslautern, Germany	3526

Procedure

To assess the stability of **HA-DTPH-dHA$^+$** hydrogels in the absence of HA degrading enzymes, prepared hydrogels as described above (see 2.4.2) were incubated in PBS over six months. For analyzing the stability, hydrogels were weight each week

2.7 Biocompatibility of HA Hydrogel Compounds

2.7.1 Cell culture

Material

Material	Company	Cat.- No.
Cell culture flask T25, T75		-
Fibroblast Growth medium	Promocell, Heidelberg, Germany	C-23110
Fibroblast supplement mix (Fibroblast growth factor, Insulin)	Promocell, Heidelberg, Germany	
Normal human dermal fibroblast (NHDF)	Promocell, Heidelberg, Germany	429Z015.1
Trypsin-EDTA		

Procedure

NHDF cells were maintained in culture in T75 cell culture flasks in Fibroblast Growth Medium with addition of 2% Supplement Mix, containing Basic Fibroblast Growth Factor (recombinant human) and Insulin (recombinant human) (PromoCell, Heidelberg, Germany). The NHDF cell line was obtained from juvenile foreskin. The flasks were kept in an incubator at 37 °C and 5% CO2. Cells were split upon reaching confluency. For experimental use, cells were washed twice with sterile PBS and detached by addition of 1 mL of Trypsin-EDTA (0.05%) (GIBCO, Rockville, Maryland). Cell aliquot was centrifuged for 4 min at 0.3 rcf until pellet was formed. The pellet was resuspended in fresh medium and cell concentration was determined by counting the cell number in a 1:1 mixture with Trypan Blue Solution, 0.4% (GIBCO, Rockville, Maryland) covering 4 counting squares of a Neubauer chamber. The required cell concentration was achieved through dilution of the stock solution.

2.7.2 NHDF Viability Assay under Treatment with dHA^{+}/HA-DTPH

Material

Material	Company	Cat.- No.
Normal human dermal fibroblast (NHDF)	Promocell, Heidelberg	429Z015.1
Fibroblast growth media kit	Promocell, Heidelberg	C-23110
dHA*	Self-made (2.1.4)	-
HA-DTPH$^{58\%}$	Self-made (2.1.1)	-
CellTiter 96® Aqueous One solution Cell Proliferation Assay Kit	Promega, Madison, Wisconsin USA	L3224
Phosphate buffered saline (PBS)	Sigma-Aldrich, Deisenhofen, Germany	D8537

Procedure

The viability assay was performed using the CellTiter 96® AQueous One Solution Cell Proliferation Assay kit (Promega Corporation, Madison, Wisconsin). Preliminary measurements were conducted to determine the optimal number of cells and crosslinker concentration for the experiment as well as the linear range of the assay.

Based on the acquired data, cells were seeded in 96-well plates in 50 µl/well volume for 24 h and 48 h measurement according to the following Fig. 14.

<table>
<tr><th></th><th>No treatment</th><th>0.01 [mg/mL]</th><th>0.1 [mg/mL]</th><th>1 [mg/mL]</th></tr>
<tr><td>A</td><td>10000 cells/well</td><td colspan="3" rowspan="5">1250 cells/well</td></tr>
<tr><td>B</td><td>7500 cells/well</td></tr>
<tr><td>C</td><td>5000 cells/well</td></tr>
<tr><td>D</td><td>3725 cells/well</td></tr>
<tr><td>E</td><td>2500 cells/well</td></tr>
<tr><td>F</td><td>1250 cells/well</td><td colspan="3" rowspan="3">0 cells/well</td></tr>
<tr><td>G</td><td>625 cells/well</td></tr>
<tr><td>H</td><td>0 cells/well</td></tr>
</table>

Figure 14 Seeding and treatment scheme for cell viability assay. NHDF treatment with dHA+/HA-DTPH58% for 24/48 hours.

After seeding, the plates incubated at 37 °C and 5% CO_2 overnight and are treated then with either 1.0, 0.1 or 0.01 mg/mL **dHA^{+}/HA-DTPH$^{58\%}$** dissolved in 50 µL medium for 24/48 hours. Cell viability was measured after 24/48 hours by adding of 5x CellTiter 96® AQueous solution to each well and further incubation for 3 hours at 37°C and 5% CO2 followed by absorbance measurement at wavelength 490 nm on TECAN Spark (Männedorf, Switzerland).

2.8 Cell morphology on HA hydrogel

Material

Material	Company	Cat.- No.
Normal human dermal fibroblast (NHDF)	Promocell, Heidelberg	429Z015.1
Fibroblast growth media kit	Promocell, Heidelberg	C-23110
Syringes Tuberkulin	Braun	15N14C8
Parafilm "M"	Bemis	-
HA-DTPH-dHA$^+$	Self-made (2.4.2)	-
HA-DTPH-dHA$^+$+RGD	Self-made (2.4.3)	-
Phosphate buffered saline (PBS)	Sigma-Aldrich, Deisenhofen, Germany	D8537

Procedure

All steps are carried out under the cell culture hood (HareSafe, *Thermo fisher Scientific*) in sterile conditions. Cells were washed two times with sterile PBS and subsequently treated with trypsin-EDTA solution (1 mL/25 cm^2) and incubated for 3 min at 37 °C and 5% CO_2 (HeraCell240, *Thermo Fisher scientific*). Detached cells are checked under a bright field microscope (DMi1, *Leica Germany*). 7 mL cell culture medium are added to inactivate trypsin and cell suspension is centrifuged at 0.8 rcf for 5 min to remove trypsin. The cell pellet is re-suspended in 1 mL of cell culture medium and cells were counted using a hemocytometer (Neubauer, *Blaubrand Germany*). Cells are diluted and 300 µL of cell suspension are added on top of each hydrogel, which is prepared under sterile conditions as described in 2.4.1. Hydrogels with cells on top were placed in a 24 well-plate and incubated for 24 hours at 37°C

and 5%CO_2 to allow cell adhesion on **HA- DTPH- dHA$^+$** hydrogels. Cell were imaged with a bright field microscope and, subsequently stained with DAPI and Phalloidin.

2.9 Cell Encapsulation in HA Hydrogel

Material

Material	Company	Cat.- No.
Normal human dermal fibroblast	Promocell, Heidelberg	429Z015.1
Fibroblast growth media kit	Promocell, Heidelberg	C-23110
Syringes Tuberkulin	Braun	15N14C8
Parafilm "M"	Bemis	
HA-DTPH-dHA$^+$	Self-made (2.4.2)	-
Peptid GRDGSPK(Acrylamide)-amide	PSL, Heidelberg, Germany	Custom made
Phosphate buffered saline (PBS)	Sigma-Aldrich, Deisenhofen, Germany	D8537

Procedure

After UV sterilization of **HA-DTPH$^{58\%}$** and the **dHA$^+$** under the hood, the components are dissolved in FGM2 and borate buffer, respectively. Afterwards the crosslinker solution is added to the **HA- DTPH$^{58\%}$** solution by gently pipetting and the mixture left for gelation for 60-120 minutes until the viscosity is sufficient to prevent fast-flowing/dripping of the mixture inside the tube. To gain RGD incorporated hydrogels, RGD is first incubated for 1 hours with the dissolved HA under sterile conditions. Then, the gelatinous liquid is slowly pipetted onto the previously prepared NHDF cell pellet (FGM2 supernatant was removed carefully) and the pellet is gently resuspended (using a cut 200 µl tip) to achieve cell dispersion within the entire

pre-gelled liquid. Finally, the liquid-cell mixture is pipetted into several provided containers (cut syringes/Teflon cylinders) and left for the remaining gelation reaction under the sterile hood overnight (ca. 20 h) covered with parafilm (obviously without mutagenic UV-exposure). Additionally, one control hydrogel without cell embedding is prepared. The stable cell-containing hydrogels and the control are then transferred to a 12-well plate the next day and covered with 2 ml FGM2. These hydrogels are stored in the 37 °C CO_2-incubator for further analysis.

2.9.1 Imaging with Fluorescence Microscopy

2.9.1.1 DAPI/Phalloidin Staining

Material

Material	Company	Cat.-No.
Cell on HA-DTPH-dHA$^+$/HA-DTPH-dHA$^+$+RGD	Self-made (2.4.2/2.4.3/2.8)	-
Cell in HA-DTPH-dHA$^+$+RGD	Self-made (2.9)	-
Phalloidin FITC	Sigma-Aldrich, Deisenhofen, Germany	P1951
DAPI	Sigma-Aldrich, Deisenhofen, Germany	D9542
Paraformaldehyd (PFA)	Sigma-Aldrich, Deisenhofen, Germany	158127
Trtion™ X-100	Sigma-Aldrich, Deisenhofen, Germany	X100
Bovine Albumin Serum (BSA)		
Phosphate buffered saline (PBS)	Sigma-Aldrich, Deisenhofen, Germany	D8537

Procedure

Hydrogels with cells on top and cells inside were first incubated with 4% PFA in PBS for 20 min. and subsequently permeabilized with 0.1% Triton X-100 in PBS for 5 min. After the permeabilization procedure samples were treated with 1% BSA in PBS for 10 min. Subsequently, samples were treated with DAPI (1:1000) and Phalloidin FITC (1:100) and imaged.

2.9.1.2 Life/Dead Staining

Material

Material	Company	Cat.-No.
Cell viability/cytotoxicity	Invitrogen, Carlsbad, Kalifornien, Vereinigte Staaten	L3224
Phosphate buffered saline (PBS)	Sigma-Aldrich, Deisenhofen, Germany	D8537

Procedure

After 24 hours incubation of cells inside the hydrogels cell culture medium is removed from the wells and hydrogels are gently washed with PBS once. 200 µL of staining solution are added on top each hydrogel and incubated for 45 min. Afterwards, staining solution was removed and hydrogels were placed on a cover slip and imaged. The staining solution contains cell-permeable dye calcein AM yielding green fluorescence (excitation maximum: 494 nm; emission maximum: 517 nm), to stain live cells and red fluorescent dye ethidium homodimer-1 (excitation maximum: 517 nm; emission maximum: 617 nm) to stain dead cells.

2.9.1.3 Imaging with Leica DMi8

Cells seeded on top of the hydrogel or encapsulated inside of the hydrogel for live cell imaging experiments imaged with a Leica DMi8 inverted fluorescent widefield microscope equipped with a X-Cite 200DC light source (200 W), a sCMOS camera (Leica DFC9000GT) using either 10x objective (HC PL FLUOTAR, NA 0.32, PH1) or 63x objective (HC PL APO CS2, NA 1.40 OIL UV). To generate composites and adjust the brightness contrast of the images “Fiji” (ImageJ 1.15h) is used.

3 Result and Discussion

Designing a 3D biomaterial, like a hydrogel has to fulfill several requirements. In the first place the used components have to be biocompatible, non-immunogenic and biodegradable. Furthermore, the hydrogel synthesis should avoid toxic coupling agents and harsh reaction conditions. Last but not least for the use as a biomaterial it is desired to have a hydrogel, which responses to environmental changes, like pH and temperature.

Due to its properties, such as biocompatibility, biodegradability and its high abundance and functionality in the human body, HA is an attractive molecule as a compound for 3D - biomaterials. Under physiological conditions, HA is a polyanion associated with extracellular cations (Na^+, Ca^{2+}, Mg^{2+}, K^+) (Mero and Campisi, 2014). A characteristic of HA is the formation of several intramolecular hydrogen bonds, which stabilize the macromolecule in aqueous solutions. These bonds are formed both within the macromolecule between the neighboring hydrocarbon residues and the neighboring polymer chains (Haxaire *et al.*, 2000). Hydrogen bonds are formed between the oxygen of the carboxyl group and the hydrogen of the acetyl amine group either directly or through an additional molecule of water that serves as a bridge. Additional hydrogen bonds are formed between the hydrogen of the hydroxyl group in the equatorial plane and the oxygen of the glycosidic bond (Chase, 1999) (Fig.15).

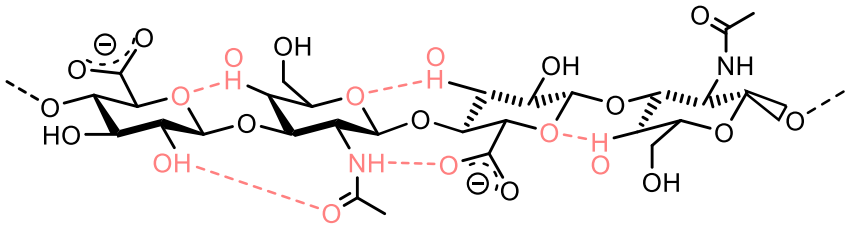

Figure 15 HA tetrasaccharide structure. *A tetrasaccharide fragment of HA comprising of two repeating disaccharides. Indicated are the five hydrogen bonds that stabilize the two-fold helix.*

Due to its conformation and molecular weight, HA can form molecular networks in solution. However, it is not able to form a structural stable gel by itself. In order to obtain such a

physically stable and mechanically robust HA-based hydrogel, a modification on the HA molecule structure needs to be inserted. Chemical modifications can be introduced at two functional sites of HA: the carboxylic acid group and the hydroxyl group. Additionally, an amino group can be recovered by deacetylation of the N-acetyl group.

3.1 Influence of Physical Cross-links on Hydrogel Formation

3.1.1 Chemical Conjugate vs. Chemical Cross-link

HA hydrogels can be formed via chemically and physically cross-linking modified in two different ways: cross-linking or conjugation (Gregoritza, Goepferich and Brandl, 2016). Both, HA conjugation and HA cross-linking are based on the same reactions. However, for HA conjugation a compound is grafted onto one HA chain by a single bond only (Vogus *et al.*, 2017), which can then form physical cross-linking via hydrogen bonds and electrostatic interactions, resulting in a physical cross-linked hydrogel. For HA cross-linking different HA chains are linked together by covalent bonds (Dicker et al., 2012) (Fig.16).

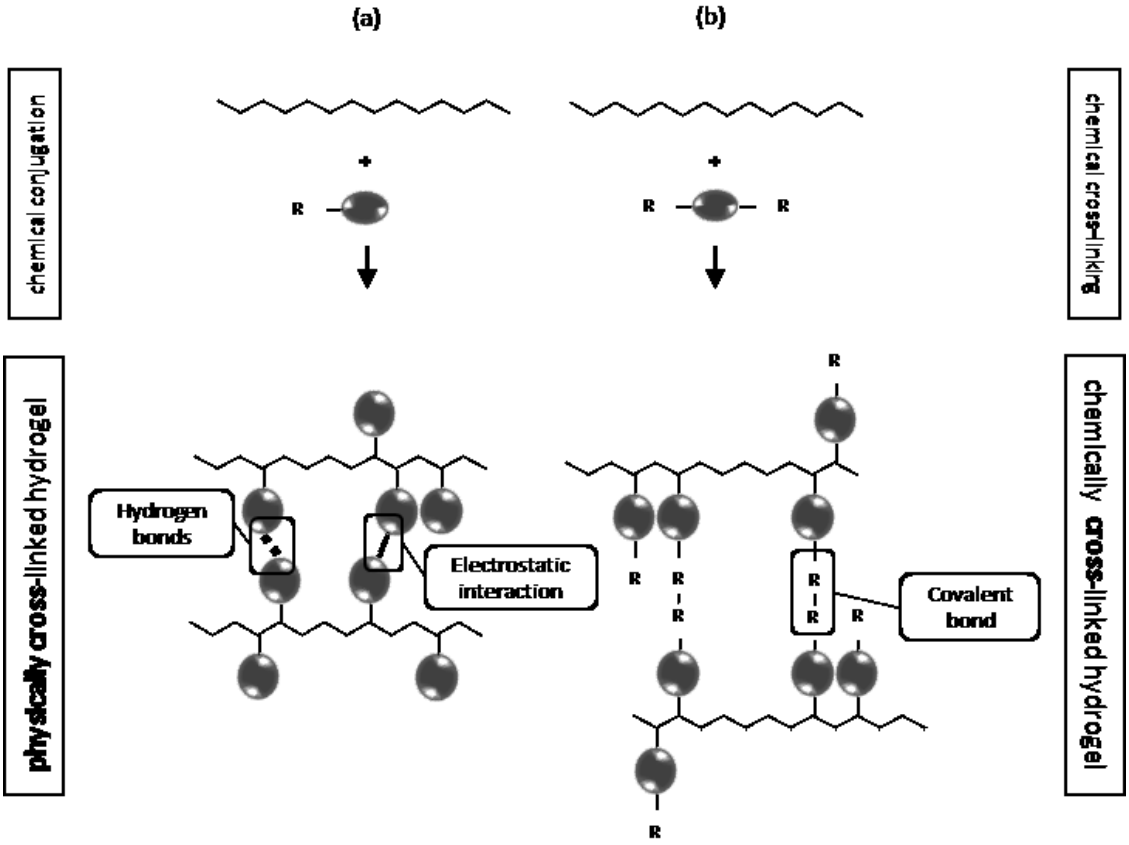

Figure 16 Scheme of physically cross-linked hydrogel (a) based on chemical conjugate and chemically cross-linked hydrogel (b) based on chemical cross-link on polymer chain adapted from Schante, Zuber, & Vandamme, (2011).

In order to develop a HA based hydrogel, which is formed under mild reaction conditions without any toxic coupling or toxic side products, I modified HA with hydrazides through carbodiimide-mediated coupling resulting in an HA-conjugate and an HA-cross-linking polymer chain. For the chemical conjugate (Fig. 17 a) I used 3-hydroxypropanehydrazide (R^1) (HPH), which is able to form hydrogen bonds but no covalent bonds with another functionalized polymer chain, resulting in **HA-HPH**. For the chemical cross-linking (Fig.17 b) I used 3,3-dithiobis (propanoic hydrazide) (R^2) (DTP) resulting in **HA-DTPH**, which is able to form disulfide bonds with another polymer chain. Successful functionalization was confirmed by NMR measurements (see Appendix 6.1.1).

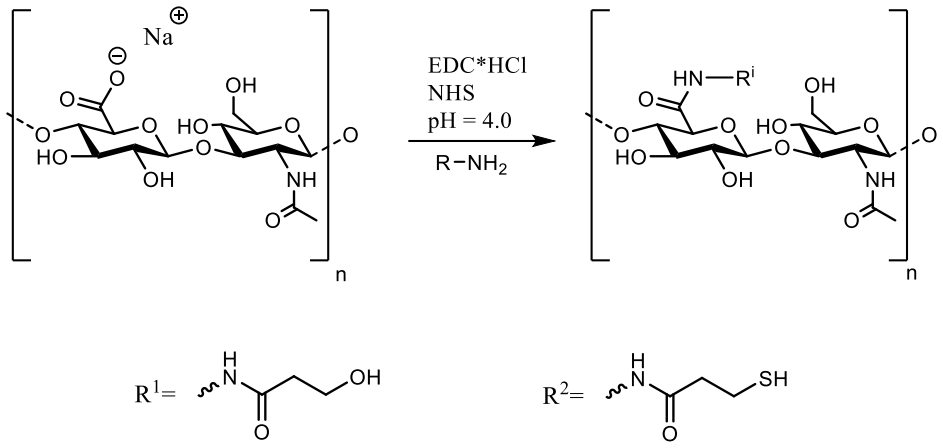

Figure 17 Functionalization of HA (74 kDa) with 3-hydroxypropanehydrazide (R1) (HPH) resulting in HA-HPH and 3,3-dithiobis (propanoic acid) (R2) (DTP) resulting in HA-DTPH. The products were purified via dialysis to yield: HA-HPH = 25.1 mg (41%) and HA-DTPH = 18.7 (35%); functionalization degree of HA = 58%.

In an attempt to examine whether functionalized **HA-DTPH** and **HA-HPH** are capable to form hydrogels, the flow inverted tube method was applied. **HA-DTPH** and **HA-HPH** showed no hydrogel formation under oxygen nor argon atmosphere at RT within a pH range from 7.5-8.5 (in PBS or 150 mM borate buffer) within 24 hours. This study has not confirmed previous research on hydrogel formation of **HA-DTPH** of Shu et al. (2002), who showed hydrogel formation after 30 min under oxygen atmosphere. One main difference is the molecular size used, which might be the cause for the different results. Whereas Shu et al. used HA of 120 kDa, 74 kDa experiments was used in the experiments reported here. Similarly, Hornof et al. (2003) showed that thiolated chitosan, with a molecular weight of 20 kDa did not form a hydrogel, but rapid gel formation was observed when the molecular weight was increased to 300 kDa.

3.1.2 Introduction of additional Physical Cross-links

3.1.2.1 Physico-Chemical Properties of dHA^+

In an attempt to increase the stability of the network and thereby to increase the viscosity of the hydrogel a synthesized positively charged molecule specifically designed for HA networks was added. The designed molecule, based on the HA structure is synthesized by deacetylation of the acetamide group and acid catalyzed degradation of HA, resulting in a positively charged disaccharide unit of HA (**dHA^+**) (Fig.18) (synthesis see 2.1.4; NMR see appendix 6.1.1). This synthesized **dHA^+** includes various advantages: (1) the maintenance of the biocompatibility, since the structure is based on HA, (2) it contains several hydroxy groups, which are able to form hydrogen bonds (Sintchak, 2000) and thus stabilizes the network and (3) it is positively charged and due to that capable to form electrostatic interactions and simultaneously form hydrogen bonds with the negatively charged groups on the polymer chain (Deng et al., 2020) resulting in a so called salt bridge (Schueler and Margalit, 1995). The advantage of such a positively charged molecule is the shielding effect of the remaining negative charge on the functionalized HA, resulting in less repulsive interaction and thus stabilizing the whole network (Noda *et al.*, 2008). The second advantage of adding such a positively charged molecule is the ability to form physical cross-links, such as hydrogen bonds and salt bridges with the polymer chain, which also leads to higher stabilization and possible hydrogel network formation (Haxaire *et al.*, 2000). Furthermore, by using a charged molecule I expect a higher response to environmental changes since charged molecules, for example, depending on the pH can associate or dissociate with hydrogen ions (O' Brien et al., 2013). Due to the negative charge on the carboxylic group the whole molecule is neutral at physiological pH. The **"+"** symbol indicates throughout the thesis the additional positive charge at the HA disaccharide unit and **"d"** will be used to refer to the disaccharide unit. The acid catalyzed degradation and deacetylation was performed based on Vibert et al. (2009).

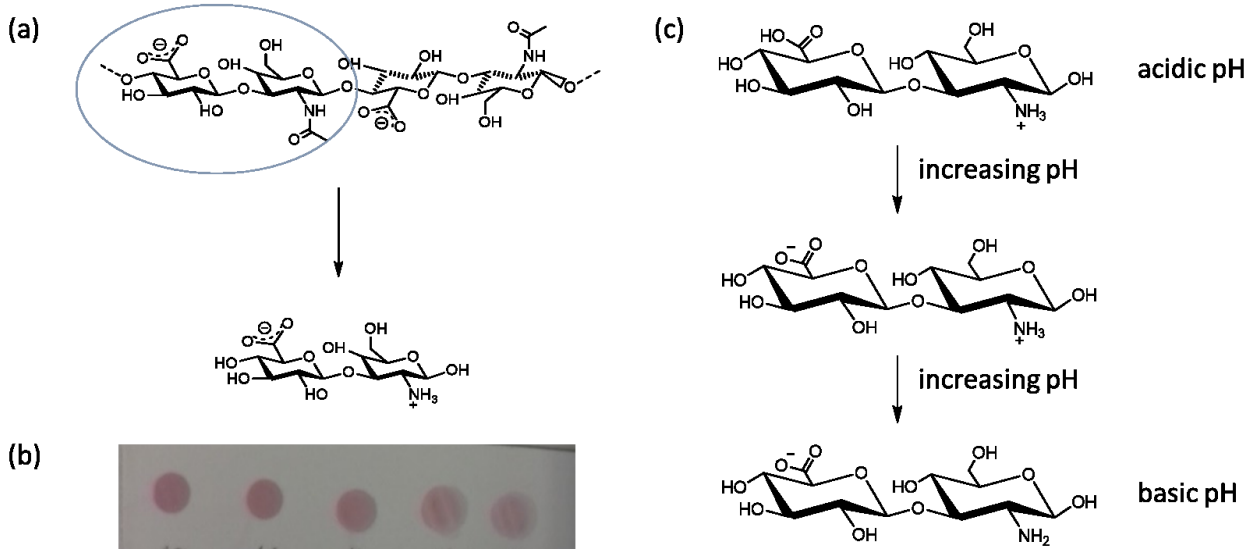

Figure 18 Structure of positively charged disaccharide unit of HA (dHA⁺). *The ionic cross-linker structure is based on the disaccharide unit of HA and is synthesized according to Vibert et al. (2009) and was in this process deacetlyated to generate a positively charged molecule (a) (see NMR Appendix). The positively charged amine groups were detected with a ninhydrin solution, and resulted in a pink color (b), charges of dHA⁺ at varying acidic, neutral and basic pH c)*

3.1.2.2 Impact of dHA⁺ on Hydrogel Formation

In order to investigate the possible interaction of **dHA⁺** with the polymer chain, **dHA⁺** was added in a ratio of 1.0 to free remaining negatively charged groups on the functionalized HA of **HA-HPH** and **HA-DTPH**. Functionalization degree was determined beforehand by using Ellman's assay for **HA-DTPH** to determine the amount of thiol groups on the polymer chain. The functionalization degree for **HA-HPH** was estimated to be the same as for **HA-DTPH** due to the same reaction conditions and reaction time. To test for potential gel formation a flow test utilizing an inverted tube test method was used (Fig.19).

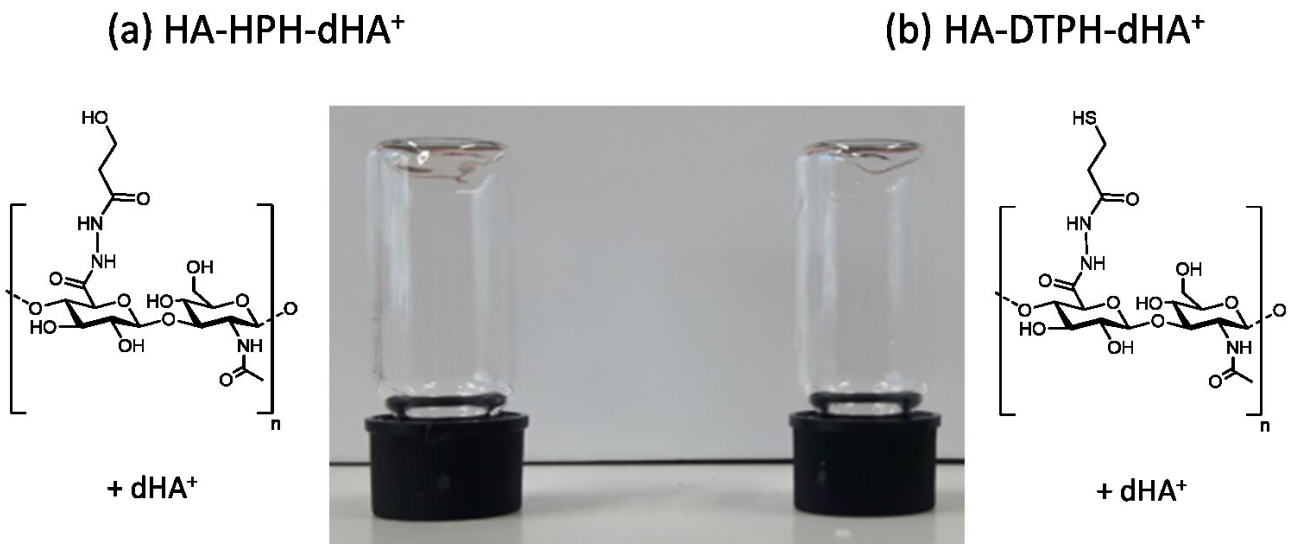

Figure 19 Inverted tube test method for HA-HPH-dHA⁺ (a) and HA-DTPH-dHA⁺ (b). *HA-HPH-dHA⁺ and HA- DTPH- dHA⁺ showed a solution (flow) – gel (no flow) transition after 24 hours of incubation under argon atmosphere at RT after 24 hours of incubation.*

For both, **HA-HPH-dHA⁺** and **HA-DPTH-dHA⁺**, I observed a solution (flow)- gel (no flow) transition at RT after 24 hours (Fig.19). This result supports the idea of increasing network stability, resulting in an increase in viscosity, due to the formation of physical cross-links induced by **dHA⁺**.

To resolve the gel formation over time of **HA-HPH-dHA⁺** and **HA-DTPH-dHA⁺**, I used shear rheology. This method was chosen because it provides information about the cross-linking density within the network, by measuring the storage modulus G' and loss modulus G'' (Franck et al., 2012). G' represents the stored deformation energy and due to this the elastic portion (solid state behavior) of the viscoelastic behavior of the hydrogel sample during a shear process. G'' is characterized by the dissipated energy and represents the viscous portion of the viscoelastic behavior (Yan et al., 2011) (Metzger et.,2017). During the evolution of G' and G'', G' and G'' cross each other, which is defined as the "gel-point". However, Winter et al. (1987) proclaimed that the crossover of G' and G'' depending on the used polymer might not be the exact "gel point" but still in vicinity. After the crossover G' exceeding G'' results in a more elastic like behavior. G' > G'' occurs due to the formation of cross-links within the

hydrogel network. Therefore, monitoring the temporal progress of G' and G'' a gelation process might be observed (Fig.20).

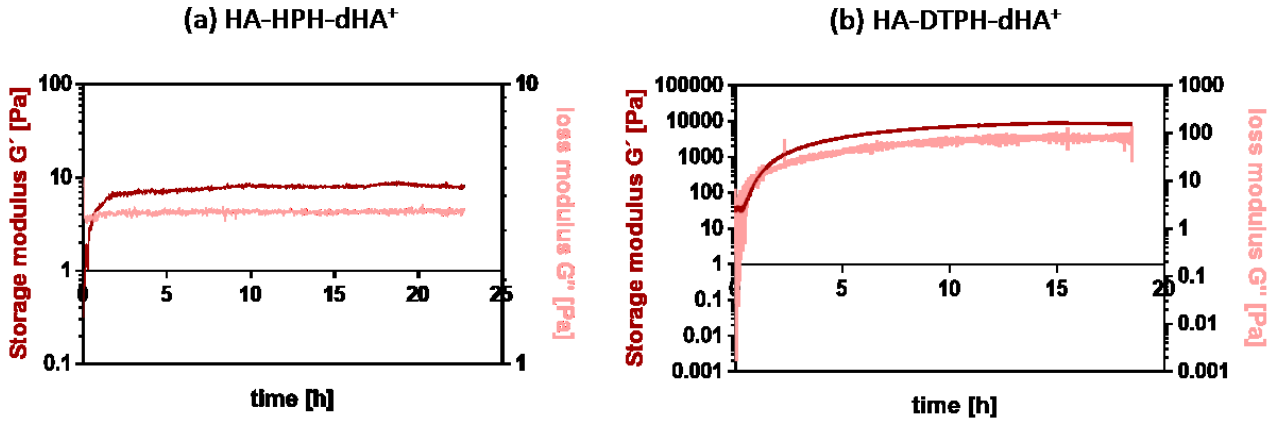

Figure 20 Progression of storage modulus G' and loss modulus G'' of HA-HPH-dHA⁺ (a) and HA-DTPH-dHA⁺ (b). *Data are measured over the course of 24 h with a solvent trap to prevent drying of the formed HA-HPH-dHA⁺ and HA- DTPH-dHA⁺ hydrogels. Both HA functionalities showed an increase of the storage modulus G' and loss modulus G'', reaching a plateau beyond the crossover point of G' and G''. G' and G'' are plotted in log10 scale.*

These measurements showed an increase in storage modulus G' and loss modulus G'' for both functionalized polymer samples, **HA-HPH-dHA⁺** and **HA-DTPH-dHA⁺**. Starting the reaction, the storage modulus G' exceeded the loss modulus G'' after a certain time. The measured G' at the plateau for **HA-HPH-dHA⁺** is 8 Pa and for **HA-DTPH-dHA⁺** it is 9 kPa. The measured "gel- point" for **HA-HPH-dHA⁺** is 1.2 h and for **HA-DTPH-dHA⁺** 0.6 h. As mentioned above G' > G'' indicates a more elastic behavior of the hydrogel sample and an increase in cross-links within the network. This cross-links as suggested before might be the formation of hydrogen bonds and salt bridges. Noda et al. (2008) reported an increase of the elastic modulus of HA after adding sucrose. Sucrose, which is also a saccharide, has the ability to form hydrogen bonds but in comparison to **dHA⁺**, it does not have a charged amine group. Noda et al. claims that sucrose increases the statistical interaction between hyaluronan macromolecules, which leads to a more rigid HA (Noda *et al.*, 2008). This finding concurs well with the results I have gained. However, this might be valid for both hydrogel samples but nevertheless the measurements revealed a higher G' for **HA- DTPH- dHA⁺**. This can be explained by different

origins of network formation. **HA-HPH** is a chemical conjugate which, only forms hydrogen bonds with another polymer. Only upon the addition of the ionic cross-linker **dHA$^+$** additional formation of physical cross-links was induced. Thus, increasing storage modulus is mainly based on physical cross-links. As for **HA-DTPH-dHA$^+$**, **HA-DTPH** is a chemical cross-link with the ability to form covalent cross-links, mainly disulfide bonds, via the oxidation of thiol groups. Therefore, possible formed disulfide bonds could be the cause of the difference of the storage modulus G' between **HA-HPH-dHA$^+$** and **HA-DTPH-dHA$^+$**. Moreover, the "gel-point" of **HA- HPH- dHA$^+$** is lower than **HA-DTPH-dHA$^+$**, which also supports the idea, that **HA- HPH- dHA$^+$** hydrogel formation is just based on physical cross-links, which cross-links the functionalized polymer chains faster than the formation of a possible chemical cross-link, in case of **HA- DTPH- dHA$^+$** hydrogel formation.

In an attempt, to investigate now the structural stability, caused by the physical cross-links, of **HA-HPH-dHA$^+$** and **HA-DTPH-dHA$^+$** hydrogels over time, gels were prepared as described in defined teflon molds (r = 3 mm, h = 3 mm) (Fig. 21 a) (see 2.1.1) and incubated in an oxygen-free atmosphere for 24 hours.

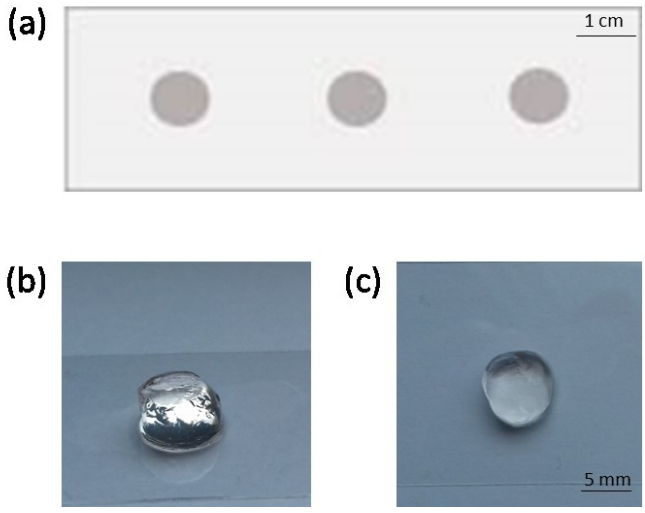

Figure 21 HA-DTPH-dHA$^+$ hydrogel. After incubation of HA-DTPH-dHA$^+$ solution in defined teflon molds (a) for 24 hours a structurally stable hydrogel was obtained. Side view (b); top view (c); diameter of the hydrogels is ~ 7 mm to 9 mm.

After 24 hours the **HA-HPH-dHA$^+$** solution was highly viscous without being able to maintain its structural integrity. Contrary to that, **HA-DTPH-dHA$^+$** gels maintained their structural stability character (Fig.21 b- c). All together, the findings of this experiments indicates that **HA-HPH**, as a chemical conjugate, showed with **dHA$^+$** an increase in G', due to the formed physical cross-links, but was not able to maintain the structure, supposedly because of its disability to form covalent bonds. Adding **dHA$^+$** to **HA-DTPH** lead to a higher G' compared to **HA-HPH-dHA$^+$** and afterwards this was supported by the formation of a structurally stable hydrogel. I have to highlight that the difference of **HA-HPH** and **HA-DTPH** is the capability of **HA-DTPH** to form disulfide bonds via thiol groups, which might be the reason for the higher G' and stable network structure. The most striking result to emerge from this experiments is that **HA-DTPH** is incapable to form hydrogels without **dHA$^+$** and adding **dHA$^+$** lead to a stiffer structurally stable hydrogel, supporting the idea that physical cross-link has an influence on hydrogel formation. In his analysis of the influence of especially hydrogen bonds Ballard et al., (2019) showed that the formation of honeycomb microstructure formed and given stability by hydrogen bonds. So further experimental investigations are needed to estimate the influence of the physical cross-link on the hydrogel formation and the physical properties, like mechanical stiffness, and possible participation of disulfide bonds in the hydrogel formation process.

3.2 Impact of Physical and Chemical Cross-links on Hydrogel Formation

Next I investigated the mechanisms underlying the gel formation: physical cross-link via hydrogen bond and salt bridge formation, and chemical cross-link via disulfide bond formation. To study the influence of the physical cross-link, I used two different ionic cross-linker, additionally to **dHA$^+$**, varying the capability of hydrogen bond formation. To examine the chemical cross-link, I varied the functionalization degree of the polymer chain.

3.2.1 Introduction of $GluA^+$ and NH_4^+

To vary the hydrogen bond formation ability of the ionic cross-linker, I used glucosamine hydrochloride (**$GluA^+$**), which is a positive charged ionic cross-linker like **dHA^+**. Though **$GluA^+$** is only one building block of the disaccharide unit of HA it forms less hydrogen bonds than **dHA^+**. Ammonium chloride (**NH_4^+**), is also positively charged and can form in total only four hydrogen bonds. As they all contain a positively charged amine group they are able to form salt bridges, leading to stabilizing effect on the network (Fig.22).

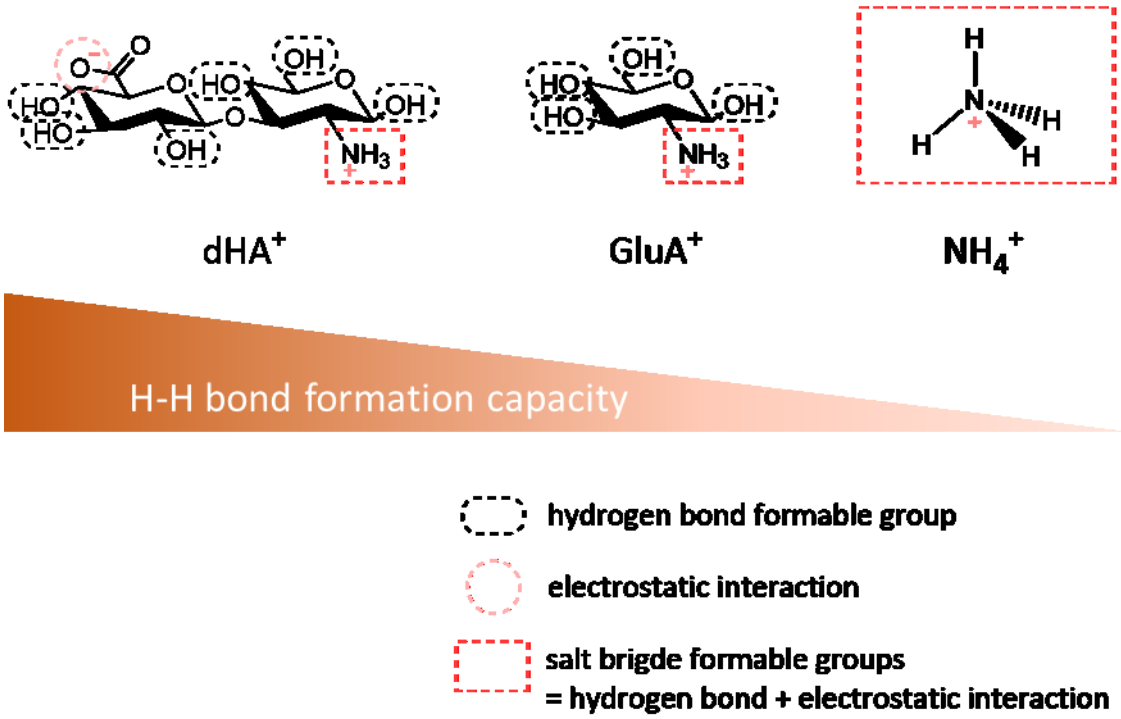

Figure 22 Scheme of the used ionic cross-linkers. *dHA^+ (disaccharide unit of HA), $GluA^+$ (positively charged glucosamine) and NH_4^+ (ammonium chloride). The capability to form hydrogen bonds is decreasing from dHA^+ to $GluA^+$ to NH_4^+. All of them can form salt bridges. Additionally, dHA+ is negatively charged on the carboxyl group of the glucuronic acid moiety.*

3.2.2 Impact of $GluA^+$ and NH_4^+ on Hydrogel formation

In order to test the ability of the ionic cross-linker **$GluA^+$** and **NH_4^+** to enhance the possible hydrogel formation based on **HA-DTPH** an inverted tube assay was performed. Therefore, **$GluA^+$** and **NH_4^+** were added to a **HA-DTPH** solution.

The solution (flow) - gel (no flow) transition was tested after 24 hours under argon atmosphere at RT (Fig.23).

Figure 23 Inverted tube assay for HA-DTPH-$GluA^+$ (a) and HA-DTPH-NH_4^+ (b). *Both hydrogels, showed a solution (flow) – gel (no flow) transition under argon atmosphere at RT after 24 hours of incubation.*

Addition of **$GluA^+$** and **NH_4^+** to the **HA-DTPH** solution with subsequent incubation under argon atmosphere induces an observable solution (flow)- gel (no flow) transition and thus gel formation after 24 hours at RT (Fig.23). These transition confirms the idea that adding an ionic cross-linker, which is capable to form physical cross-links enhances the hydrogel formation. Regarding, these results it has to be highlighted that **NH_4^+**, which has the lowest capability to form hydrogen bonds already has an enhancing effect on the hydrogel formation.

3.2.3 Varying the Chemical Cross-link

The number of possible chemical cross-links was modified by varying the degree of functionalization on the carboxyl groups of the glucuronic acid moiety of HA. The degree of functionalization was determined by the free thiol groups using the Elman´s assay (see in 2.5.1).

Table 2 Different degrees of thiolation for 74 kDa HA were achieved with longer reaction times. This table summarizes the different reaction times, in conjugation with the resulting degrees of thiolation for 74 kDa. HA-DTPH with a thiolation degree of 29 ± 4%, 42 ± 2 and 58 ± 5% were used.

Molar ratio of HA : DTP : EDCl	**HA batch (*Lifecore-Biomdical*)**	**Reaction time**	**Degree of thiolation HA-DTPH^{x}**
1:1:1	024367	20 min	29 ± 4%
1:1:1	024367	40 min	42 ± 2%
1:1:1	024367	60 min	58 ± 5%

Different degrees in thiolation of HA using DTPH were achieved by increasing the reaction time (Tab.2). Throughout this thesis the functionalization degree of the used **HA-DTPH** will be indicated by the superscript number **"x"** in **HA-DTPH^{x}**. Varying the amount of free thiols by different functionalization degrees, provides the possibility of a changing amount of formed disulfide bonds. Breakspear et al. (2019) reported already the influence of the amount of free thiol groups on the formation of possible disulfide bonds by establishing a keratin based hydrogel based on the amount of formed disulfide bonds. He concludes that increasing disulfide bonds leads further to a higher mechanical strength, which I will examine in the further experiments.

3.2.4 Taking a Closer Look on the Hydrogel Formation

3.2.4.1 Progress of Hydrogel Formation Depending on Physical and Chemical Crosslinks

To further investigate the hydrogel formation in dependency of physical cross-links, based on the used ionic cross-linker, and chemical cross-links, based on the functionalization degree of **HA- DTPH**, the progression of G' and G'' was monitored as described in 2.5.2.1 (Fig. 24).

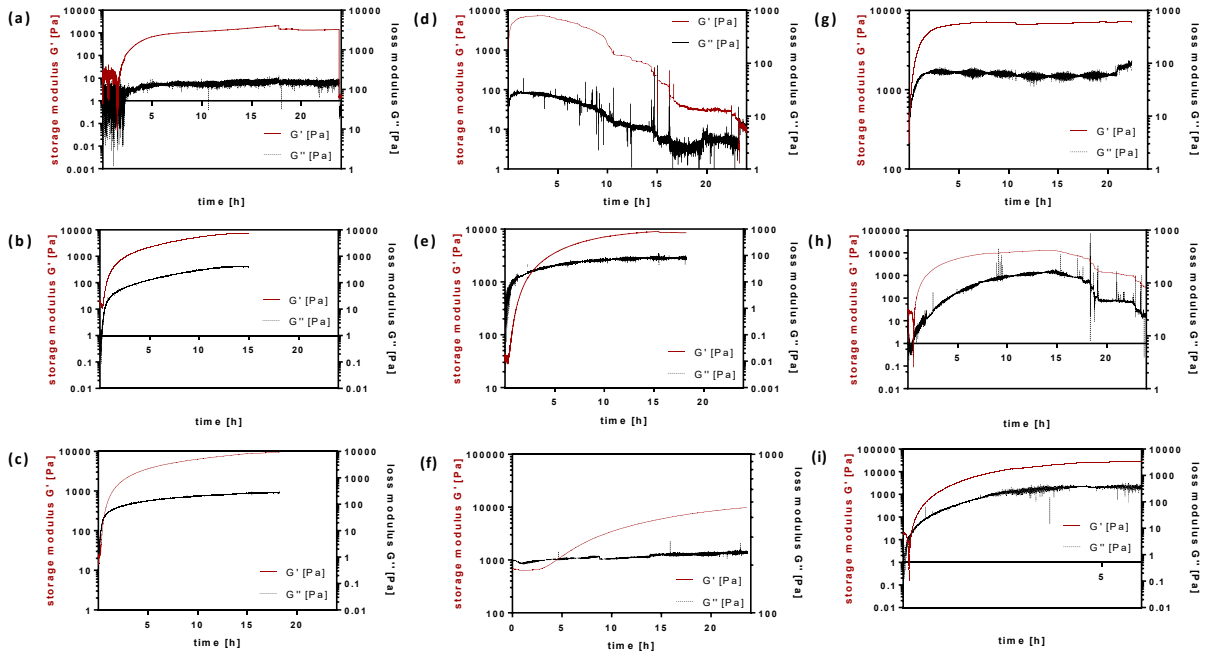

Figure 24 Progression of storage modulus G' and loss modulus G'' during gelation of HA-DTPH$^{29\%}$-NH_4^+ (a), -$GluA^+$ (b),- dHA^+ (c); HA-DTPH$^{42\%}$-NH_4^+ (d), -$GluA^+$ (e),- dHA^+ (f); HA-DTPH$^{58\%}$-NH_4^+ (g), -$GluA^+$ (h),- dHA^+ (i). *Ionic cross-linker ratio of 1.0 to remaining free negative charged groups on HA-DTPH.G' and G'' are plotted in log10 scale.*

A typically progress could be observed for most of the hydrogel conditions (Fig.24). Initially G'' is higher than G'. In the course of the polymerization process, G' is exceeding G'' and finally reaching a plateau. In the beginning, higher G'' means that the sample behaves as a viscous-liquid system first. When the sample starts to gel, G' grows faster as the cross linking reaction starts. When G' is equal to G'' the "gel point" is reached and with further cross-linking within the hydrogel G' exceeds G''. The time, when both curves are flattening indicates the end of

the cross-linking reaction (Fig.24). However, this method has some unexpected limitations. (1) Few hydrogel conditions (Fig.24 a, b, d, g) showed at the beginning of the gel formation progress G' > G'' with a missing crossover of G' and G'', is caused likely, because hydrogel formation occurred while loading the sample. (2) Due to the experimental setup the formed hydrogels dried out, which is indicated by the decrease of G' and G'' after reaching the plateau (Fig. 24 d, h). To prevent the evaporation of the solvent, measurements were stopped directly after G' reached the plateau (Fig. 24 b-c, e-f, i). Despite the limitations of this method, and consequently the results, however suggests a successful gelation process. To gain a better overview and for comparison purposes the "gel-point" and the storage modulus G' of the plateau, for each hydrogel condition respectively, "gel-point" and storage modulus G' values are extracted out of the curves (Fig.24) and listed in Tab.3.

Table 3 Determination of the gelation time t "gel point" and storage modulus G' at the plateau in dependency of the thiolation degree and applied ionic cross-linker. Gelation time defined as t at the time point, when the storage modulus G' is equal to the loss modulus G'''. This indicates the start of cross-link formation and gelation of the solution. Each data point was measured after 5 min, for some hydrogels cross-over time point is before the first 5 min of measurements, thus visualization was not possible. The storage modulus G' measured at the plateau is increasing with the increasing capability of the used ionic cross-linker and with increasing thiolation degree.

Thiolation degree of HA-DTPH	**Used ionic cross-linker**	**t at „gel point" [min]**	**Storage modulus G' [kPa]**
29%	dHA^+	15	9.6
	$GluA^+$	> 5	7.2
	NH_4^+	> 5	1.4
42%	dHA^+	270	9.9
	$GluA^+$	168	8.5
	NH_4^+	> 5	7.3
58%	dHA^+	30	13.7
	$GluA^+$	12	12.3
	NH_4^+	> 5	7.2

From Tab. 3 it can be noted, that the "gel-point" was decreasing from **HA-DTPH-dHA$^+$** to **HA- DTPH-GluA$^+$**, and **HA-DTPH-NH$_4^+$** showed the lowest "gel-point". Further it is increasing with increasing thiolation degree, with the exception that **HA-DTPH$^{42\%}$** has a higher "gel-point" than **HA-DTPH$^{58\%}$**. As for the storage modulus, it was increasing from **HA-DTPH-NH$_4^+$** to **HA-DTPH-GluA$^+$** and **HA- DTPH-dHA$^+$** showed the highest storage modulus. The same trend was observed with increasing thiolation degree. This is consistent with the idea that the possible formation of disulfide bonds influences directly the hydrogel formation (Cao *et al.*, 2019).
The differences of the occurring "gel-point" in dependency of the used ionic cross-linker could be caused by the molecule size of the ionic cross-linker. Since, the so called "gel-point" is referred to the critical point where the gel first appears (Krog and Version, 2010), it is based on the first interaction of the ionic cross-linker and **HA-DTPH**. Considering the size of the ionic cross-linker **NH$_4^+$**, as the smallest ionic cross-linker, the diffusion within the polymer chain is favored and results in a faster first interaction (Sandrin et al., 2016). Additionally, the thiolation degree has also an influence on the "gel-point". This could occur, because of the decreasing entanglement of the polymer chain with increasing thiolation degree (Bi *et al.*, 2010) (Phys and Grest, 2016). Increasing functionalization of the negative charged carboxyl group leads to a decrease in repulsion of the polymer chains with each other or also within one polymer chain, which could result in an increase in entanglement (Tanaka, Adachi and Chujo, 2010). However, these results thus need to be interpreted with caution, due to the limitations of the experimental set up. Still, the increasing storage modulus G' with increasing thiolation degree leads to the assumption that the thiol groups may play a key role in the hydrogel formation.

3.2.4.2 Disulfide Bond Formation during Hydrogel Formation

To investigate the possible participation of the thiol groups on the hydrogel formation, the amount of reacted thiols inside the hydrogels during hydrogel formation is measured with an adapted Ellman's assay as described in 2.5.1 (Fig.25). In total five hydrogel conditions were tested: (1) **HA-DTPH** without an ionic cross-linker (2) **HA-DTPH** with the three different ionic cross-linker **HA-DTPH-Cl$^+$, "Cl$^+$"** indicates here any positively charged ionic cross-linker (**NH$_4^+$,**

GluA⁺, dHA⁺) and (3) **HA- DTPH- Ox.** The last one (**HA-DTPH-Ox.**) was established by Zheng et al. (2003). It is a disulfide bond based HA hydrogel system, which refers to the oxidized form of **HA-DTPH.** It is synthesized by the incubation of **HA-DTPH** for 72 hours under oxygen atmosphere and subsequently oxidized with 0.3% hydrogen peroxide. In this thesis **HA- DTPH- Ox.** will serve as a comparable hydrogel system, which is just based on chemical cross-link, mainly disulfide bonds and helps to distinguish the influence of the physical cross-link formed by the added ionic cross-linker on the properties of the hydrogel. The abbreviation **"Ox."** indicates throughout this thesis the oxidized hydrogel form of **HA-DTPH**.

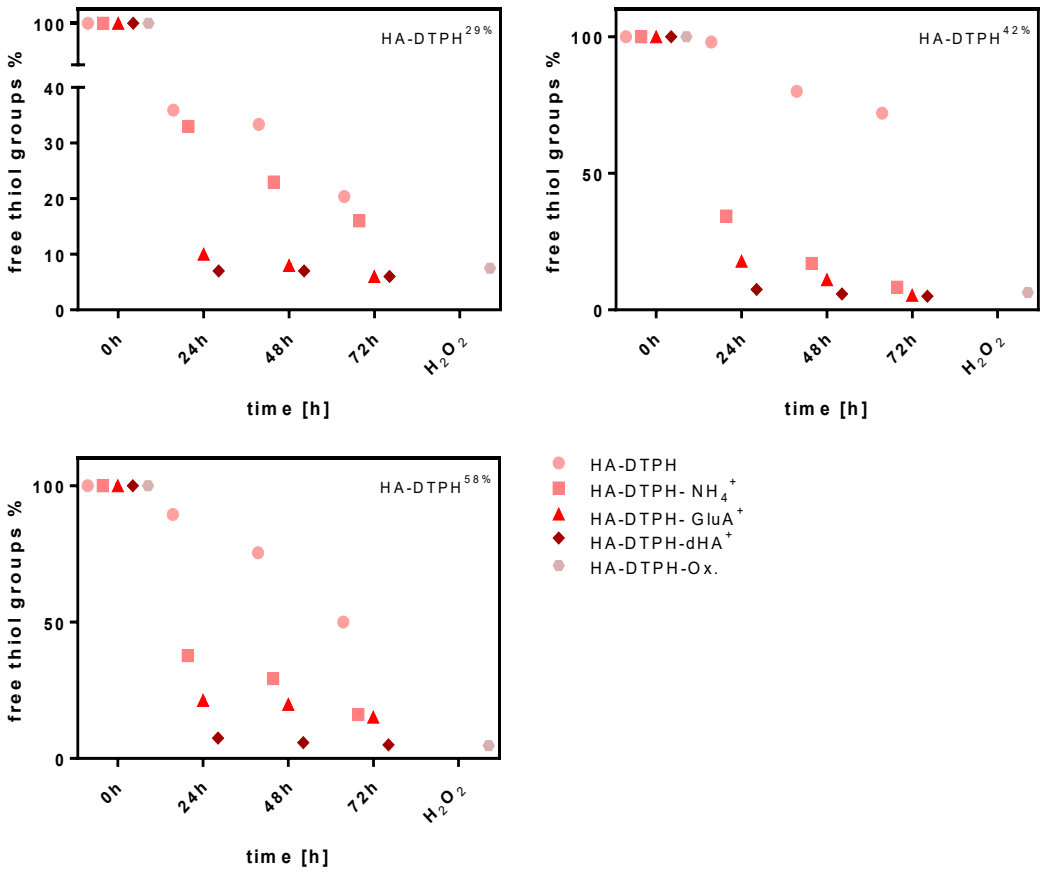

Figure 25 Detection of free thiol groups of HA-DTPH, HA-DTPH-Cl⁺ and HA-DTPH-Ox. hydrogels based on Elman's assay. Elman's were performed at defined time points after preparing the gel solution. For HA-DTPH-Cl⁺ a rapid decrease of free thiol groups occurred within 24 hours. Much slower decrease of free thiol groups were observed for HA-DTPH solutions without an ionic cross-linker. Subsequently oxidizing HA-DTPH to HA-DTPH-Ox. lead to a decrease of free thiol groups. representative values of one of three independent experiments; icon size exceeds SD; mean and standard deviation of triplicate are presented.

The Elman's assay showed a significant difference between the amount of free thiol groups of **HA- DTPH-Cl$^+$** and **HA-DTPH** hydrogels. Interestingly a rapid decrease of free thiol groups is observed for **HA-DTPH-Cl$^+$** hydrogels. In comparison a much slower decrease is observed for **HA-DTPH**. For **HA-DTPH$^{29\%}$** I measured a decrease from 100% free thiol groups to 36 ± 0.08% within 24 hours, whereas for **HA-DTPH$^{29\%}$-NH$_4^+$** a decrease from 100% to 33 ± 0.03%, for **HA-DTPH$^{29\%}$-GluA$^+$** from 100% to 10%±0.02 and for **HA-DTPH$^{29\%}$-dHA$^+$** from 100% to 7 ± 0.02% was observed. The same trend is seen for **HA-DTPH$^{42\%}$** and **HA-DTPH$^{58\%}$** with and without cross-linker, respectively. The decrease of the amount of free thiol groups within 72 hours gets slower. The amount of free thiol groups of **HA-DTPH$^{29\%}$** decreases within 72 hours from 36 ± 0.08% to 20 ± 0.03%. Subsequently, incubation of **HA-DTPH$^{29\%}$** with 0.3% H_2O_2 lead to a decrease of free thiol groups from 20 ± 0.03% to 7.5 ±0.08 %.

The most striking result to emerge from the data is that the free thiol groups reacted rapidly to disulfide bonds upon addition of the ionic cross-linker after 24 hours. Considering the hypothesis that the used ionic cross-linker stabilizes and tightens the hydrogel network, due to the formation of hydrogen bonds and salt bridges, the results are on the same page, resulting in an enhancement of the covalent network formation, mainly the disulfide bond formation. The ionic cross-linker **dHA$^+$** forms the highest amount of hydrogen bonds within the tested cross-linker and therefore has the capability to stabilize the system the most and thus brings the thiol groups in a close proximity, to enable their reaction with each other (Hobert *et al.*, 2014). The less formed disulfide bonds upon using **GluA$^+$** and **NH$_4^+$**, is consistent with idea that with decreasing capability to form hydrogen bonds the stabilizing and tightening effect is decreasing and free thiol groups are in less proximity to react with each other (Rajpal et al., 2013). Additionally, to the effect of the formed hydrogen bonds and salt bridges, some examples in the literature revealed that the pK_a of thiols can be shifted, induced by electrostatic interaction with neighboring ionizable groups and polar residues or both. Resulting in the ease of oxidation of the free thiol groups to the corresponding disulfide (Kuo, Swann and Prestwich, 1991). Considering the results of **HA-DTPH-NH$_4^+$** and **HA-DTPH** after 72 hours has further strengthened the idea of the stabilizing effect of physical cross-links. **HA-DTPH** is not able to maintain its structural integrity, although the amount of free thiol group

of **HA-DTPH-NH_4^+** and **HA-DTPH** is almost the same, only upon incubation with H_2O_2 the amount of free thiol groups is reduced. Incubation with 0.3% H_2O_2 led as reported by Weinfurtner et al. (2018) to the oxidation of free thiol groups and results in the formation of disulfide bonds. But it should be noted that oxidizing of **HA-DTPH** is not feasible before 72 hours, implicating that a certain amount of free thiol groups has to be formed to withstand the diffusion of H_2O_2. This is in good agreement with the work of Rehor et al. (2008), who measured, after exposing cysteine thiols to air for 48 hours, 22% of free thiols from the initial number.

Taken together, these findings support the idea of utilizing charged positive molecules with the capability to form hydrogen bonds, such as **dHA^+**, **$GluA^+$** and **NH_4^+,** as ionic cross-linker. Two impact factors of **dHA^+**, **$GluA^+$** and **NH_4^+** has to be highlighted: (1) inducing the disulfide bond formation and (2) stabilizing and tightening the hydrogel network via formation of hydrogen bonds and salt bridges. Resulting in a hybrid double cross-linked hydrogel, **HA-DTPH-Cl^+**, consisting of chemically and physically cross-links.

A suggested possible structure of the formed **HA-DTPH-Ox.** and **HA-DTPH-Cl^+** hydrogels are shown in Fig. 26. Main advantage of the developed **HA-DTPH-Cl^+** hydrogel system is first the avoidability of a coupling toxic agent, such as H_2O_2, like it is needed for **HA-DTPH-Ox.** This makes the hydrogel system suitable for any kind of cell included study. Moreover, it consists of just one main component, namely HA, so based on the bottom-up approach of the synthetic biology it is suited to study the role of the ECM only concentrated on HA without any disturbing site effects of other proteins or components of the ECM. This is a great benefit to study cell behavior or by added factors induced cell behavior in a reduced ECM environment.

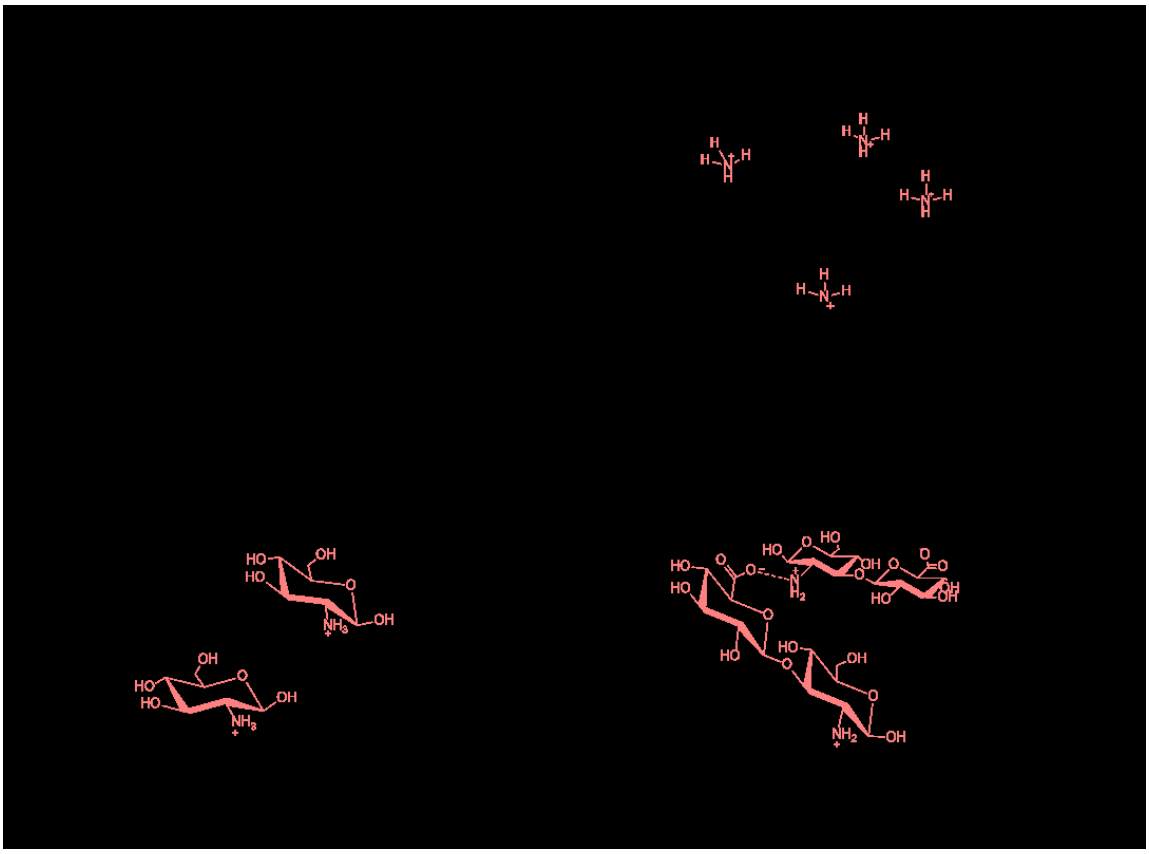

Figure 26 Suggested network formation of HA-DTPH-Ox. hydrogel and HA-DTPH-Cl⁺ hydrogels (b-d). *a Formation of HA-DTPH-Ox. hydrogels are based on disulfide formation b-d Formation of HA-DTPH-NH_4^+ (b), HA-DTPH-$GluA^+$(c) and HA-DTPH-dHA^+ hydrogels are based on additional physical cross-links like hydrogen bonds and salt bridges.*

3.3 Physical and Chemical Cross-link influence on Mechanical Stiffness

As mentioned above G' gives information about the mechanical properties and the influence of physical and chemical cross-links within the hydrogel. Moreover, it gives insight into the elastic behavior of the hydrogel system. However, by definition the storage modulus G' resembles the stored energy of an applied force but not the exact stiffness of the hydrogel.

Therefore, **HA-DTPH-Cl⁺** and **HA-DTPH-Ox.** hydrogels were prepared as described in 2.4.1/2.4.2 and the so called Young's modulus of fully in water swollen hydrogels was measured via compression in bulk rheology (Fig.27).

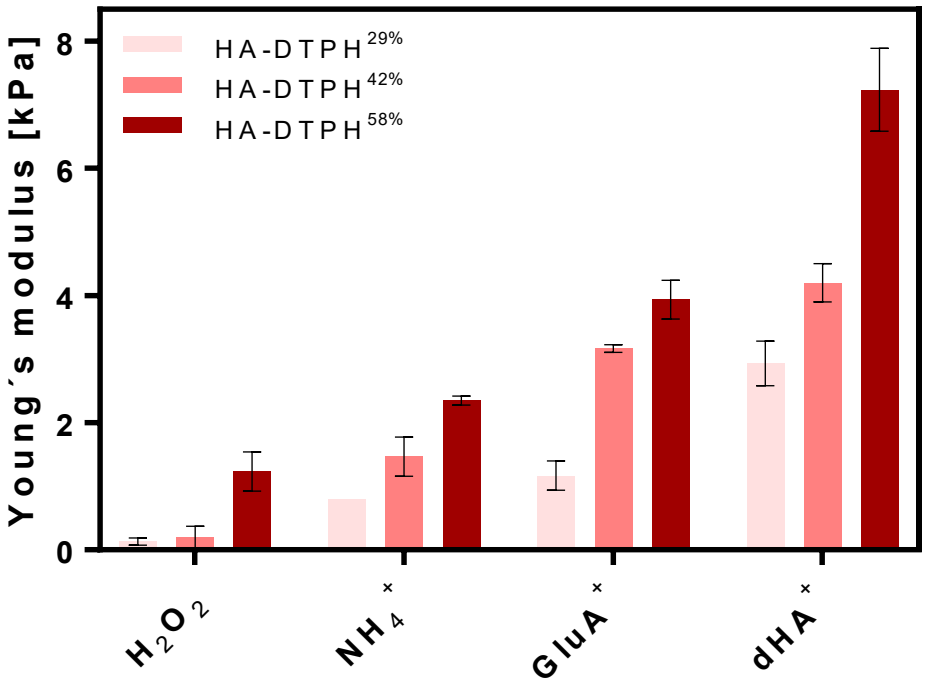

Figure 27 Young's modulus of HA-DTPH-Cl⁺ and HA-DTPH-Ox. after being swollen in water. *Young's moduli of HA- DTPH- Cl⁺ are increasing with the capacity to form hydrogen bonds based on the used cross-linker and with increasing thiolation degree. Young's moduli of HA-DTPH-Ox. hydrogels are lower compared to the respective thiolation degree of HA-DTPH-Cl⁺; mean and standard deviation of triplicates are presented.*

The analysis of the Young's modulus revealed a significant difference between **HA-DTPH-Ox.** **HA-DTPH-CL$^+$** hydrogels. **HA-DTPH$^{29\%}$-Ox**. hydrogels after being swollen in H_2O have the lowest Young's modulus with 0.1 ± 0.06 kPa, increasing with increasing thiolation degree to 0.4 ± 0.2 kPa for **HA-DTPH$^{42\%}$** and 1.2 ± 0.3 kPa for **HA-DTPH$^{58\%}$**. As for **HA-DTPH-Cl$^+$** hydrogels the Young's modulus is increasing with increasing capability to form hydrogen bonds of the used ionic cross-linker. A common trend for both, **HA-DTPH-Ox.** and **HA-DTPH-Cl$^+$,** is the increasing Young's modulus with increasing thiolation degree. The Young's modulus for **HA- DTPH$^{29\%}$-NH$_4^+$** is 0.8 kPa, for **HA-DTPH$^{42\%}$-NH$_4^+$** 1.5 ± 0.3 kPa and for **HA-DTPH$^{58\%}$-NH$_4^+$** 2.4 ± 0.08 kPa. For **HA-DTPH-GluA$^+$** the Young's modulus is increasing from 1.3 ± 0.2 kPa for the lowest thiolation degree, to 3.2 ± 0.06 kPa for **HA-DTPH$^{42\%}$** and for the **HA-DTPH$^{58\%}$** it is 4.0 ± 0.3 kPa. The highest Young's modulus was measured for **HA-DTPH-dHA$^+$**. For a thiolation degree of 29% it is 2.9 ± 0.6 kPa, for a thiolation degree of 42% it is 4.2 ± 0.3 kPa and for 58% thiolated HA it is 7.2 ± 0.7 kPa. The differences of the Young's modulus between **HA-DTPH-Ox.** and **HA-DTPH-Cl$^+$** hydrogels strengthened the hypothesis of the influence of additionally formed physical cross-links on the mechanical stiffness. Due to the formation of hydrogen bonds and salt bridges the network tightens and get stiffer. The results regarding the used ionic ross-linker correlates satisfactorily with the previous findings regarding the storage modulus G'. The increasing Young's modulus from **dHA$^+$** to **GluA$^+$** and to **NH$_4^+$** supported the idea of the increasing capability to from hydrogen bonds, hereby stabilizing and tightening the network.

3.3.1 Disulfide Dependent Mechanical Stiffness

By plotting the amount of free thiol groups within each hydrogel against the Young's modulus the influence of the formed chemical cross-links is highlighted (Fig.28).

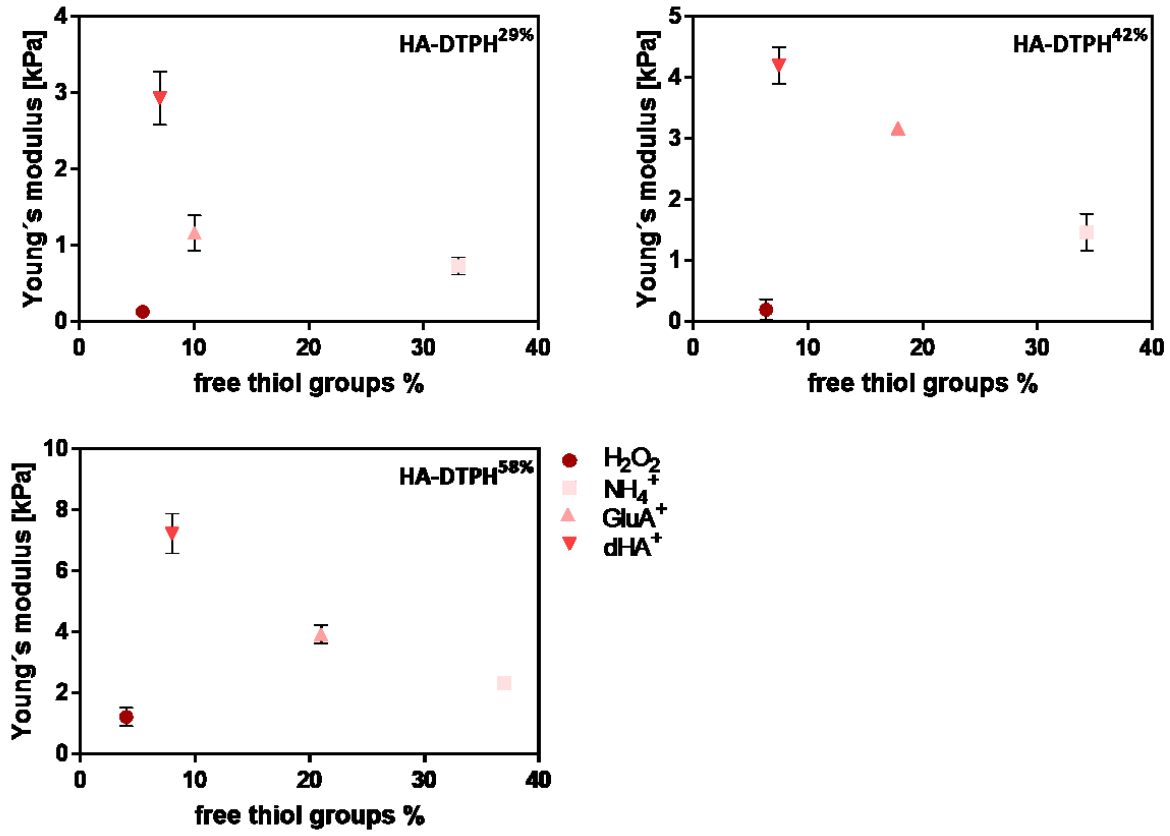

Figure 28 Young's modulus of HA-DTPH-Cl⁺ and HA-DTPH-Ox. for three different thiolation degrees against the amount of free thiol groups in % within the hydrogel measured by using the Ellman's assay. For HA-DTPH-Cl⁺ the Young's modulus is correlating with the amount of free thiol groups. With increasing free thiol groups the Young's modulus is decreasing. As for HA-DTPH-Ox. a negative correlation can be observed. Less free thiol groups result in a very soft hydrogel.

Plotting the Young's modulus against the amount of free thiol groups reveals an increase in free thiol groups for **HA-DTPH-Cl⁺** hydrogels resulting in a decrease of the Young's modulus. In comparison to **HA-DTPH-Ox.** hydrogels the correlation between Young's modulus and the amount of free thiol groups is negative for all thiolation degrees. Hence, two conclusions can

be made for **HA-DTPH-Cl$^+$** hydrogels: (1) More reacting thiol groups lead to more disulfide bonds which results in a tighter network. This is observed in an increase in the Young's modulus from **dHA$^+$** to **GluA$^+$** to **NH$_4^+$** cross-linkers. (2) An increase of the thiolation degree leads to more chemical cross-links within the network and this results in an increase of the Young's modulus. Comparing **HA-DTPH-Cl$^+$** hydrogels to **HA-DTPH-Ox.** hydrogels, the influence on the stiffness of the physical cross-link is remarkable. Although **HA-DTPH-Ox.** has less free thiol groups, resulting in more disulfide bonds, **HA-DTPH-Ox.** hydrogels are a softer. It is plausible that one limitation may have influenced the results obtained. Lee et al. (2017) showed that mechanical force, like compression and tension, mediates disulfide bond rapture. He exposed gels to range of compression strains from 0 to 40% for 30 seconds and observed the beginning of the rupture of the disulfide bonds at 10% strain. Since due to technical limitations I used a strain of 10% in my measurements, which may have led to the rapture of disulfide bonds and resulted in a lower Young's modulus. However, overall the results indicated that the strain-responsive nature of the gels allows accurate control over stiffness through thiol density.

3.3.2 Varying the Amount of dHA$^+$

Since, previous results showed that the Young's modulus can be varied by using different thiolation degrees which ends up in different amounts of disulfide bonds leading to varying tightening effect of the network. Next, I varied the ratio of **dHA$^+$** to the remaining free negative charged groups on **HA-DTPH$^{58\%}$** to analyze the influence of physical cross-links on the Young's modulus (Fig.29).

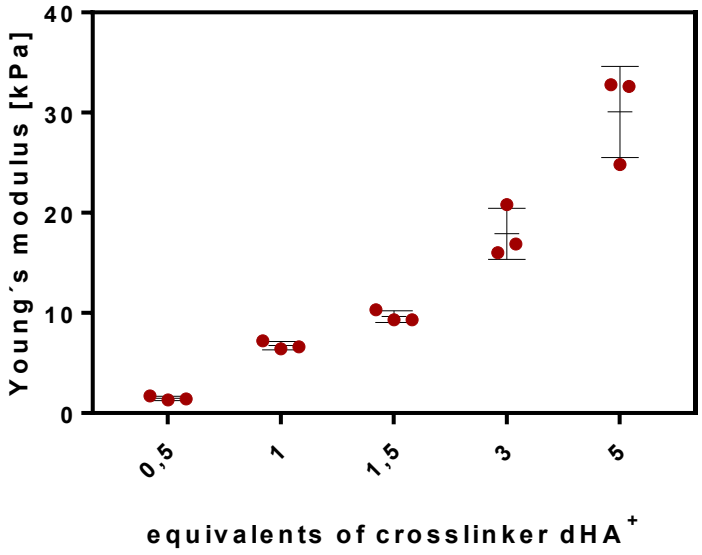

Figure 29 Young's modulus of HA-DTPH$^{58\%}$-dHA$^+$ in dependency of dHA+. dHA$^+$ was varied from 0.5 to 5 to the free remaining negative charged groups on HA-DTPH$^{58\%}$. Young's modulus of HA-DTPH-dHA$^+$ hydrogels is increasing with increasing cross-linker ratio; triplicates are presented.

Adding **dHA$^+$** in different concentrations a clear trend occurred. Below the ratio of 1.0 of the ionic cross-linker to the negative charged groups on the polymer chain the Young's modulus is 1.4 ± 0.2 kPa. Increasing the cross-linker concentration leads to increase of the Young's modulus up to 30.6 ± 4.5 kPa for cross-linker ratio 5.0.

This result shows that the hydrogel stiffness can be clearly varied by using different ionic cross-linker, with different abilities to form physical cross-links. Moreover, hydrogel stiffness can be

varied by varying the concentration of used ionic cross-linker. This is explained by the fact that more hydrogen bonds are be formed and thus the stiffness of the gel is increasing. The main conclusion is, that the chemical cross-link is especially responsible for the structural stability and mediates the formation of a stable backbone. Upon adding an ionic cross-linker disulfide bonds are formed and a structural stable backbone via disulfide bonds is generated. By this oxidation of thiol groups with hydrogen peroxide is avoided. The here presented hybrid double cross-linked HA-based hydrogels thus present a biocompatible system. Furthermore, the usage of ionic cross-linker holds the potential to form hydrogels with tunable stiffness depending on the number of physical cross-links, such as hydrogen bonds. Although hydrogen bonds are an order of magnitude weaker than ionic and covalent bonds, I have established a form stable, dynamic network structure combining physically and chemically cross-links. Despite the weakness of each physical cross-link, the multiplicity of such links makes the gel network structures quite stable (R. Zhang et. al). Overall, this system has several advantages including: (1) simple chemistry, (2) tunable mechanical stiffness, and (3) biocompatible hydrogel synthesis. Given the ability to control and tune the mechanical stiffness makes the hydrogel system usable for various biomedical application (Hu *et al.*, 2015). This includes cell study behavior and differentiation studies of stem cells in a 3D environment. For example, mesenchymal stem cells (MSCs) cultured in hydrogels with stiffness of lower (0.1–1 kPa), intermediate (8–17 kPa) or higher ranges (34 kPa) can differentiate into neural, myogenic or osteogenic phenotypes, respectively (Engler *et al.*, 2006).

3.4 Swelling Behavior of Hybrid Double Cross-linked Hydrogel

One of the most remarkable properties of HA is its high water affinity. Due to the negative charge of the carboxylic group within the chain, one HA polymer can bind and retain a high amount of water (Papakonstantinou, Roth and Karakiulakis, 2012). Hydration plays a key role in all cellular progresses and functions, therefore the characterization of the established hydrogel regarding the water uptake ability is indispensable. Especially in respect of future biomedical applications field of the designed ECM mimetic. A characteristic of hydrogels built

up of polymers is, that they swell but not dissolve when water or a solvent enters it (Kim *et al.*, 2012). The swelling properties, which usually use degree of swelling to define hydrogels, depend on many factors, such as the network density, nature of the solvent as well as polymer solvent interaction parameters. Generally, the degree of cross-linking influences the area permitted for diffusion across the hydrogel network and, subsequently, the capacity for hydrogels to take up water (Brannon-peppas & Peppas, 1990).

3.4.1 Swelling Ratio in Water

In order to analyze the water uptake capacity of the hydrogels presented in this work, I determined the swelling ratio Q_M of **HA-DTPH-Ox.** and **HA-DTPH-Cl$^+$** hydrogels in water at room temperature. Therefore, hydrogels were prepared as described in the 2.4.1/2.4.2 and were subsequently placed in water. Equilibrium of swelling was reached within one hour (Fig.30).

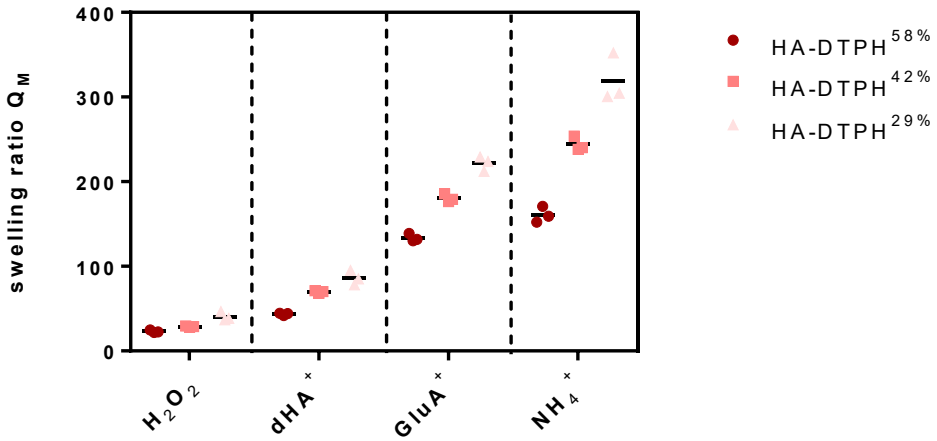

Figure 30 Swelling ratios of HA-DTPH-Cl$^+$ and HA-DTPH-Ox. hydrogels in water at room temperature after reaching equilibrium. *Swelling ratios of HA-DTPH-Cl$^+$ and HA-DTPH-Ox. hydrogels in water at room temperature show lower swelling ratios for HA-DTPH-Ox. in comparison to respective HA-DTPH-CL$^+$ hydrogels and an overall decreasing swelling capacity with increasing degree of thiolation. Swelling ratios are calculated by dividing the weight of the hydrogels in the respective solution by the dry weight of the hydrogels (determined by freeze-drying), triplicates are presented.*

For **HA-DTPH-Cl$^+$** a clear trend of the swelling behavior is observed. Swelling ratio is increasing from **dHA$^+$** and **GluA$^+$** to **NH$_4^+$**. Oxidized hydrogels **HA-DTPH-Ox.** show lowest swelling ratios compared to hydrogels with ionic cross-linker **HA-DTPH-Cl$^+$**. This difference is most obvious for **HA-DTPH$^{29\%}$-NH$_4^+$** hydrogels with 319.1 ± 28.7 and decrease to 40.6 ± 5.2 for **HA- DTPH$^{29\%}$- Ox.** hydrogels. Another interdependence is the increasing swelling ratio with decreasing degree of thiolation. For example, when **dHA$^+$** is used as a cross-linker, swelling ratios are ranging from 43.5 ± 1.5 for **HA-DTPH$^{58\%}$** to 86.2 ± 8.4 for **HA-DTPH$^{29\%}$**. As for the cross-linker **GluA$^+$** swelling ratio is increasing from 133.7 ± 4.6 for **HA-DTPH$^{58\%}$** to 221.6 ± 8.7 for **HA-DTPH$^{29\%}$**. For hydrogels with **NH$_4^+$** as a cross-linker swelling ratios are ranging from 160.7 ± 9.4 for **HA-DTPH$^{58\%}$** to 319.1 ± 28.7 for **HA-DTPH$^{29\%}$**. Swelling ratios of **HA-DTPH-Cl$^+$** are correlating with the used ionic cross-linker and used functionalization degree of **HA-DTPH**. Mainly, swelling ratio is decreasing with (1) increasing capacity to form hydrogen bonds of the used ionic cross-linker and (2) increasing number of thiol bridges at higher degrees of thiolation. This can be attributed to the rising cross-links within the hydrogel network which results in a decreasing capacity of the hydrogels to take up water.

By plotting the swelling ratio for each hydrogel against the Young's modulus the correlation between swelling ratio and Young's modulus is highlighted (Fig.31).

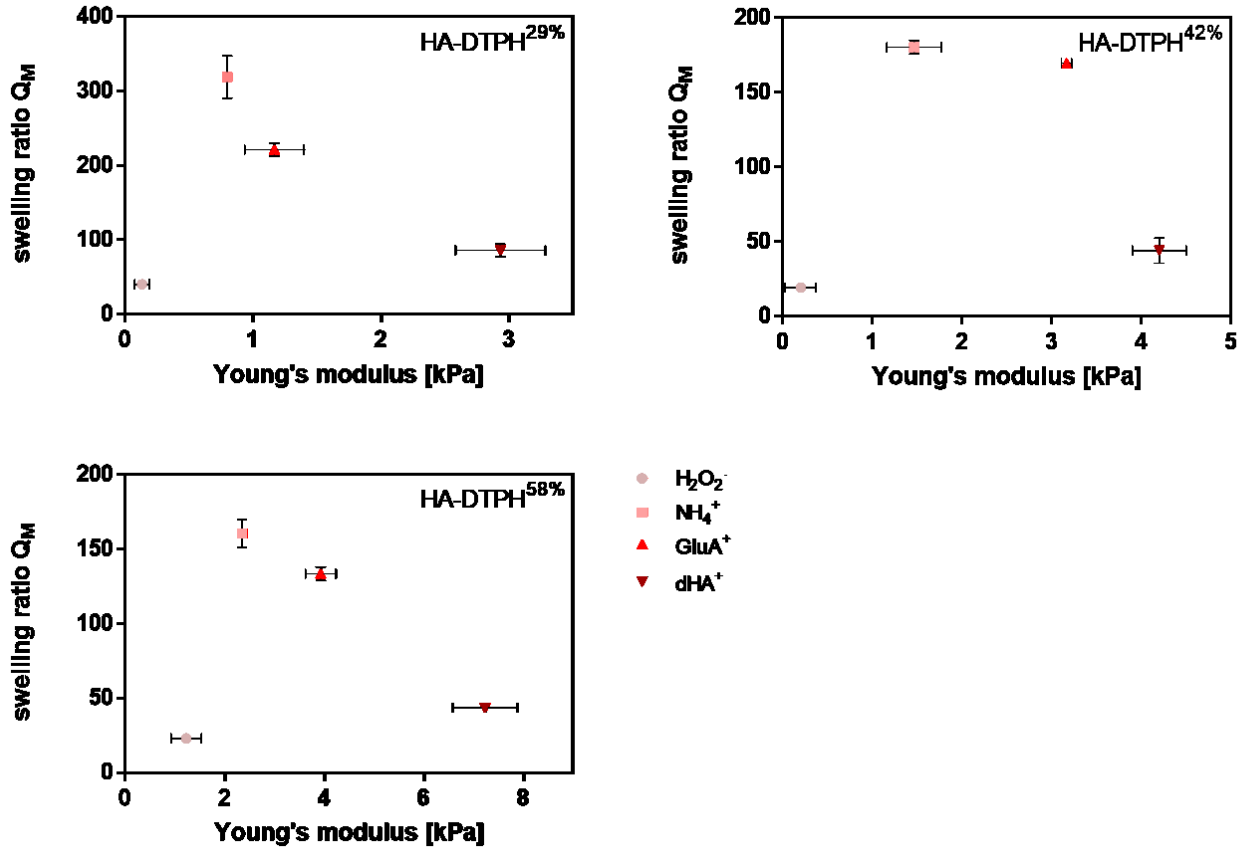

Figure 31 Swelling ratios of HA-DTPH-Cl⁺ and HA-DTPH-Ox. hydrogels against the obtained Young's modulus in 3.3. Swelling ratios of HA-DTPH-Cl⁺ are decreasing with increasing Young's modulus. HA-DTPH-Ox. albeit it is softer than HA- DTPH-Cl⁺, HA-DTPH-Ox shows the lowest swelling ratio.

Swelling ratios obtained for **HA-DTPH-Cl⁺** are in accordance with hydrogel stiffness as swelling ratio is lower with higher Young's modulus based on increasing covalent and/or physical cross-links. A remarkably surprising result is the swelling ratio of **HA-DTPH-Ox.** compared to the swelling ratio of **HA-DTPH-Cl⁺**. Albeit it is according to its Young's modulus softer, **HA- DTPH- Ox** shows the lowest swelling ratio. The cause for this different swelling behavior of **HA-DTPH-Cl⁺** and **HA-DTPH-Ox.** hydrogel could be ascribed to several different mechanisms. By introducing different ionic cross-linkers with several hydrophilic chemical residues like hydroxyl groups (-OH) in case of **dHA⁺** and **GluA⁺** the water absorbing properties

within the network increases. Another mechanism could be by the so called forward osmosis. In this case water molecules diffuse, following the osmotic pressure, from a solution with lower osmotic pressure to another solution with higher osmotic pressure. By adding charged molecules to the hydrogels, the osmotic pressure inside the hydrogel network increases and thus the water diffusion inside the hydrogel. Such a mechanism of osmotic driving forces during the hydrogel swelling process, gives the opportunity to tune the dependence between stiffness and swelling ratio. This could be further examined by analyzing the swelling ratio with increasing ionic cross-linker concentration within the hydrogel. Tuning the dependence of hydrogel stiffness and swelling ratio was also described by Cha et al. (2011). He incorporated a polymer chain with hydrophobic moieties inside of a poly (ethylene glycol) diacrylate (PEGDA) hydrogel and observed a decrease in the Young's modulus, by tuning the cross-links within the hydrogel, which caused just a minimal increase in the swelling ratio, due to the hydrophobic moieties.

3.2.1.1 Calculated Mesh Size of in Water Swollen Hydrogels

In order to analyze the different swelling behavior in consideration of the mesh sizes of **HA- DTPH- Cl⁺** and **HA-DTPH-Ox.** hydrogels, the mesh sizes are calculated as described in 2.5.5. These calculations are based on the swelling ratios of **HA-DTPH-Cl⁺** and **HA-DTPH-Ox.** hydrogels in water (Fig.32).

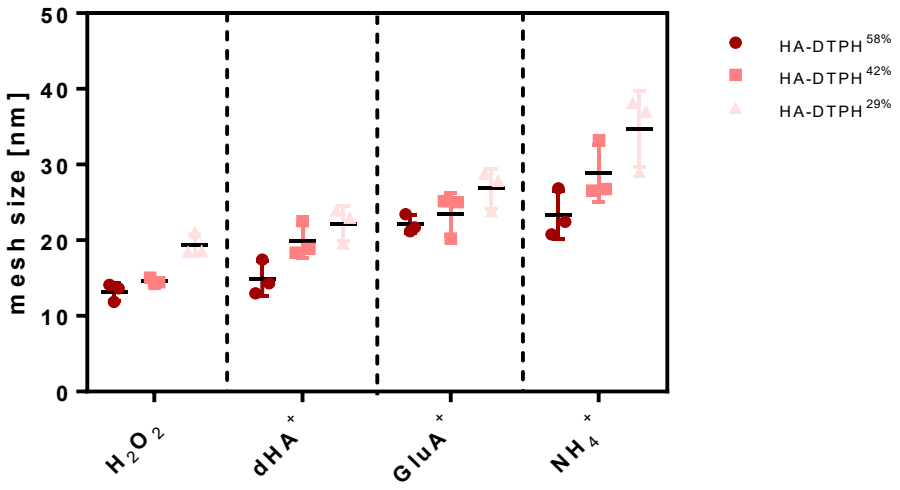

Figure 32 Mesh sizes for HA-DPTH-Cl⁺ and HA-DTPH-Ox. calculated from the corresponding swelling ratios Q_M. Mesh sizes of HA-DTPH-Cl⁺ and HA-DTPH-Ox. in water at room temperature are increasing for HA-DTPH-Cl⁺ respectively for the used ionic cross-linker and its increasing capability to form hydrogen bonds and are decreasing with increasing thiolation degree. HA-DTPH-Ox. hydrogels compared to HA-DTPH-Cl⁺ the mesh sizes are smaller and increasing of thiolation degree has a smaller effect on decreasing mesh sizes. Mesh sizes are highly correlated with the swelling ratios, triplicates are presented.

In accordance to the swelling ratios, mesh sizes for **HA-DTPH-Cl⁺** hydrogels are increasing with decreasing capacity to form hydrogen bonds of the used ionic cross-linker. Additionally, mesh sizes are decreasing with increasing thiolation degree. Comparing the mesh size depending on the degree of thiolation **HA-DTPH-Cl⁺** are always higher than comparable mesh sizes of **HA-DTPH-Ox.** hydrogels (Fig.32). For example, when **dHA⁺** is used as a cross-linker, mesh sizes are ranging from 15 ± 3 nm for **HA-DTPH$^{58\%}$** to 23 ± 2.3 nm for **HA-DTPH$^{29\%}$**. As for the cross-linker

GluA^{+} mesh size is increasing from 22 ± 1.7 nm for **HA-DTPH**$^{58\%}$ to 27 ± 2.7 nm for **HA-DTPH**$^{29\%}$. For hydrogels with **NH**$_4^{+}$ as a cross-linker, mesh sizes are ranging from 23 ± 3 nm for **HA-DTPH**$^{58\%}$ to 35 ± 5 nm for **HA- DTPH**$^{29\%}$. Mesh sizes of **HA-DTPH-Ox.** are increasing from 13 ± 1.2 nm for **HA-DTPH**$^{58\%}$ to 19 ± 1.5 nm for **HA-DTPH**$^{29\%}$**.**

By plotting mesh sizes against the amount of free thiol groups within the network, the influence of the formed disulfide bonds on the mesh size is determined (Fig. 33).

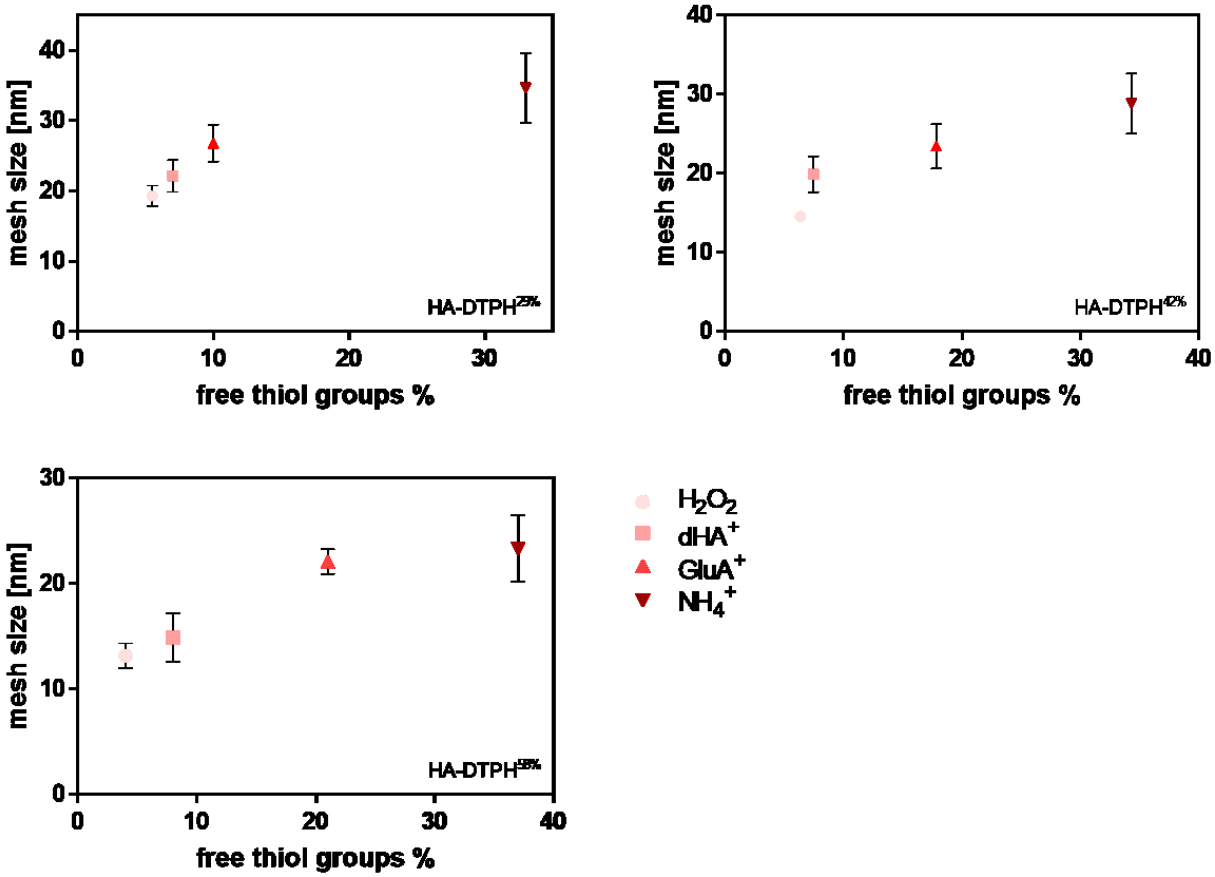

Figure 33 Mesh sizes of HA-DTPH-Cl^{+} *and HA-DTPH-Ox. for three different thiolation degrees against the amount of free thiol groups in % within the hydrogel measured by using the Ellman's assay suggest a strong correlation of the amount of formed disulfide bonds with mesh sizes. Mesh sizes are correlating with the amount of free thiol groups with increasing amount of disulfide bonds mesh sizes are decreasing since the network has more covalent cross-links.*

Figure 33 depicts the correlation of mesh sizes and free thiol groups of **HA-DTPH-Cl**$^{+}$ and **HA-DTPH-Ox**. hydrogels. The mesh size is increasing with increasing free thiol groups within the hydrogel network. Conversely, this means that with increasing number of disulfide bonds the mesh size is decreasing. Another observation is the increase of the mesh size with decreasing thiolation degree. Typically, more disulfide bonds are equated with more covalent cross-links, which is mainly the cause for varying mesh sizes. Since physical cross-links are dynamic and reversible the influence on the mesh size is not as crucial as the formation of covalent cross-links like disulfide bonds (Miwa, Kurachi, Kohbara, & Kutsumizu, 2018).

These findings support the idea of increasing amount of formed disulfide bonds leading to the increase of the amount of formed pores. Various biomedical applications are utilizing the mesh size. For example, controlled drug delivery is dependent on the mesh size. It determines the diffusion of drugs through the hydrogel network and is controlled due to the steric interaction between the drug and the polymer network. In case of a larger mesh than the drug, the diffusion process is independent from the mesh size and the drug will be released without control (Li and Mooney, 2018). When the mesh size approaches the drug size, the diffusion of the drug experience a steric hindrance (Lin *et al.*, 2005). Larger drugs than the mesh is effectively immobilizing the drug inside the hydrogel network and released upon hydrogel degradation. Since, controlled drug delivery is desired, by knowing the mesh size the diffusion of molecules in and through the hydrogel network can be predicted.

3.4.2 External stimuli dependent swelling behavior

Biomedical applications, such as drug delivery are not only dependent on the mesh size but also on the swelling of the hydrogel upon environmental changes, such as temperature, pH and ionic concentration. As a hydrogel swells, the mesh size increases and the entrapped molecules are released at the desired target site upon the external stimuli. Therefore, the ability to display a measurable change in volume in response to external stimuli is crucial. Some hydrogels exhibit this volume change by swelling and shrinking, while others undergo transitions between sol and gel phases (Brannon-Peppas & Peppas, 1990) (Jeong, Wan, & Han,

2002). Therefore, swelling ratios of **HA-DTPH-Cl$^+$** hydrogels and **HA-DTPH-Ox.** hydrogels are analyzed in the presence of different pH values and different ionic concentrations. Furthermore, they were exposed to different temperature. As a first step, hydrogels were swollen in water at defined temperatures. To contrast the effect of the thiolation degree only the smallest (**HA-DTPH$^{29\%}$**) and the highest (**HA-DTPH$^{58\%}$**) thiolation degree were used in the following experiments.

3.2.1.1 Temperature-Dependent Swelling Behavior

In general, temperature sensitive hydrogels are often used as a drug delivery system and therefore need to be designed for the relevant physiological conditions, which include all solution conditions exposed to while in transit to the intended anatomical target. In human blood plasma, the physiological temperature is 37 °C (Ribeiro *et al.*, 2018). Therefore, hydrogel swelling behavior was analyzed at room temperature (22 °C) and 37 °C. **HA-DTPH-Cl$^+$** hydrogels and **HA-DTPH-Ox.** hydrogels were prepared as described in 2.4.1/2.4.2 and successively incubated in water at 22 °C and 37°C under shaking until reaching equilibrium (Fig.34).

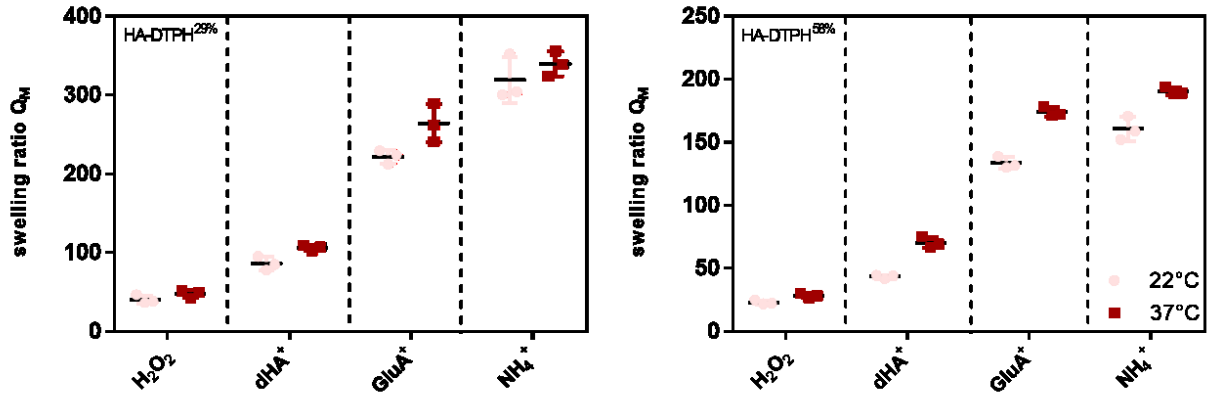

Figure 34 Swelling ratio Q_M of HA-DTPH-Cl$^+$ and HA-DTPH-Ox. hydrogels with two different thiolation degrees (29%, 58%) at two different temperatures 22 °C (light pink) and 37 °C (dark red). *Swelling ratio Q_M is increasing with increasing temperature for both hydrogel systems. For HA-DTPH-Cl$^+$ hydrogels an increase of swelling ratio Q_M with increasing capacity to form hydrogen bonds can be observed, triplicates are presented.*

Increasing the temperature to 37°C led to the same trend for the swelling behavior for both hydrogel systems as described in 3.2.1. but resulted in higher swelling ratios Q_M compared to incubation temperature of 22°C. This confirms previous findings in the literature by S. J. Kim et al. (2004), who established a polyelectrolyte HA/Chitosan based hydrogel, which increased in swelling with increasing temperature.

3.2.1.2 Ionic Solution Dependent Swelling Behavior

The ability of ionic strength sensitive hydrogels to uptake and bind ions is one of the most important feature of these. It is used in the biomedical field as well as in the industrial field. For example, Javed et al. (2018), showed the successful removal of heavy metal ions from aqueous media by using a poly (methacrylic acid) hydrogel. Therefore, I characterized the response of the **HA-DTPH-Cl**$^+$ and **HA-DTPH-Ox.** hydrogel system towards three different ionic solutions. Choosing three different concentrations of NaCl: 50 mM, the physiological value of 150 mM, and 300 mM. To differentiate the influence of monovalent und divalent cations, I used in the same concentrations as for NaCl also for $MgCl_2$ and $CaCl_2$ (Fig. 35).

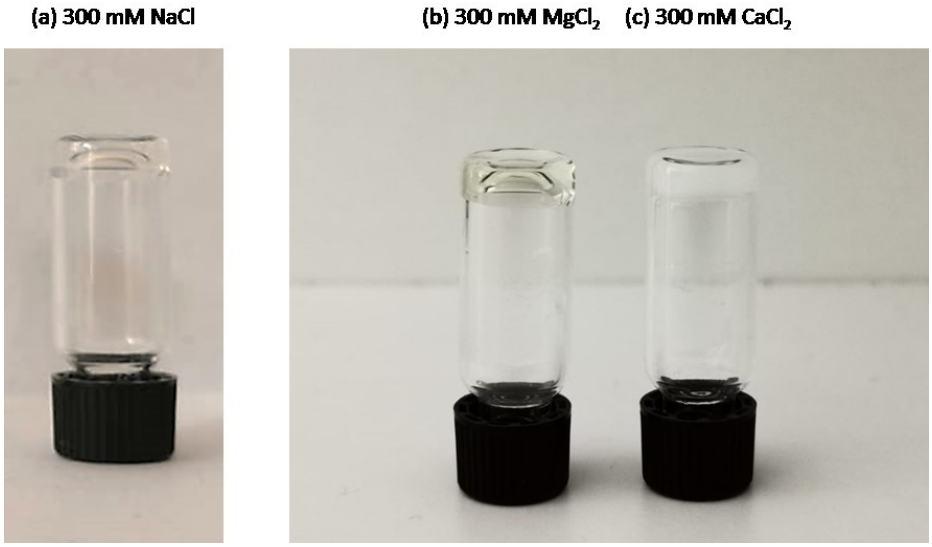

Figure 35 HA-DTPH-NH_4^+ hydrogels after incubation for 24 h in 300 mM NaCl (a), 300 mM $MgCl_2$ (b) and $CaCl_2$ (c) solution for 24 hours. Hydrogel in NaCl and $MgCl_2$ showed no significant change in morphology, but hydrogel in $CaCl_2$ showed hardening and whitening.

All hydrogel samples at first experienced swelling in all used solutions. Water molecules diffused into the hydrogels at the beginning of the swelling tests so that their volume underwent expansion. However, hydrogel samples immersed in 300 mM $CaCl_2$ solution showed a different swelling morphology. **HA-DTPH-NH_4^+** hydrogels in NaCl and $MgCl_2$ solution were transparent and flexible. However, the hydrogels in $CaCl_2$ solution appeared white and more solid (Fig.35). The main reason for this observation is that the formation of complexing cross-linking sites increased the network density of the hydrogel. The different reaction of $MgCl_2$ and $CaCl_2$ may give a hint that the formation constant of Ca^{2+} with the carboxyl group of HA is higher than the formation constant of Mg^{2+} with the carboxyl group, which leads to a stronger complex formation with $CaCl_2$. However, there has been little discussion about these cations and the complex formation with HA. Müller et al. (2017) established an amorphous hyaluronic acid cartilage system, where he observed the exchange of Ca^{2+} against Mg^{2+}. Thus, indicating a higher formation constant for $Ca^{2+}$with HA than Mg^{2+} with HA.

To further characterize this behavior, **HA-DTPH-Cl$^+$** and **HA-DTPH-Ox.** hydrogels were incubated in NaCl, $MgCl_2$ and $CaCl_2$ solution with a concentration for each cation of 50 mM, 150 mM and 300 mM. Thereby the ionic strength dependent swelling ratio was determined (Fig.36).

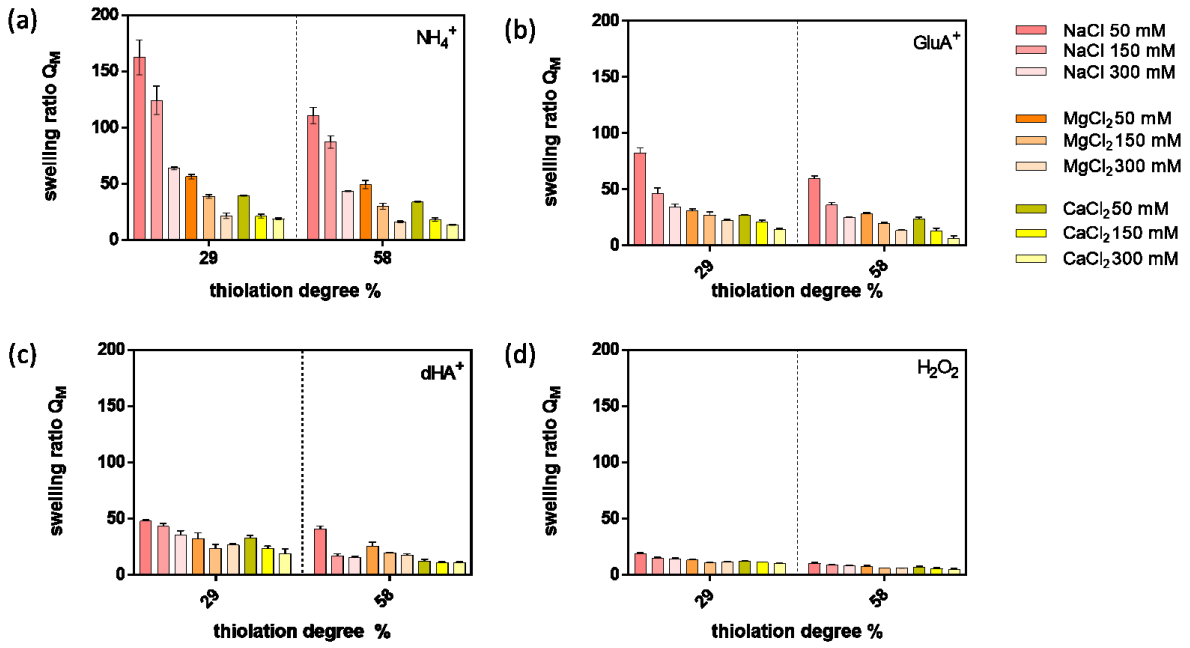

Figure 36 Swelling ratio Q_M of HA-DTPH-Cl$^+$ and HA-DTPH-Ox. hydrogels with two different thiolation degrees (29%, 58%) in different ionic solution. *Swelling ratio Q_M decreases with increasing ionic concentration and increasing formation ability of the monovalent NaCl and divalent $CaCl_2$ and $MgCl_2$. Swelling ratio Q_M of HA-DTPH-NH_4^+ and HA-DTPH-GluA$^+$ is lower after incubation in $MgCl_2$ and $CaCl_2$ than swelling ratio Q_M of HA-DTPH-dHA$^+$ and HA-DTPH-Ox. mean and SD of triplicates are presented.*

Figure 36 depicts the swelling ratio of hydrogels in solutions with varying ionic concentrations and different cations. A common trend for each hydrogel system is the decreasing swelling ratio with increasing ionic concentration. This accounts for all ions tested. The second trend is the decreasing swelling ratio from NaCl to $MgCl_2$. The lowest swelling ratio was determined for hydrogels incubated with $CaCl_2$. The third feature is the decreasing swelling ratio with increasing thiolation degree. Another remarkable observation was the response of **HA-DTPH-NH_4^+** and **HA-DTPH-GluA$^+$** in $MgCl_2$ and $CaCl_2$ compared to **HA-DTPH-dHA$^+$** and **HA-DTPH-Ox.**

Although hydrogels with **NH_4^+** and **$GluA^+$** show the highest swelling ratio in water, the swelling ratio for example in 300 mM $CaCl_2$ solution for **HA-DTPH$^{29\%}$-NH_4^+** is 19 ± 0.8 and for **HA- DTPH$^{29\%}$-$GluA^+$** 15 ± 0.8 and for the comparable hydrogel with **dHA^+** the swelling ratio is 19 ± 4. The swelling capacity of the hydrogels in dependence of the ionic strength of the swelling solution can be explained by the difference in osmotic pressure for intake of solvent molecules into the hydrogels. The decrease of the swelling ratio among the ions could be caused by the different binding behavior of the ions to the polymer chain. Divalent cations such as Ca^{2+} and Mg^{2+} in aqueous solutions cross-link with HA polymer bearing carboxylate groups. Gao et al. (2018) has been demonstrated that depending on the Ca^{2+} concentration, intramolecular and intermolecular complexation takes place. This complexing ability of the carboxylate groups with Mg^{2+} and Ca^{2+} leads to the decreasing swelling ratio of the hydrogels. These cations can even act as cross-linkers in the network due to the complex formation ability. However, the monovalent cation Na^+ in aqueous solutions cannot form complex with the carboxylate groups so the effect of NaCl on the swelling ratio of the hydrogels is reduced. The swelling behavior of hydrogels with **NH_4^+** and **$GluA^+$** could be caused by their decreased capacity to form hydrogen bonds. Due to the diffusion of the cations within the hydrogel dissociation of physically cross-linked sites could take place and complex formation of carboxylate groups with Mg^{2+} and Ca^{2+} could occur (Gao *et al.*, 2018). However, these results revealed that higher concentrations of salt solutions have a strong influence on swelling properties by the complex formation. It was already shown that hydrogel systems with these properties can be used, for example, in horticulture. The uptake and absorbance of Ca^{2+} inside the hydrogel led to growth improvement of *P. eupharatica* (Chen and Zommorodi, 2004). Additionally, such a system could also be used in a chelation therapy to treat metal-interactions by selectively binding metal-ions like shown by Polomoscanic et al. (2005). He established hydrogels containing hydroxamic acid groups as chelators for iron in the gastrointestinal tract.

3.2.1.3 pH Dependent Swelling Behavior

Another important application for hydrogel systems is the controlled drug delivery. In such cases, the drug has to be delivered in response to the body at a distinct site and defined time point. The specific time patients take their medication is very important as it has significant impact on treatment success. If symptoms of a disease display circadian variation, drug release should also vary over time (Traitel & Kost, 2004). One possibility to accomplish the controlled drug release is the response of hydrogels to certain stimuli in the body, like the pH (Rizwan et al., 2017.).

In order to investigate the sensitivity of the **HA-DTPH-Cl$^+$** hydrogel system to changing pH in the environment, I determined the swelling behavior in different pH solutions. It has been shown that degradation of HA occurs at pH < 4 and pH > 11 (Maleki and Nystro, 2008), but mostly at alkaline pH. Therefore, I used a pH range from 3 to 10. Hydrogels were incubated in each pH solution until reaching the equilibrium, the mass of each replicate was determined and the gels were transferred to the next pH solution (Fig.37).

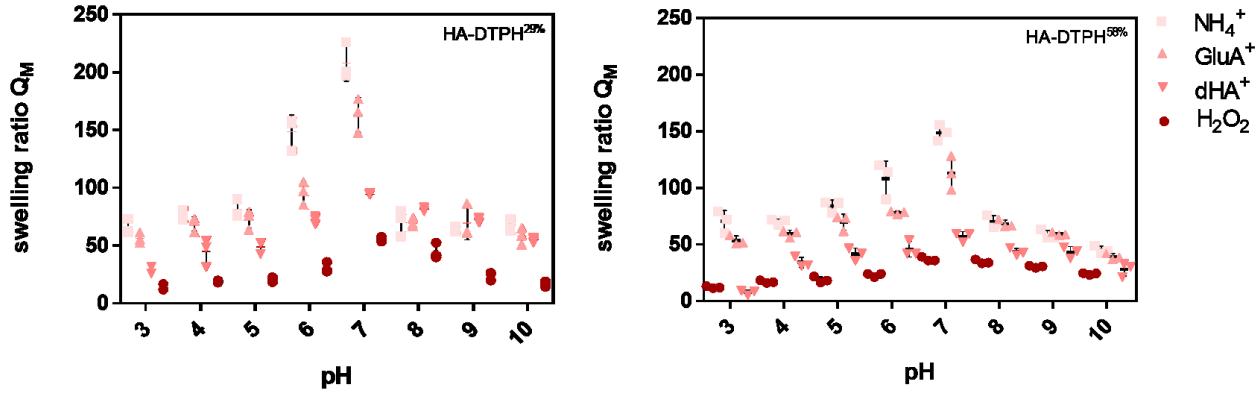

Figure 37 Swelling ratio Q_M of HA-DTPH-Cl$^+$ and HA-DTPH-Ox. hydrogels (29%, 58%) in different pH solution ranging from 3 to 10. *All hydrogel systems showed the same trend: with increasing pH until 7 the swelling ratios increase. At pH 8 to 10 the swelling decreases. HA-DTPH-NH_4^+ showed the highest swelling ratio and HA-DTPH-Ox. the lowest, triplicates are presented.*

As expected, all hydrogels were sensitive to a pH gradient (Fig.37). **HA-DTPH-Ox.** hydrogels showed the weakest response to the changes in pH. The swelling ratio started to increase at a pH of 6 and reached its maximum at pH 7 with a swelling ratio of 55 ± 2 for **HA-DTPH$^{29\%}$** and decreased with increasing thiolation to 37 ± 2 for **HA-DTPH$^{58\%}$**. For **HA-DTPH-Cl^{+}** hydrogels swelling ratio Q_M decreased with increasing capacity to form hydrogen bonds and with increasing thiolation degree. The swelling ratio Q_M for **HA-DTPH$^{29\%}$-NH$_4^{+}$** started to increase at a pH 6 (Q_M = 148 ± 14) until it reached its maximum at a pH 7 to (Q_M = 208 ± 15) and decreased at pH 10 (Q_M = 67 ± 5). **HA-DTPH-GluA^{+}** and **HA-DTPH-dHA^{+}** hydrogels showed the same pH response as **HA-DTPH-NH$_4^{+}$**. Swelling ratio Q_M started to increase from pH 6 to pH 7 and then slowly decreased slowly.

In general, pH dependent swelling of hydrogels containing an acidic moiety on the polymer chains depends on the pH of the surrounding medium relative to the respective pK_a (Rizwan et al., 2007). In the case of the carboxylic groups of HA, the ionization of the acidic groups occur in the presence of pH medium > pK_a 3, which induces the generation of fixed negative charges on the polymer chains and mobile positive charges in the solution (Qiu and Park, 2001). This leads to an increase in hydrophilicity, an increase in the number of immobilized negative charges and an increase of the electrostatic repulsion between the chains. All these mechanisms taken together result in swelling of the hydrogels (Wang *et al.*, 2012). The hybrid double cross-linked hydrogel systems presented here shrink at low pH (pH 3-5) and > 8 and start to swell as expected with increasing pH (pH 6 – 7). Swelling at pH 6 can be explained by the fact that carboxyl groups are partially ionized and thus influence the swelling behavior. As **HA-DTPH-NH$_4^{+}$** hydrogels are according to the Young's modulus the softest it is expected that swelling is increased due to the bigger mesh size. As for **HA- DTPH- GluA^{+}** and **HA-DTPH-dHA^{+}** the network is tighter swelling is reduced compared to **HA-DTPH-NH$_4^{+}$** hydrogels. Such a controlled tunable pH responsive hydrogel is optimal as a drug delivery system. Sharpe et al. (2015) has successfully established a poly(methacrylic acid) (PMAA) based hydrogel and showed the release of the encapsulated drug in the small intestine upon responding to the surrounding pH by swelling. By encapsulating the drug inside the hydrogel, it was protected from the harsh conditions of the stomach.

3.4.2.1 Extraordinary Swelling Behavior of HA-DTPH-dHA$^+$

Reversible Swelling and Shrinking Behavior of HA-DTPH-dHA$^+$

A remarkable observation in this here presented work was that the pH induced swelling effect of the **HA-DTPH-dHA$^+$** hydrogels was fully reversible. In order to study this, hydrogels were incubated in solutions of pH 7 and pH 3, respectively, until having reached equilibrium, and their respective weight was assessed by weighing the hydrogel (Fig.38).

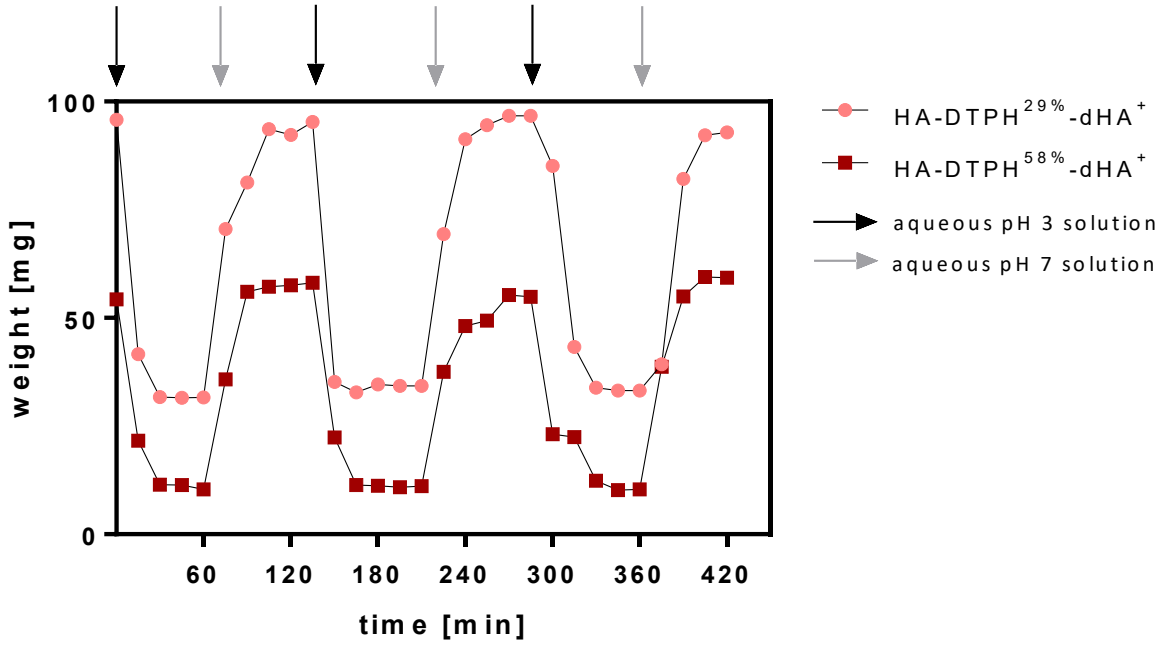

Figure 38 pH induced shrinking and swelling behavior of HA-DTPH-dHA$^+$ of different thiolation degrees. *HA- DTPH- dHA$^+$ hydrogels were incubated in an aqueous solution of pH 7 until having reached equilibrium and subsequently incubated in a pH solution of pH 3.*

A reversible swelling and shrinking behavior could be observed by placing the hydrogels alternately in a fresh aqueous solution of pH 7 and pH 3.

Acidifying Effect of HA-DTPH-dHA⁺

Incubation of **HA-DTPH-dHA⁺** hydrogel overnight in a defined aqueous solution of pH 7 led to the most striking observation (Fig.39).

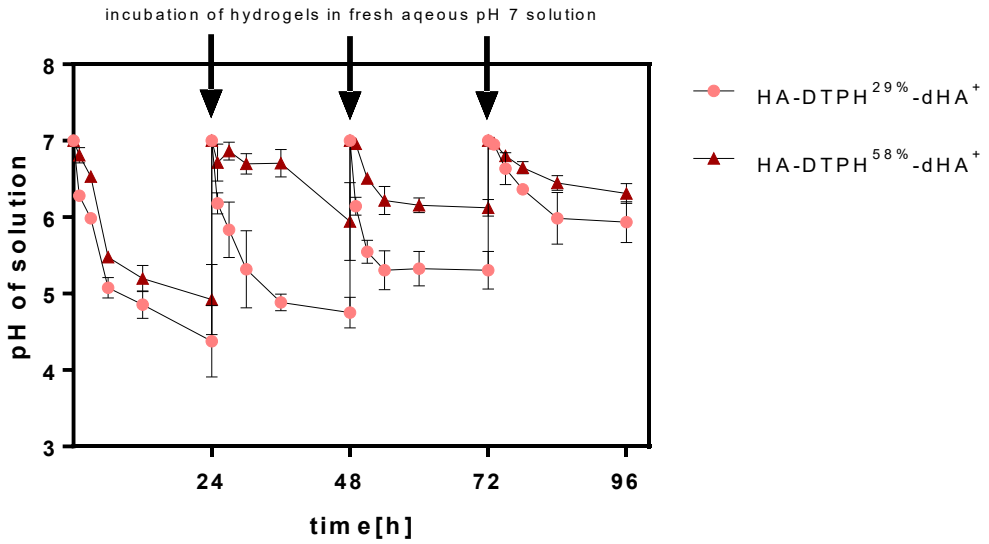

Figure 39 Influence of HA-DTPH-dHA⁺ hydrogels on the pH of the incubated solution while swelling. *Incubation of HA-DTPH-dHA⁺ in an aqueous solution of pH 7 over a certain time led to the acidifying of the solution. Acidifying effect of the HA-DTPH-dHA⁺ hydrogel decreases after each cycle and the effect of HA-DTPH$^{29\%}$-dHA⁺ is higher than the effect observed for HA-DTPH$^{58\%}$-dHA⁺ hydrogels. triplicates are presented.*

Incubation of the **HA-DTPH-dHA⁺** hydrogels in an aqueous solution of pH 7 resulted in a decrease of the pH combined with a shrinking of the hydrogel during the swelling process. Repeating this process, showed a less decrease of the pH. One possible conclusion is, that the ionic cross-linker **dHA⁺** leaked out in the swollen state of **HA-DTPH-dHA⁺**, acidified the solution and in a feedback loop led to the shrinkage of the hydrogel which in turn stops the leaking process. After refreshing the pH solution, the hydrogels swelled again, which could lead again to a leaking of **dHA⁺** into the solution and acidification of the solution. Eventually the pH change decreased and the cycle ends when no further **dHA⁺** diffused out anymore. This

suggests that a certain amount of **dHA⁺** remained in the network. In general, this mechanism could be caused by the acidic carboxylic moiety at **dHA⁺**.

Osmolarity of pH solution

To study the correlation between the swelling behavior and the acidification of the incubated solution, the osmolarity of the solution was measured (Fig.40). The osmolarity is a general measure to determine how concentrated the solute is within one liter of solution.

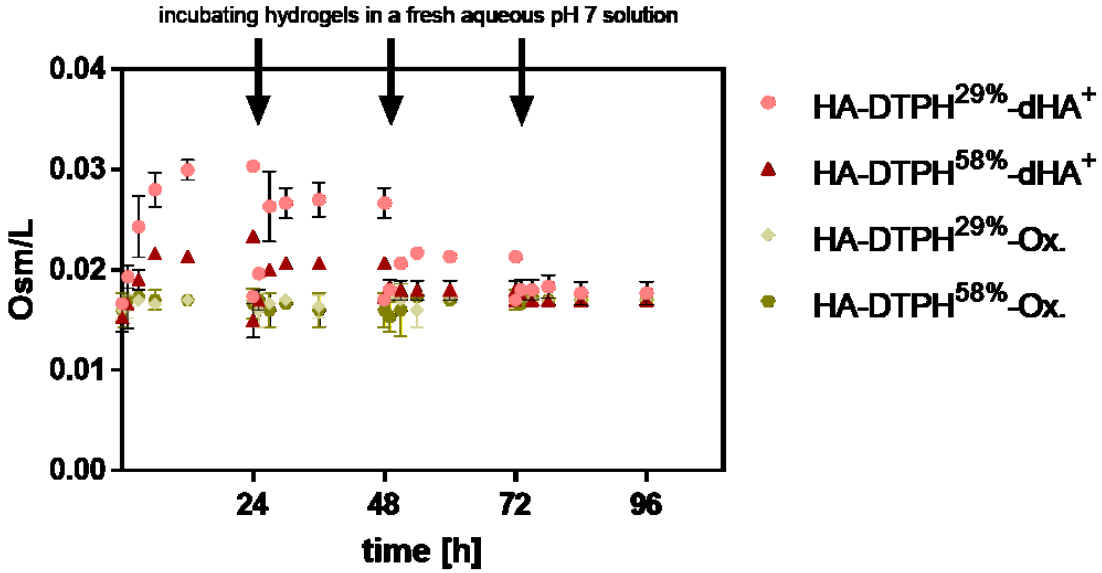

Figure 40 Osmolarity measurement of the solution, in which HA-DTPH-dHA⁺ hydrogels are incubated. *The osmolarity of the solution is increased during the hydrogel swelling process. Osmolarity of the solution in which HA- DTPH$^{29\%}$-dHA⁺ is incubated was higher than the osmolarity of the solution of HA-DTPH$^{58\%}$-dHA⁺. HA-DTPH-Ox. showed no influence on the osmolarity. The osmolarity was measured after 0 h, 1 h, 3 h, 6 h, 12 h, 24 h, 48 h, 72 h and 96 h. triplicates are presented.*

Measuring the osmolarity of **HA-DTPH-dHA⁺** and **HA-DTPH-Ox.**, revealed that the osmolarity of the solution, in which the **HA-DTPH-dHA⁺** was incubated, increased. Whereas the osmolarity of the solution in which **HA-DTPH-Ox.** was incubated was constant over time. The general trend could be observed, that with each cycle of **HA-DTPH-dHA⁺** incubation in pH 7 solution the increase of the osmolarity decreased and in general the osmolarity increased with

decreasing thiolation degree. Whereas the osmolarity of the solution in which **HA-DTPH-Ox**. was incubated stayed constant and did not change over time. These results are consistent with the results of the acidifying of the pH solution based on the leakage of **dHA$^+$** into the solution. These results give the opportunity to use the established hybrid double cross-linked HA hydrogel system as a pH dependent controlled drug delivery system, for example for drug delivery to the colon. The pH of the colon is alkaline (Koziolek *et al.*, 2015), which would lead to the swelling of the hydrogel and subsequently to the drug release.

3.5 HA-DTPH-dHA$^+$ Dependent Biological properties

To fulfill the task of a biomaterial aiming for an application in a biomedical field, certain properties have to be fulfilled, such as high biocompatibility, adhesiveness/non-adhesiveness and biodegradability. To accomplish the property of biocompatibility hydrogel synthesis should avoid toxic components which might be released upon degradation or any toxic coupling agents used in order to mediate network formation. To fulfil the property of adhesiveness several features have to be kept in mind, such as surface roughness, surface charge and stiffness of the biomaterial. And since the hydrogel system is made out of HA, which is known to be biodegradable in the ECM *in vivo*, the hydrogel system should be degradable. This attribute is especially crucial for cells, as it enables them to move through the highly viscous ECM and to remodel it depending on their needs. The requirements of biocompatibility are fully accomplished in the presented **HA-DTPH-dHA$^+$** hydrogel system, since no toxic coupling agent, such hydrogen peroxide to oxidize the thiol groups, is needed for hydrogel formation. Nevertheless, the biocompatibility of the hydrogel system and accompanying utilized compounds has to be examined and proofed. Primary normal human dermal fibroblasts (NHDF), which are involved in HA synthesis (Acid *et al.*, 2020) (Terazawa *et al.*, 2015) and degradation (Stair-nawy, Cso and Stern, 1999) in the human dermis, therefore are also interesting for dermatological research as well as wound healing studies. Thus, NHDF cells, isolated from juvenile foreskin are employed to study the biocompatibility on the one

hand and, regarding future biomedical applications, such as tissue engineering or cell delivery, cells were embedded into the hydrogel on the other hand.

3.5.1 Biocompatibility of dHA^+ and HA-DTPH

Cell viability assays are widely used to analyze the effect of a compound on cell viability as well as conclude on its toxicity, leading to cell death. To analyze the cell viability of NHDF cells upon **dHA^+** and **HD-DTPH$^{58\%}$** incubation, I utilized a tetrazolium reduction based assay (Fig.41). 3-(4,5-dimethylthiazol-2-yl)-5-(3-carboxymethoxyphenyl)-2-(4-sulfophenyl)-2H-tetrazolium (MTS) is a water-soluble tetrazolium reagent which can be bioreduced by viable cells to a colored formazan product, that is as well soluble in medium. The conversion is assumed to be accomplished through NADPH/NADH-mediated reduction by metabolically active, hence live, cells.

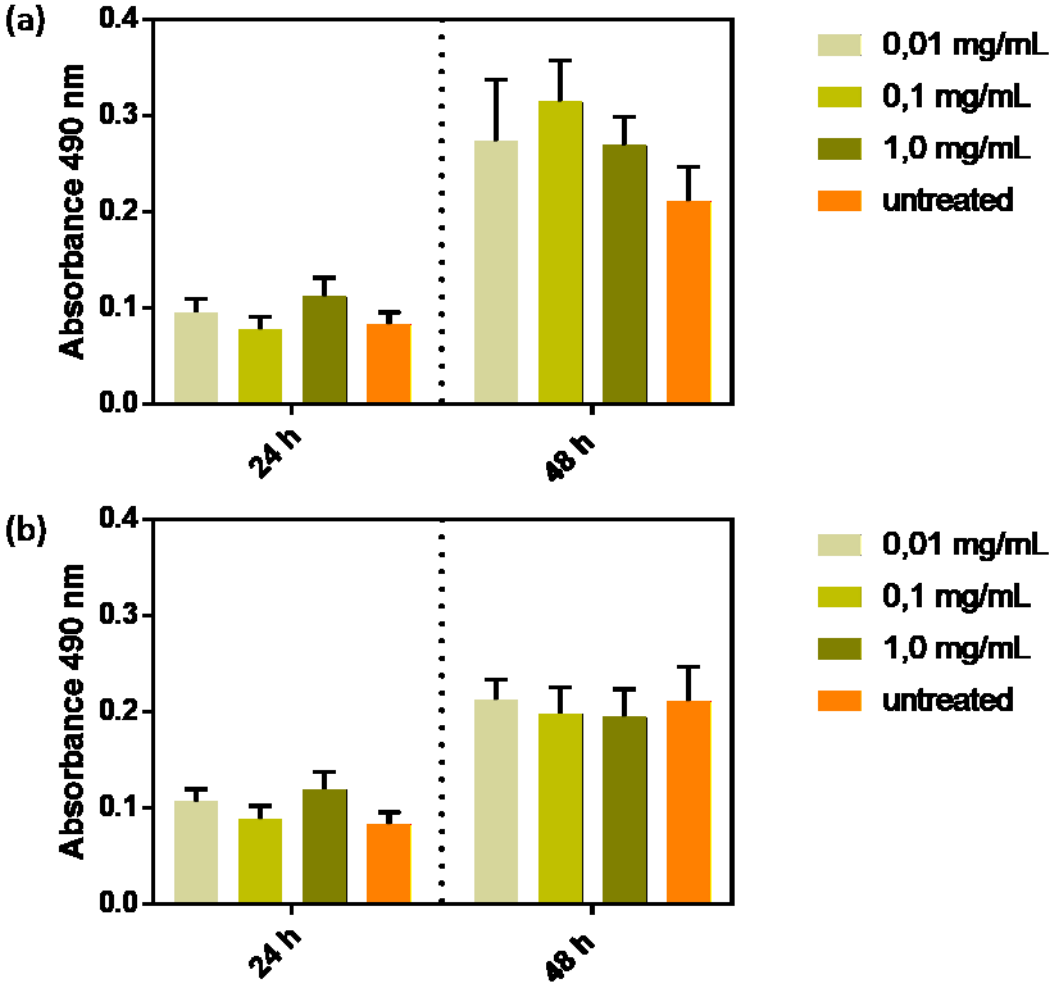

Figure 41 Effect of ionic cross-linker dHA⁺ and HA-DTPH on NHDF cells. 3750 NHDF/ cm² were seeded and cultivated for 24 hours before being treated with dHA⁺ (a) and HA-DTPH (b) being solved in fibroblast growth media (FGM2) for 24 hours/48 hours and subsequently incubated with MTS for 3 hours. After 3 hours the absorbance of reduced MTS tetrazolium at 490 nm was measured. Incubation with dHA⁺ shows a higher reduction of MTS tetrazolium after 48 hours compared to untreated cells (a). No differences in reduction of MTS tetrazolium could be observed for NHDF cells incubated with HA-DTPH after 24 hours and 48 hours (b). The background absorbance was subtracted from these data. Each data represents the mean ± SEM of three replicates of three independent experiments.

The measurement of viability of NHDF cells upon treatment with **dHA⁺** indicated an increased metabolic activity in comparison with control under all three chosen treatment concentrations, especially 0.1 mg/mL of **dHA⁺** after 48 hours post treatment. **dHA⁺** treatment at 0.01 and 0.1 mg/mL resulted in slightly elevated metabolic activity for NHDF cells after 48 hours post treatment. NHDF viability measurement under **HD-DPTH$^{58\%}$** treatment showed no

differences to the control sample. In summary, viability measurement has not delivered a certain result, concerning the enhancement of cell viability under **dHA^{+}** / **HA-DTPH$^{58\%}$**. However, it has been determined, that both compounds do not have a cytotoxic effect on NHDF cells, which makes **HA- DTPH$^{58\%}$-dHA^{+}** hydrogels suitable for cell included studies.

3.5.2 Cell Adhesion on HA-DTPH-dHA^{+}

Beside the requirement of biocompatibility, the adhesiveness of hydrogels, is also a property which distinguishes the biomedical application. On the one hand adhesive hydrogels are desired for example in wound dressing models to guarantee a complete closure of the wound site to prevent the penetration of bacteria inside the wound. On the other hand, for example, the synovial fluid in the joints has to be inert to maintain the agility of the joint. In case of an inflammation the synovial fluid granulates and gets adhesive, which results in osteoarthritis. In this case, hydrogels are also used as an inert filler, where no adhesiveness is wanted. In order to assess the adhesiveness of the established **HA-DTPH-dHA^{+}** hydrogel, NHDF cells were seeded on the hydrogels as described in 2.8. Two different ionic cross-linker **dHA^{+}** eq. 0.5 and 1.0 to the free remaining negative charge on **HA-DTPH$^{58\%}$** were used. Since it was above shown the by varying the ionic cross-linker amount the mechanical stiffness is tunable, the cell adhesion can be analyzed on softer and stiffer hydrogel. As a positive control, to compare cell adhesion and spreading behavior on the hydrogels, cells are simultaneously seeded on a **HA-DTPH$^{58\%}$-dHA^{+}** hydrogel system with incorporated linear 5% equivalent linear RGD to free thiol groups of **HA-DTPH$^{58\%}$** inside (Fig.42). The RGD motif consists of three defined amino acids arginine, glycine and aspartate and is present in several ECM proteins, such as fibronectin, vitronectin and laminin. RGD binding motif serves as ligands for a subset of integrin receptors, and guarantee cell adhesion. Adding RGD serves two different intentions: (1) comparison of cell adhesion by integrin-RGD interaction with cell attachment via CD44 -HA binding. (2) analyzing the tunability of the hydrogel system by increasing the complexity. RGD is incorporated by utilizing Thiol-Michael addition click reaction (see 2.4.3).

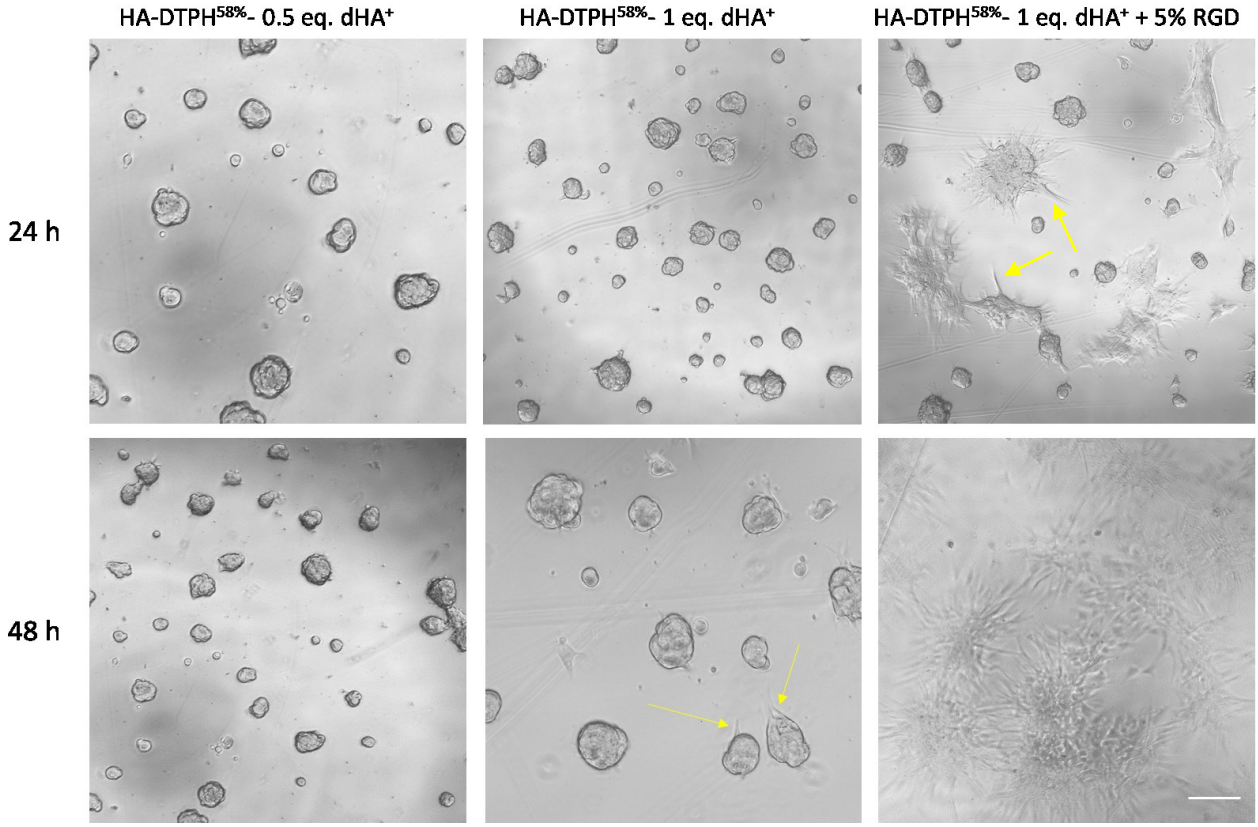

Figure 42 1000/cm² NHDF cells seeded on hydrogel with varying dHA⁺ concentration (0.5 eq. and 1 eq. to free remaining negative charges of HA-DTPH58%) and on HA-DTPH-dHA⁺ hydrogel with incorporated linear RGD motive. After 24 hours NHDF cells are in clusters on all three hydrogel conditions, on the HA-DTPH-dHA⁺-RGD hydrogel are additionally spindle shaped cells. After 48 hours, NHDF cells are still in formed cluster on HA-DTPH- 0.5/1.0 eq. dHA⁺, yellow arrows indicate a tendency of formation of focal adhesion HA-DTPH- /1.0 eq. dHA⁺. NHDF cells are fully spreaded on HA-DTPH-dHA⁺-RGD hydrogel. Scale bar = 50 µm

The images of NHDF cells on top of the hydrogel revealed a cluster formation for all hydrogel conditions after 24 hours post-seeding. **HA-DTPH$^{58\%}$-dHA^{+}** with linear RGD showed, beside cluster formation, already after 24 hours spreaded cells with spindle shaped long focal adhesions indicated by yellow arrows. After 48 hours NHDF cells on **HA-DTPH$^{58\%}$-dHA^{+}** are still in formed clusters, however on **HA-DTPH$^{58\%}$-1.0 eq dHA^{+}** hydrogels a tendency of filopodia formation on the edge of the cluster can be seen (yellow arrow). On the **HA-DTPH$^{58\%}$-dHA^{+}-RGD** hydrogels cells are fully spreaded.

To support these findings, seeded NHDF cells were fixed and stained with DAPI, which stains the nucleus and Phalloidin, which stains the actin cytoskeleton and thereby outlines the cell area as described in 2.9.1.1, 48 hours post-seeding (Fig.43).

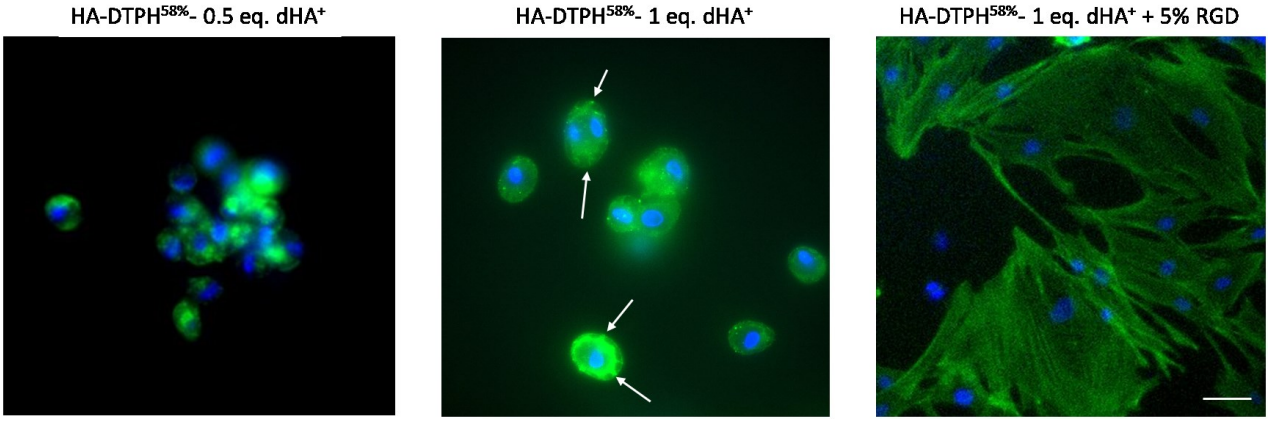

Figure 43 Morphology of NHDF cells on HA-DTPH-0.5/1.0 eq. –dHA⁺ and HA-DTPH-1.0 eq. - 5% RGD. *Cells on the adhesive control surface HA-DTPH-1.0 eq. dHA⁺- 5% RGD are much more spreaded and form a confluent cell layer after 48 hours. Cells on the hydrogel HA-DTPH-0.5 eq. – dHA⁺ hydrogel are round and still in a cluster like formation. NHDF cells on HA-DTPH-1.0 eq. –dHA⁺ are showing a filopodia formation in the hydrogel indicated by yellow arrow. Scale bar = 25 µm*

Images of stained NHDF cells with DAPI and Phalloidin revealed different adhesion behavior: (1) On **HD-DTPH-0.5 eq. dHA⁺** single cells and also cluster formation can be seen. Cells are adherent but showed no spreading behavior. (2) More single cells could be observed on the **HA- DTPH- 1.0 eq.-dHA⁺** hydrogel, which are attached to hydrogel surface and showing a tendency to form filopodia, which are first hint for the spreading behavior. (3) On the hydrogel with incorporated RGD NHDF cells are fully spreaded and adherent to the surface.

Taken all together, NHDF cells are adherent on the **HA-DTPH-dHA⁺** hydrogel, which indicates a possible non-integrin mediated cell adhesion. However, it is plausible that a number of certain parameters may also cause the adhesion behavior. Cell adhesion and spreading is not only occurring by receptor and ligand binding but is influenced by the surface charge, by the surface roughness and by the stiffness of the substrate. The latter were supported by the results obtained from NHDF cells on hydrogels with varying ionic cross-linker. On the hydrogel

with higher ionic cross-linker concentration, thereby stiffer hydrogel, cells were forming filopodia, which is a hint for cell spreading. Hence, decreasing of the ionic crosslinker leads to softer hydrogels and less cell adhesion or spreading. To further investigate non-integrin mediated cell adhesion, experiments have to be performed in which the receptor CD44 or RHAMM, which are mainly responsible for cell adhesion and spreading upon HA binding, are inhibited. However, NHDF cells on hydrogels with incorporated RGD showed adherent and fully spreaded cells, which is most likely integrin mediated. Despite the fact that these results contain some uncertainties it can be concluded that the **HA-DTPH-dHA$^+$** is tunable regarding its adhesiveness, which makes suitable for adhesive and less adhesive studies or biomedical applications. Furthermore, adding RGD proved the stability of the system with increasing complexity.

3.6 Enzymatic Degradability and Stability of HA Hydrogel

Regarding our system as an ECM mimetic the degradability of the **HA-DTPH-dHA$^+$** compared to **HA-DTPH-Ox.** by HA degrading enzymes is interesting for fundamental insights into HA degradation in correlation with the stability of additional physical cross-links in case of the **HA-DTPH-dHA$^+$** hydrogel. Degradability and stability is also an important property for various biomedical applications. For example, hydrogels used as drug delivery system, should be degraded after delivering their cargo whereas hydrogels used as tissue fillers has to be stable upon a long time.

3.6.1 Cross-linking Dependent Enzymatic Degradation

To analyze the influence of the physical cross-link on the stability of the hydrogel upon enzymatic degradation, two HA degrading enzymes are chosen: (1) hyaluronidase IV and (2) hyaluronate lyase. To compare the degradation of different hydrogels in different enzyme solutions, the half-life ($t_{1/2}$) of each hydrogel is calculated. Half-life represents the time frame

in which the hydrogel lost half of its initial weight, expecting a first order exponential decay (Fig.44).

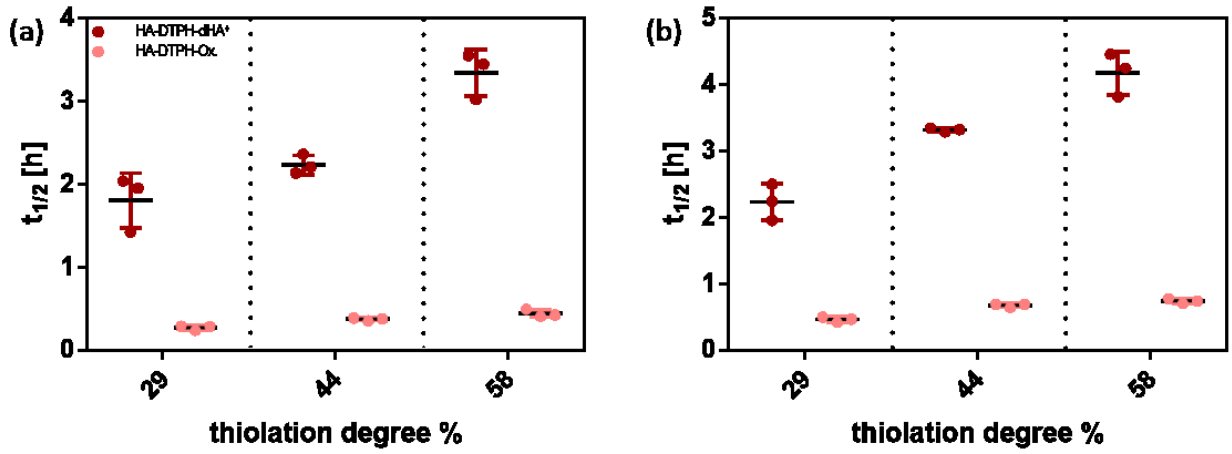

Figure 44 Half-lives of HA-DTPH-dHA⁺ and HA-DTPH-Ox. hydrogels (with 29%, 44% and 58%, respectively thiolation degree) in hyaluronidase solution (a) and lyase solution (b) at room temperature show thiolation- and cross-linking dependent degradation kinetics. For both enzymes half-lives of HA-DTPH-Ox. hydrogels are shorter than the corresponding HA-DTPH-dHA⁺ hydrogels. Additionally, half-lives are increasing with increasing degree of thiolation. Triplicates are presented.

Half-lives of **HA-DTPH-dHA⁺** and **HA-DTPH-Ox.** hydrogels are increasing with increasing degree of thiolation of **HA-DTPH**. **HA-DTPH-Ox.** have shorter half-lives than comparable **HA- DTPH- dHA⁺** made with the same **HA-DTPH** (Fig. 45). For hyaluronidase IV half-lives are ranging from 2.2 ± 0.3 h for **HA-DTPH$^{29\%}$-dHA⁺** to 0.5 ± 0.03 h for **HA-DTPH$^{29\%}$-Ox.**. Half-lives for hyaluronate lyase are shorter with 1.8 ± 0.3 h for **HA-DTPH$^{29\%}$-dHA⁺** to 0.3 ± 0.03 for **HA-DTPH$^{29\%}$-Ox.**. With increasing half-life, stability of hydrogels against enzymatic degradation is increasing. Therefore, the two general trends for degradation with both enzymes can be attributed to the amount of cross-link within the hydrogel system. With increasing thiolation degree the chemically cross-link is increasing and by adding **dHA⁺** additional physical cross-links are formed, by which the system is further stabilized. In general, this results showed, that the **HA-DTPH-dHA⁺** hydrogel system is degradable and thus, fulfills an important property for biomedical application. In conclusion, the **HA-DTPH-dHA⁺** hydrogel system enables the tuning

of the enzymatic degradation, which makes it more flexible and adjustable. Since, the **HA-DTPH-dHA$^+$** hydrogel system is suitable, for cell studies it was further analyzed upon its stability over long time in the absence of HA degrading enzymes.

3.6.2 Long-Term Stability of HA-DTPH-dHA$^+$

To analyze the stability of the established **HA-DTPH-dHA$^+$** hydrogel system in the absence of degrading enzymes, hydrogels were prepared as described in 2.4.1 and incubated over a time period of six months in a weekly fresh PBS solution (Fig.45).

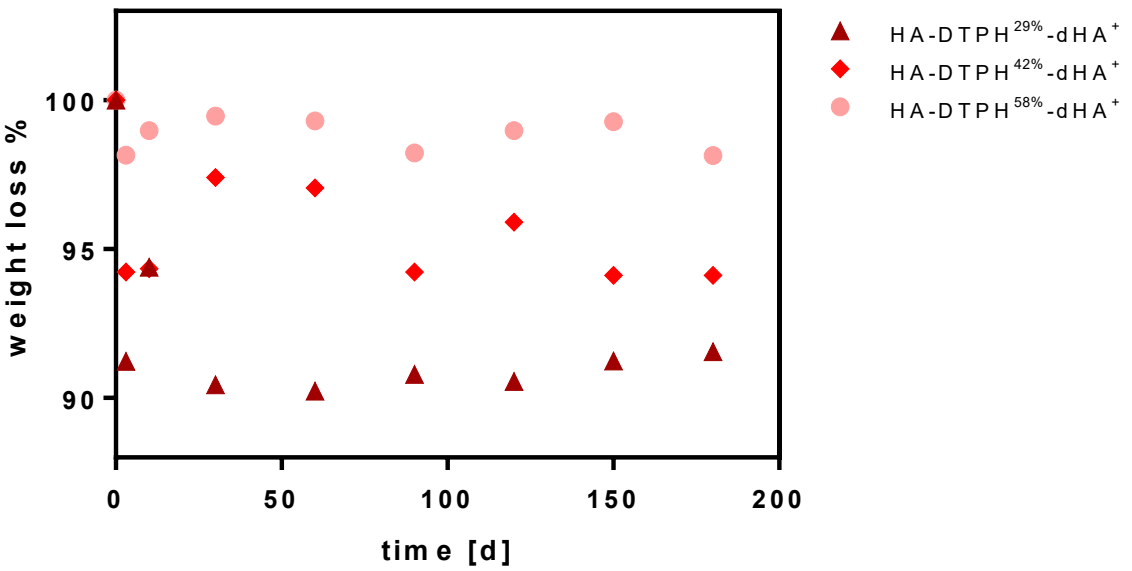

Figure 45 No degradation of HA-DTPH-dHA$^+$ can be observed in PBS. The weight of the hydrogel is constant over the course of six months.

HA-DTPH-dHA$^+$ hydrogels showed a great stability in PBS (Fig.45) and no degrading processes were observed, which makes it suitable for long term cell studies or as tissue filler applications, where no HA degrading enzymes are present.

3.7 Cell encapsulation in HA-DTPH-dHA$^+$ Hydrogel

Biodegradable hydrogels are often used for tissue engineering applications. Therefore, cells are encapsulated inside the hydrogel network, which provides either a structural 3D environment or additional bioactive molecules are incorporated into the hydrogel to induce desired cell behavior and tissue growth (Nicodemus, Bryant and Ph, 2008). In order to embed cells into a hydrogel two main strategies are used. Either cells are seeded on top of a pre-formed porous hydrogel with subsequent migration of cells into the gel, or cells are encapsulated directly during hydrogel formation. Such cell encapsulation involves mixing cells with precursors in a liquid solution followed by gelation and thus encapsulation of cells. The liquid precursor solution as well as the process by which gelation occurs must be mild and cell-friendly. Considering these requirements **HA-DTPH-Ox.** hydrogels are not suitable for cell encapsulation, since oxidizing with hydrogen peroxide is required to gain a stable hydrogel. Hydrogen peroxide is known to be cytotoxic and inducing cell death by producing highly reactive hydroxyl radicals (Whittemore, 1995). Whereas the developed **HA-DTPH-dHA$^+$** hydrogel avoids such cytotoxic cross-linking agents and as already been shown above the ionic cross-linker **dHA$^+$** proofed to be biocompatible (Fig.42). However, the successful establishment of an NHDF cell encapsulation protocol required several changes in the hydrogel synthesis. First of all, the before used Teflon molds (Fig.21 a) were not suitable anymore, since providing nutrition for the cell were not possible using these molds. To provide nutrition for the embedded cells, without taking them out of the cell encapsulation container disposable 1 ml syringes (B. Braun Melsungen AG, Germany) were cut at 0.1 ml mark below the tip of the syringe to obtain a cylindric well with the syringe plunger serving as a movable bottom (based on a technique by Khetan et al.). After transferring the hydrogel solution in the syringe, hydrogel was covered with cell culture medium and encapsulated cells were cultivated inside of the hydrogel in the syringe. Another setup was used in order to achieve sterile embedding conditions and for further optical studies, like the possibility of taking microscope images. Here embedding is performed in a cylindric teflon mold (made in the PCI

werkstatt) which sits in a FGM2 medium filled small petri dish modified with a glass bottom to improve microscopy analysis and nutritional supply (Fig.46)

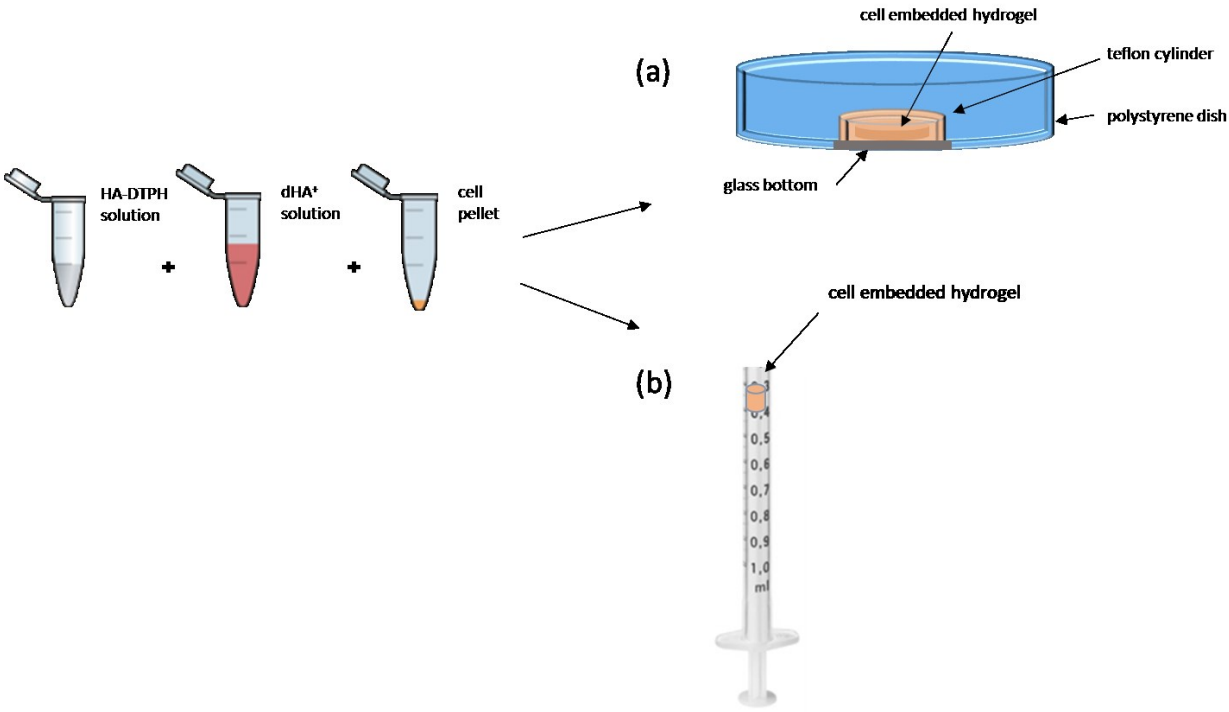

Figure 46 Scheme of cell encapsulation procedure in two different experimental setups.

Another change of the protocol was made regarding the solvent. Instead of borate buffer, fibroblast growth medium (FGM2) was tested as a solvent for both **HA-DTPH** and the ionic cross-linker **dHA**$^{+}$ to promote biocompatibility on the one hand and to provide nutrition within the hydrogel on the other hand (Fig. 47).

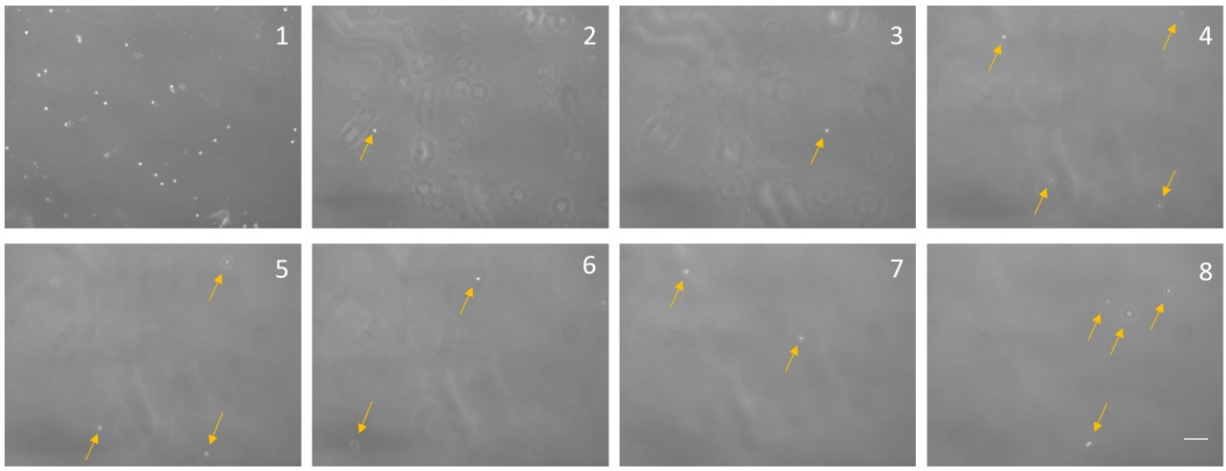

Figure 47 Cells embedded inside of HA-DTPH$^{58\%}$-dHA^{+} hydrogel using fibroblast growth medium (FGM2) as a solvent. Images were taken of 8 layers of the hydrogel. A small number of cells could be found in different layers of the gel (indicated by yellow arrow). However, these hydrogels proved to be unstable in FGM2 at 37 °C releasing the embedding cells. Scale bar 100 nm.

However, the hydrogel was not sufficiently stable to retain the cells which resulted in a drop of the entire cell-content to the bottom of the gel/plate (Fig. 47-1). A few NHDF cells are found in different layers, however the distribution of NHDF cells within the hydrogel was not satisfying.

Another possible change of the above described preparation (see 2.4.2) was again modified regarding the solvent. While the cross-linker was dissolved in FGM2, 150 mM borate buffer pH = 8.5 was used to dissolve **HA-DTPH$^{58\%}$** (Fig.48).

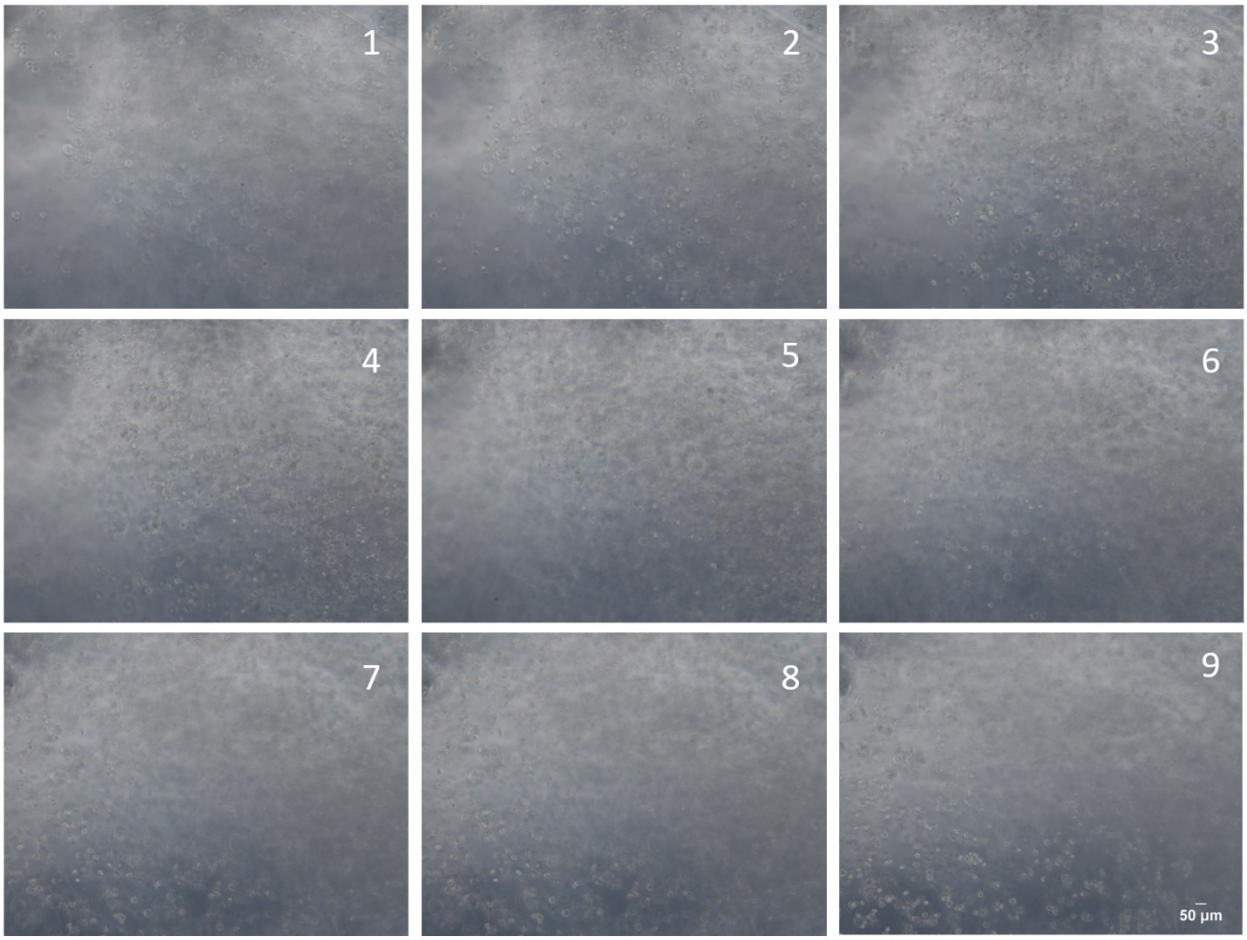

Figure 48 Encapsulated NHDF cells after 24 hours incubation in fibroblast growth medium. *NHDF cells were homogenously distributed within the hydrogel. NHDF cells were rounded and did not showed the spindle like morphology.*

Hydrogels, thereby dissolving **HA-DTPH$^{58\%}$** in borate buffer and **dHA^{+}** in FGM2 resulted in stable gel formation and successful embedding at post-mixture timepoint = 80 min. These cell-containing hydrogels were stable after transferred to FGM2 in 37 °C. In this setup NHDF cells were observed in different layers of the gel (Fig. 50) though without spreading (round appearance). Transferring hydrogels out of the syringe in cell culture medium did not lead to

cell release from the gel matrix but to stable embedding. Embedding of the cells were also confirmed by imagining via SEM (see appendix). After the successful embedding of the NHDF cells inside the hydrogel the cell viability was proved with a live/dead staining kit, containing calcein AM and ethidium homodimer, after 24 hours post-embedding (Fig.49).

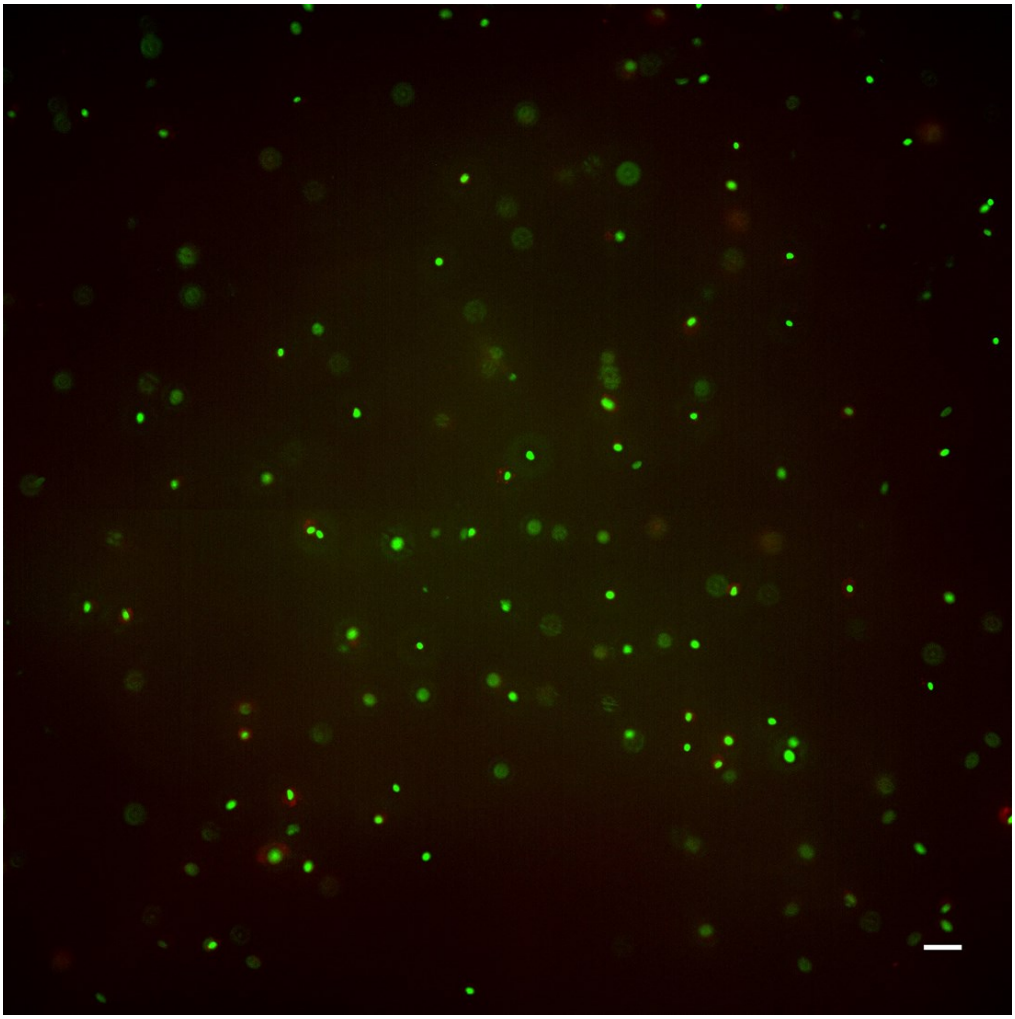

Figure 49 .Live/Dead staining of NHDF embedded in HA-DTPH$^{58\%}$-dHA^{+}. Homogenous distribution of NHDF cells inside the hydrogel. Living cell (green fluorescence) and dead cell (red florescence). Image were taken as a Z-stack and max. intensity were performed via ImageJ. Scale bar = 50 µm

Generally, a homogenous distribution of NHDF cells were observed and the life/dead assay was able to prove the high viability of NHDF cells inside the **HA-DTPH-dHA^{+}** hydrogel.

To promote cell attachment inside the hydrogel the before used approach of incorporation of linear RGD was carried out and again stained with DAPI and Phalloidin (Fig.50).

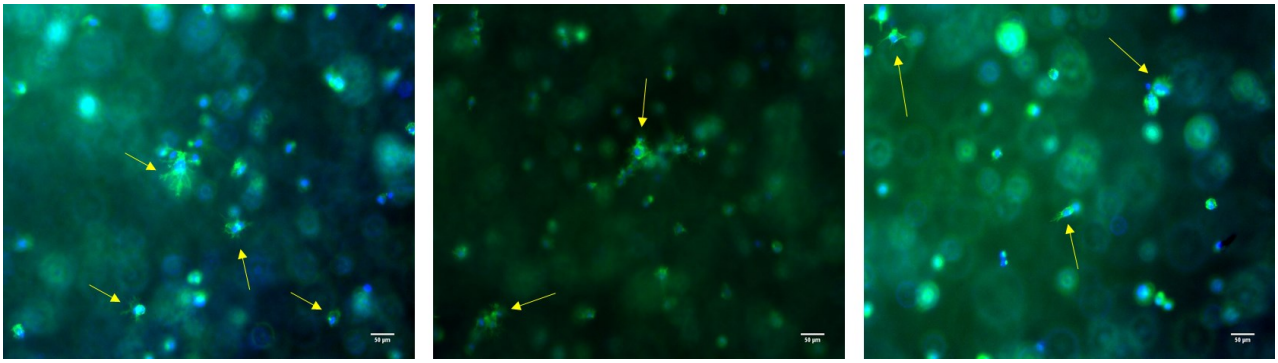

Figure 50 Composite images taken from NHDF embedded in HA-DTPH-dHA$^+$-RGD hydrogel. Spreading of fibroblasts (indicated with yellow arrows) was observed 24 hours post-embedding inside the hydrogel. Cell nuclei are stained with DAPI. Actin is directly stained with phalloidin. Scale bar = 50 µm

By incorporating RGD inside the hydrogel, spreading of the embedded cells were observable. Remarkably the phenotype of the NHDF cells were not resembling the expected spindle shape like phenotype, which can be observed on a 2D substrate, but more a star like phenotype. To examine further the biocompatibility of the hydrogel cells were again embedded and cultivated for five weeks within the hydrogel. Thereby the media was changed every third day to provide necessary nutrition (Fig.51).

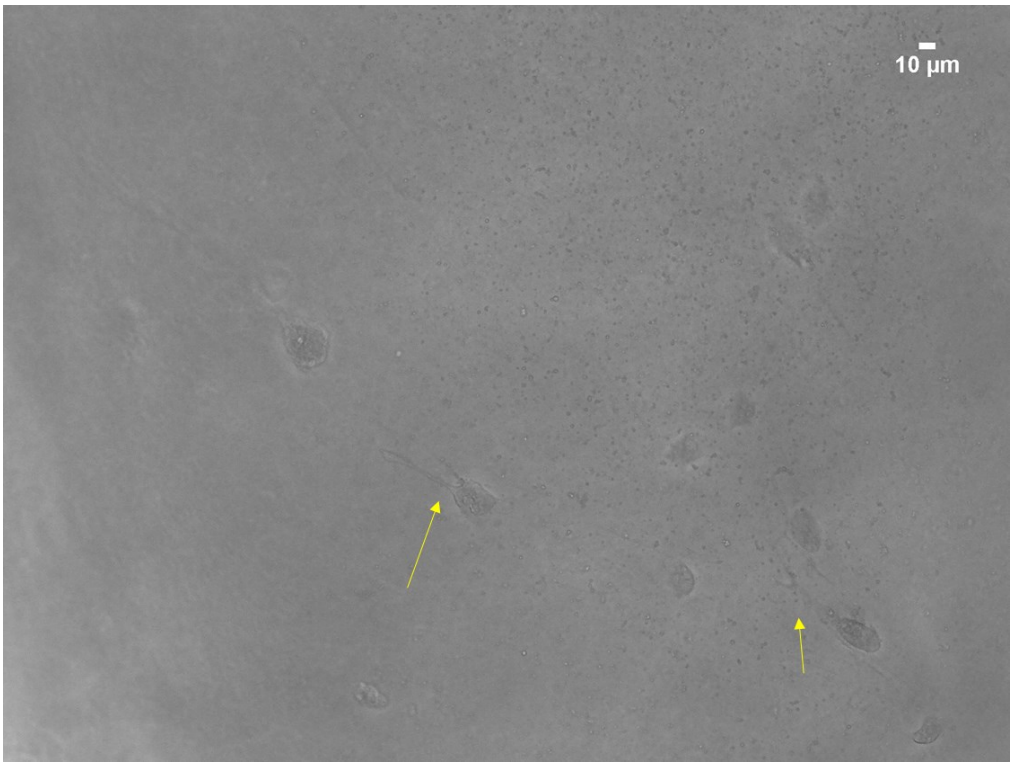

Figure 51 NHDF cells embedded in HA-DTPH-dHA⁺ hydrogel for five weeks. NHDF cells showed the formation of filopodia (indicated by yellow arrow) within five weeks post-embedding. Scale bar = 10 µm

A striking observation were made after incubation of embedded NHDF cells inside the **HA- DTPH-dHA⁺** hydrogel without an additional adhesion inducing motif after five weeks post-embedding (Fig. 51). Cells were not round anymore as seen before (Fig.50) but appeared spreaded and formed filopodia like structures (yellow arrow).

Taken all together, it can be concluded that the method of cell encapsulation inside of the **HA- DTPH-dHA⁺** was successfully established and furthermore showed a high viability of cells. It was also confirmed that incorporating RGD led to cell spreading, which makes the system suitable for example tissue engineering or organoid formation. Surprisingly, cells spread even without a spreading induced motif, like RGD, which indicates: (1) NHDF cells expressed hydrogel degrading enzymes to spread within the gel, (2) the formation of their own extracellular matrix, which induced cell spreading or (3) non-integrin mediated cell spreading via CD44 and RHAMM. These findings have to be further investigated regarding the

CD44/RHAMM expression and ECM protein expression by NHDF cells. Additionally, this experiment should be repeated with **HA-DTPH-dHA^{+}** with varying cross-linker concentration to investigate the influence of stiffness and charge to the NHDF spreading behaviour. However, this hydrogel system can be used to study cell migration, general behaviour, immobilization and release thereby offering an interesting platform for basic ECM mimicking experiments regarding the “purified” role of HA. In future, possible insights from this platform could serve as a theoretical basis for developing a material suited for application in wound dressing and tissue regeneration *in situ*. This may imply HA influencing mechanotransduction in turn stimulating intracellular response. Also, migration of fibroblasts into the hydrogel could be further investigated since this is an interesting aspect to pursue in treating chronic wounds by recruiting cells to the damaged tissues. For this purpose, seeding of NHDF on the gels surface and subsequent trancing of possible cell migration into the scaffold could be performed.

4 Conclusion and Outlook

4.1 Conclusion

In conclusion, this thesis presents a novel hybrid double cross-linked HA based hydrogel system, held together by chemical and physical cross-links, and developed under consideration of the bottom up approach of synthetic biology. The synthesized hydrogel is successfully established under biocompatible conditions for the use in a biomedical field.

Hydrogel synthesis were performed with 74 kDa HA, thiol functionalized in a range of 29% - 58% and combined with three different ionic cross-linkers. Considering the maintenance of the biocompatibility, ionic cross-linker were chosen accordingly: (1) a HA based ionic cross-linker, which is synthesized by acidic degradation and further deacetylated to generate a positively charged amine group, (2) charged glucosamine (**GluA$^+$**) and (3) ammonium chloride (**NH_4^+**). The used ionic cross-linker were also chosen due to their increasing capacity to form hydrogen bonds from **NH_4^+** to **GluA$^+$** and **dHA$^+$**: Adding the ionic cross-linker resulted in a stable, reproducible hydrogel, due to the simultaneously formed disulfide bonds and physical cross-links, such as hydrogen bonds and salt bridges. The amount of chemical cross-links is further determined by the degree of functionalization of the HA backbone as well as on the concentration and type of cross-linker. Hydrogel formation without an ionic cross-linker required oxidation of the thiol groups with hydrogen peroxide to gain a stable hydrogel. The physico-chemical properties of HA hydrogels prepared with any of the charged cross-linkers (**Cl$^+$**) depend both on chemical and physical cross-links. Thus mechanical stiffness, swelling capacity and mesh sizes can be tuned by adjusting the amount of formed chemical and physical cross-links by varying: (1) the thiolation degree, (2) the ionic cross-linker, respectively regarding its capacity to form hydrogen bonds and (3) the concentration of the used ionic cross-linker. Furthermore, the developed hybrid double cross-linked HA based hydrogel system showed a higher sensitivity to external stimuli like, temperature, ionic solution and pH, than the oxidized **HA-DTPH-Ox**. hydrogel, this opens up more tunability regarding a

biomedical application. Incubating the hydrogel system in different ionic solutions showed the impact of monovalent and divalent cations on the swelling behavior. Swelling ratio decreased from NaCl to $MgCl_2$ and $CaCl_2$, indicating a stronger interaction of the polymer chain with the divalent cations. **HA-DTPH-Cl$^+$** in pH solution ranging from pH 4 to 10 showed an increase in swelling from pH 4 to 7, reaching the maximum at pH 7 and started to shrink from 8 onwards. Moreover, the hydrogel system **HA-DTPH-dHA$^+$**, showed while incubation in a solution of pH 7 a negative feedback loop on its swelling behavior. In the swollen state of the hydrogel, ionic cross-linker leaked out of the hydrogel, subsequently acidifies the solution, which acts then as a feedback to the hydrogel and results in the shrinking of the hydrogel. This shrinking of the hydrogel stopped the leakage of the ionic cross-linker **dHA$^+$**. In addition to the physico chemical properties, biological applicability of the presented hydrogel was also confirmed and showed a different adhesive behavior of NHDF cells dependent on the physical cross-link and thereby resulting stiffness. Especially, the formed physical cross-links stabilized the system while incubation with HA degrading enzymes. Thus, **HA-DTPH-dHA$^+$** showed a higher half-life time than **HA-DTPH-Ox.** Since non-immunogenicity, biodegradability and non-toxicity was already demonstrated for the **HA-DTPH-dHA$^+$** the cytocompatibility of the gel was investigated in this work by studying more complex interaction of cells in a 3D context. Encapsulation of NHDF cells were successfully established and the viability was shown after 24 hours of incubation of the NHDF cells inside of the hydrogel. Moreover, NHDF cells showed after five weeks of incubation spreading behaviour within the hydrogel, indicating the expression of HA degrading enzymes and expression of adhesion and spreading responsible receptors. Furthermore, it was shown that the hydrogel system is stable enough to handle an increase in complexity by adding RGD. In summary this novel hybrid double cross-linked HA based hydrogel could in future make a difference in improving drug delivery strategies *in vivo*, in further promoting our understanding of cell migration and behavior in synthetic scaffolds *in vitro* or in finding yet better treatment options regarding tissue damage *in situ*.

4.2 Outlook

The developed hybrid double cross-linked HA based hydrogel is a great tool to distinguish the effect of chemical and physical cross-links in hydrogels with polyanionic polymer backbones. To further examine the influence of physical and chemical cross-link the length of HA used for the hydrogel synthesis could be varied. The use of longer HA gives the opportunity to also determine the impact of the HA structure on the hydrogel synthesis, since longer HA tends to entanglements and intermolecular formed physical cross-links. Another possibility to study the influence of physical cross-links on the hydrogel formation in an intermolecular manner, is the deacetylation of the thiol functionalized HA. By this the positive charged group is immobilized on the HA structure and can form physical cross-links within the polymer chain. The hybrid double cross-linked HA based hydrogel could also be varied in the used GAG, such as chondroitin sulfate and keratin sulfate. Regarding the desired study any other GAG could be functionalized and used as the hydrogel backbone. Several biomedical applications are suitable for the developed hybrid double cross-linked hydrogel. First of all, it can serve as a biosensor under specific pH conditions. For example, an incorporated fluorescence molecule, would diffuse out of the hydrogel upon swelling at alkaline pH, together with the ionic cross-linker **dHA**$^{+}$, and thus signalling the alkaline pH. Due to the feedback loop the diffusion of the fluorescence molecule would stop after the acidification of the solution. It could also be used as a mucosa mimicking system in the gastro intestinal tract. Here glycoproteins with cysteine groups bind to the mucosa layer via disulphide bond formation (Bernkop-schnu, 2005). If the mucosa gel layer isn't stable, which occurs in diseases like ulcerative colitis then the wall of the gastro intestinal tract is not protected (Johanson et al., 2013). Therefor the established hydrogel system could be used as a mucosa mimicking gel layer. Since, I proved that I can control the amount of free thiol groups via the added ionic cross-linker it would give the possibility with free thiol groups on the surface of the hydrogel to react with the cysteine groups of the glycoproteins via disulphide bond formation. The high biocompatibility gives also the opportunity to use the hydrogel system as a tissue engineering tool, since it has been

shown that NHDF cells can migrate within the hydrogel, thus it can mimic for example the dermis of the skin.

Figure 52 shows possible biomedical application for the established **HA- DTPH-dHA$^+$** hydrogel.

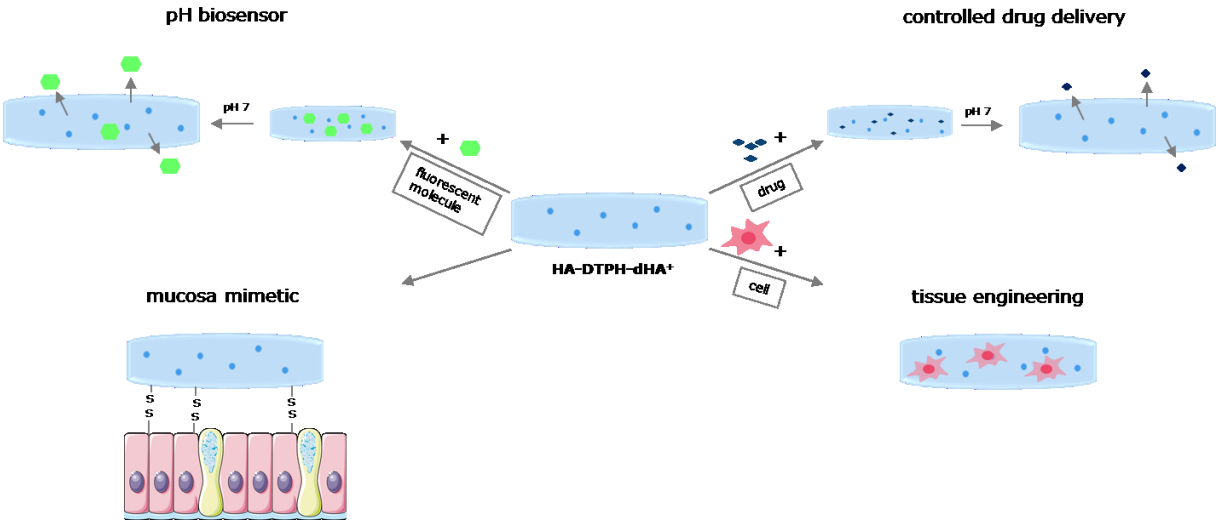

Figure 52 Possible Biomedical application for HA-DTPH-dHA$^+$ hydrogel

The developed hydrogel showed also a great potential to use as a controlled drug delivery system combined with as wound dressing. During the wound healing process, a switch of pH is observed. The pH of the acute wound is alkaline (7-8) and decreases during the healing process (4-5). The pH during the wound healing process is essential for a successful healing process, thus it has been shown that the pH of chronic wounds does not decrease (Kumar and Honnegowda, 2015). Hence, a pH-responsive release of therapeutic drugs or growth factors could be beneficial for effective treatment of wounds (Banerjee et al. 2012). Controlled drug release in combination with a pH regulating system, like the hybrid double cross-linked HA based hydrogel system, established in this thesis, could be valuable.

A possible application as a wound dressing is presented in Figure 53.

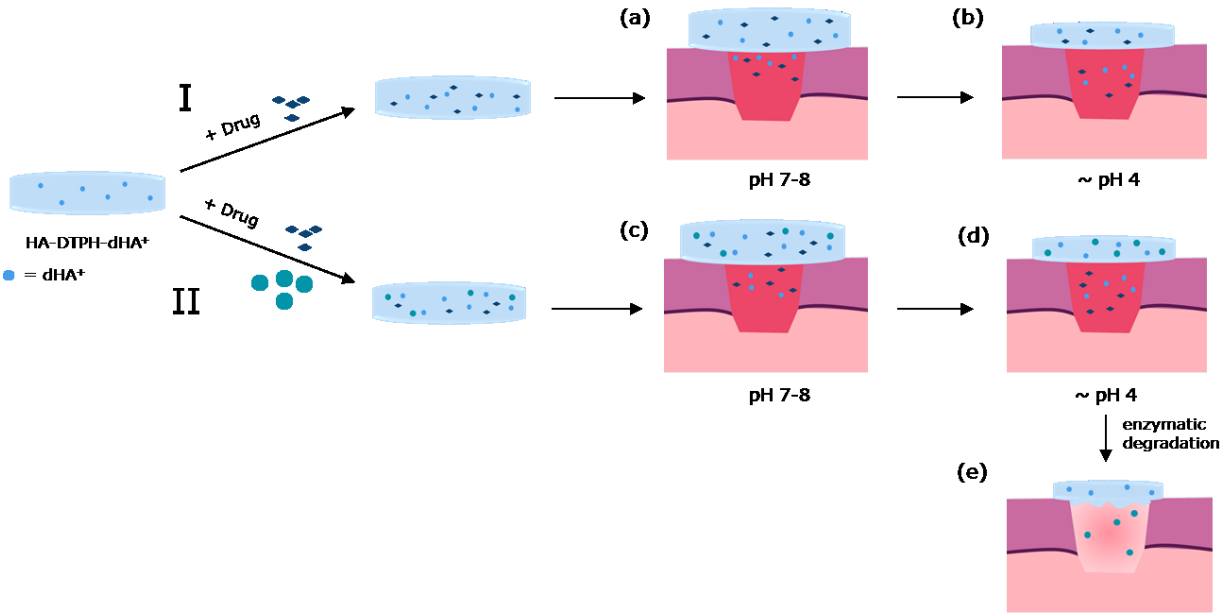

Figure 53 Possible application of the hybrid double cross-linked HA based hydrogel as a: (1) pH regulator and (2) pH controlled drug release wound dressing. (I) Drug loaded HA-DTPH-dHA+ hydrogel. Hydrogel swelling upon pH 7- 8 and release of dHA+ and possible incorporated drug a, acidification of wound site lead to shrinking of hydrogel and stop of drug release b. (II) Two in size different drug loaded HA-DTPH-dHA+ hydrogel. Hydrogel swelling upon pH 7- 8 and release of dHA+ and possible incorporated small drug c, acidification of wound site lead to shrinking of hydrogel and stop of drug release d, upon enzymatic degradation released bigger drug e.

I) Drug incorporated **HA-DTPH-dHA$^+$** hydrogel swells upon responding to the alkaline pH and release desired drug and **dHA$^+$**. Consequently, wound site acidifies, which leads to the stop of drug release and **dHA$^+$**. II) Two, in size different, drugs are incorporated inside **HA-DTPH-dHA$^+$** hydrogel and the smaller drug and **dHA$^+$** would be released upon swelling at alkaline pH and result again in acidification. Upon enzymatic degradation the bigger drug could be released. To utilize the established hydrogel as a wound dressing model, a few properties such as biocompatibility and degradability have to be characterized.

5 Appendix

5.1 Additional Information on the Presented Experiments

5.1.1 NMR Data of Synthesized Compounds

HA-DTPH:

^{1}H-NMR (600Hz, D_2O): δ = 3.18 (m, 5H, H-1/2, SH), 3.15-2.0 (m, Carbohydrate protons), 1.77 (s, 3H, C(=O) CH_3) ppm.

HA-HPH:

^{1}H-NMR (600Hz, D_2O): δ = 3.15-2.0 (m, Carbohydrate protons), 1.77 (s, 3H, C(=O) CH_3) ppm.

DTPH:

^{1}H-NMR (600Hz, D_2O): δ = 2.90 (t, 2H, CH_2C=O), 2.50 (t, 2H, S-CH_2) ppm.

dHA$^+$:

^{1}H-NMR (600Hz, D_2O): δ = 5.48 (d, $J_{1,2}$ = 3,5 Hz; GaIN H-1α), 4.72 (d, $J_{1,2}$ = 8,0 Hz; GaIN H-1β), 4.73, 4.72 (2d, $J_{1,2}$ = 7,5 Hz, 1H; GlcA H-1α,β), 4.30-4.20 (m; GaIN H-3α, H-4, GlcA H-5), 4.15-4.06 (m; GaIN H-3β, GlcA H-4), 3.80-3.70 (m; GaIN H-5, 2H-6), 3.65 (dd, $J_{2,3}$ = 11,0 Hz; GaIN H-2α), 3.56 (m; GlcA H-3α,β), 3.45 (m; GlcA H-2α,β), 3.34 (dd, $J_{2,3}$ = 11,0 Hz; GaIN H-2β) ppm.

5.2 Experimental Values of Presented Graphs

In this chapter, all experimental data points presented, following the order they appear in chapter three, are summarized

5.2.1 Experimental Values of Ellman's Assay

Experimental values of free thiol groups of **HA-DTPH-Cl⁺/HA-DTPH/HADTPH-Ox**. hydrogels determined by using the Ellman's assay after 24 hours (Tab.4) and 72 hours (Tab.5).

Table 4 Exact values of Ellman´s assay for HA-DTPH-Cl⁺ and HA-DTPH with three different thiolation degrees after 24 hours. All values represent mean standard deviation of triplicates.

24 h	HA-DTPH$^{29\%}$	HA-DTPH$^{42\%}$	HA-DTPH$^{58\%}$
NH_4^+	33.0 ± 0.03	34.3 ± 0.03	37.7 ± 0.3
$GluA^+$	10.0 ± 0.02	17.8 ± 0.01	21.3 ± 0.06
dHA^+	7.0 ± 0.01	7.5 ± 0.06	7.5 ± 0.08
Without Linker	35.9 ± 0.01	98.0 ± 0.01	89.5 ± 0.085

Table 5 Exact values of Ellman´s assay for HA-DTPH-Cl⁺ and HA-DTPH with three different thiolation degrees after 72 hours. All values represent mean and standard deviation of triplicates.

72 h	HA-DTPH$^{29\%}$	HA-DTPH$^{42\%}$	HA-DTPH$^{58\%}$
NH_4^+	16.0 ±0.02	8.3 ± 0.04	16.1 ± 0.1
$GluA^+$	6.0 ± 0.03	5.4 ± 0.04	15.2 ± 0.05
dHA^+	6.0 ± 0.02	5.0 ± 0.02	5.0 ± 0.04
Without Linker	20.4 ± 0.03	72.0 ± 0.03	50.0 ± 0.04
H_2O_2	7.5 ± 0.01	6.3 ± 0.08	4.5 ± 0.01

5.2.2 Experimental Values of Young's Moduli

Experimental values of Young's moduli of fully swollen **HA-DTPH-Cl⁺/HA-DTPH-Ox.** hydrogels with cross-linker ratio 1.0 to free remaining negative charged groups on the polymer chain (Tab.6).

Table 6 Exact values of Young's moduli of fully swollen HA-DTPH-Cl⁺/HA-DTPH-Ox. hydrogels with cross-linker ratio 1.0 to free remaining negative charged groups on the polymer chain. All values represent mean and standard deviation of triplicates.

1 equ.	HA-DTPH$^{29\%}$ Young's modulus [kPa]	HA-DTPH$^{42\%}$ Young's modulus [kPa]	HA-DTPH$^{58\%}$ Young's modulus [kPa]
H_2O_2	0.13 ± 0.058	0.2 ± 0.2	1.2 ± 0.3
NH_4^+	0.8 ± 0.05	1.5 ± 0.3	2.4 ± 0.071
$GluA^+$	1.16 ± 0.23	3.2 ± 0.06	4.0 ± 0.3
dHA^+	2.93 ± 0.35	4.2 ± 0.3	7.2 ± 0.7

5.2.3 Experimental Values of Swelling Ratio in Water and Calculated Mesh Sizes

Experimental values of swelling ratio of **HA-DTPH-Cl$^+$/HA-DTPH-Ox.** hydrogels at two defined temperatures 22 °C (Tab.7) and 37°C (Tab.8).

Table 7 Experimental values of swelling ratio of HA-DTPH-Cl$^+$/HA-DTPH-Ox. hydrogels at 22 °C. All values represent mean standard deviation of triplicates.

22°C	HA-DTPH$^{29\%}$	HA-DTPH$^{42\%}$	HA-DTPH$^{58\%}$
H_2O_2	40.5 ± 5.2	44.2 ± 8.6	23.1 ± 1.6
dHA^+	86.2 ± 8.4	19.5 ± 0.6	43.5 ± 1.4
$GluA^+$	221.6 ± 8.7	180.5 ± 4.7	133.7 ± 4.5
NH_4^+	319.1 ± 28.7	169.8 ± 1.5	160.7 ± 9.4

***Table 8 Experimental values of swelling ratio of HA-DTPH-Cl$^+$/HA-DTPH-Ox. hydrogels at 37 °C.** All values represent mean standard deviation of triplicates.*

37°C	HA-DTPH$^{29\%}$	HA-DTPH$^{42\%}$	HA-DTPH$^{58\%}$
H_2O_2	47.8 ± 4.8	55.1 ± 3.1	28.4 ± 1.8
dHA^+	106.4 ± 3.5	188.0 ± 8.5	70.5.5 ± 4.4
$GluA^+$	264.1 ± 24.1	268.0 ± 2.6	190.4± 2.9
NH_4^+	339.5 ± 15.7	55.1.8 ± 3.1	23.1 ± 1.6

Calculated values of mesh size of **HA-DTPH-Cl$^+$/HA-DTPH-Ox.** hydrogels based on swelling ratio (Tab.9)

Table 9 Calculated values of mesh size of HA-DTPH-Cl$^+$/HA-DTPH-Ox. hydrogels with HA-DTPH29% based on swelling ratio. *All values represent mean standard deviation of triplicates.*

	HA-DTPH$^{29\%}$ mesh size[nm]	**HA-DTPH$^{42\%}$ mesh size[nm]**	**HA-DTPH$^{58\%}$ mesh size[nm]**
H_2O_2	19.3 ± 1.5	14.6 ± 0.4	13.2 ± 1.2
dHA^+	22.2 ± 2.3	19.9 ± 2.3	14.9 ± 2.3
$GluA^+$	26.8 ± 2.6	23.5 ± 2.8	22.1 ± 1.2
NH_4^+	34.7 ± 5.0	28.9 ± 3.8	23.4 ± 3.2

5.2.4 Experimental Values of Swelling Ratio at pH from 3 to 10

Experimental values of swelling ratio of **HA-DTPH-Cl^{+}/HA-DTPH-Ox.** hydrogels with **HA- DTPH$^{29\%}$** (Tab.10) **HA- DTPH$^{58\%}$** (Tab.11) in pH solution ranging from 3-10.

Table 10 Exact values of swelling ratio HA-DTPH-Cl^{+}/HA-DTPH-Ox. hydrogels with HA-DTPH$^{29\%}$ in pH solution ranging from 3-10. *All values represent mean standard deviation of triplicates.*

pH	NH_4^+	$GluA^+$	dHA^+	H_2O_2
3	65.85 ± 9.56	56.36±4.57	29.88 ± 3.17	13.70 ± 2.57
4	76.62 ± 2.33	68.78 ± 6.26	44.88 ± 11.79	19.02 ± 0.97
5	81.15 ± 5.29	73.00 ± 8.08	48.82 ± 5.23	20.83 ± 2.17
6	148.74±14.30	95.79 ± 9.89	72.29 ± 3.25	30.84 ± 4.41
7	208.04±15.6	163.27±14.98	94.54 ± 0.80	55.28 ± 2.00
8	70.7 ± 11.5	69.77 ± 3.75	82.03 ± 1.85	44.85 ± 6.85
9	63.9 ± 2.4	69.64 ± 14.5	72.61 ± 2.29	24.03 ± 3.55
10	67.06 ± 5.4	58.15 ± 7.13	55.13 ± 2.07	16.91 ± 2.31

Table 11 Exact values of swelling ratio HA-DTPH-Cl^{+}/HA-DTPH-Ox. hydrogels with HA-DTPH$^{58\%}$ in pH solution ranging from 3-10. *All values represent mean standard deviation of triplicates.*

pH	NH_4^+	$GluA^+$	dHA^+	H_2O_2
3	70.46 ± 9.6	53.55±4.06	7.64±1.98	12.28±0.95
4	70.30 ± 2.3	59.52±3.20	34.18±4.54	17.14±1.22
5	83.98 ± 5.3	69.81±6.90	41.48±5.47	18.83±2.60
6	108.13±15.8	78.20±1.30	45.96±6.84	23.16±1.49
7	148.76±7.2	113.14±15.07	57.07±4.18	37.10±1.87
8	70.03 ± 5.6	68.28±3.36	43.55±3.28	34.79±1.72
9	58.51 ± 4.1	59.28±1.51	43.16±4.97	30.46±1.01
10	45.62 ± 3.4	39.25±2.94	28.24±6.02	24.12±0.75

5.2.5 Experimental Values of Swelling Ratio for Varying Ionic Strength Solution

Experimental values of swelling ratio of **HA-DTPH-Cl$^+$/HA-DTPH-Ox.** hydrogels with **HA- DTPH$^{29\%/58\%}$** in different ionic solution and different ionic concentrations (Tab.12).

Table 12 Exact values of swelling ratio of HA-DTPH-Cl$^+$/HA-DTPH-Ox. hydrogels with HA-DTPH$^{29\%/58\%}$ in different ionic solution and different ionic concentrations. *All values represent mean standard deviation of triplicates.*

Thiolation degree	**50 mM NaCl**	**150 mM NaCl**	**300 Mm NaCl**
29%	162.38±15.47	124.28±12.64	63.72±1.25
58%	110.72±7.25	87.13±5.48	43.18±0.33
	50 mM $MgCl_2$	**150 mM $MgCl_2$**	**300 mM $MgCl_2$**
29%	56.33±2.02	38.71±1.71	21.46±2.39
58%	49.25±3.68	29.88±2.63	16.00±0.72
	50 mM $CaCl_2$	**150 mM $CaCl_2$**	**300 mM $CaCl_2$**
29%	39.37±0.48	21.06±1.71	18.76±0.82
58%	33.74±0.27	17.99±1.35	13.30±0.42

5.2.6 Experimental Values of Cell Viability Assay

Experimental values of the cell viability assay upon treatment of NHDF cells with **dHA⁺** (Tab.13) and **HA- DTPH** (Tab.14).

Table 13 Exact values of cell viability (Absorbance 490 nm) upon dHA⁺ treatment of NHDF cells over 24/48 hours. *All values represent mean and SEM values of n = 9.*

Incubation time	0.01 mg/mL	0.1 mg/mL	1 mg/mL	Untreated
24 h	0.095 ± 0.014	0.077 ± 0.013	0.112 ± 0.020	0.083 ± 0.013
48 h	0.273 ± 0.064	0.314 ± 0.043	0.269 ± 0.030	0.211 ± 0.036

Table 14 Exact values of cell viability (Absorbance 490 nm) upon HA-DTPH treatment of NHDF cells over 24/48 hours. *All values represent mean and SEM values of n = 9.*

Incubation time	0.01 mg/mL	0.1 mg/mL	1 mg/mL	Untreated
24 h	0.106 ± 0.013	0.088 ± 0.013	0.119 ± 0.018	0.093 ± 0.013
48 h	0.212 ± 0.021	0.198 ± 0.027	0.195 ± 0.028	0.256 ± 0.036

5.2.7 Experimental Values of Enzymatic Degradation

Experimental values of half-lives for enzymatic degradation of **HA-DTPH-Cl^{+}/HA-DTPH-Ox.** hydrogels with **HA- DTPH$^{29\%/42\%/58\%}$** with HA degrading enzyme: hyaluronidase (Tab.15) and lyase (Tab.16).

Table 15 Exact values of half-lives of HA-DTPH-dHA^{+}/HA-DTPH-Ox. hydrogels with HA- DTPH$^{29\%/42\%/58\%}$ with HA degrading enzyme: lyase. *All values represent mean standard deviation of triplicates.*

lyase	HA-DTPH-dHA^{+} Half-life [h]	HA-DTPH-Ox. Half-life [h]
29%	1.8 ± 0.3	0.3 ± 0.03
42%	2.2 ± 0.1	0.4 ± 0.02
58%$^{+}$	3.3 ± 0.3	0.4 ± 0.04

Table 16 Exact values of half-lives of HA-DTPH-dHA^{+}/HA-DTPH-Ox. hydrogels with HA- DTPH$^{29\%/42\%/58\%}$ with HA degrading enzyme: hyaluronidase. *All values represent mean standard deviation of triplicates.*

hyaluronidase	HA-DTPH-dHA^{+} Half-life [h]	HA-DTPH-Ox. Half-life [h]
29%	2.2 ± 0.3	0.5 ± 0.03
42%	3.3 ± 0.03	0.7 ± 0.03
58%$^{+}$	4.2 ± 0.3	0.7 ± 0.04

5.3 Additional Information on Enzymatic Degradation of HA Hydrogels

Exemplary graph of Exponential Decay with Fit Values for Degradation of HA-DTPH-dHA$^+$ Hydrogel in Hyaluronidase

To determine the half-life of **HA-DTPH-dHA$^+$** hydrogel in different enzyme solutions, a first order exponential decay is fitted to the weight measurements done over time (2.6.1) (Fig.54). For **HA- DTPH$^{29\%}$- dHA$^+$** one exemplary data set with fit values is shown Tab.17.

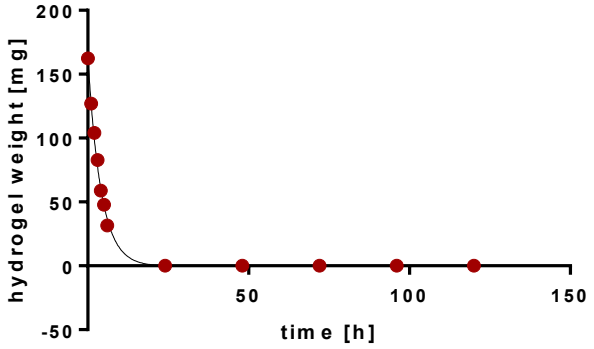

Figure 54 Degradation of HA- DTPH$^{29\%}$- dHA$^+$ on hyaluronidase follows an exponential decay first order. The weight loss of the hydrogel over time can be fitted and half-life can subsequently be calculated from the fit.

***Table 17 Fit values for first order exponential decay for HA- DTPH$^{29\%}$- dHA$^+$ degradation in hyaluronidase.** Values are given after analysis in "Graph Pad Prism7" (version 7.0c, GraphPad Software Inc.).*

Best-Fit parameter	#1
Y0	164,1
NS	-0,4538
K	0,2461
HalfLife	2,817
Std. Error	
Y0	2,512
Goodness of Fit	
Degrees of Freedom	9
R square	0,9977

Absolute Sum of Squares	80,22

5.4 Additional Information on Swelling behaviour of HA-DTPH-dHA^{+}

In an attempt to visualize the swelling behavior **HA-DTPH$^{58\%}$-dHA^{+}**, it was recorded over time during the swelling process in an aqueous solution of pH 7 (Fig.55).

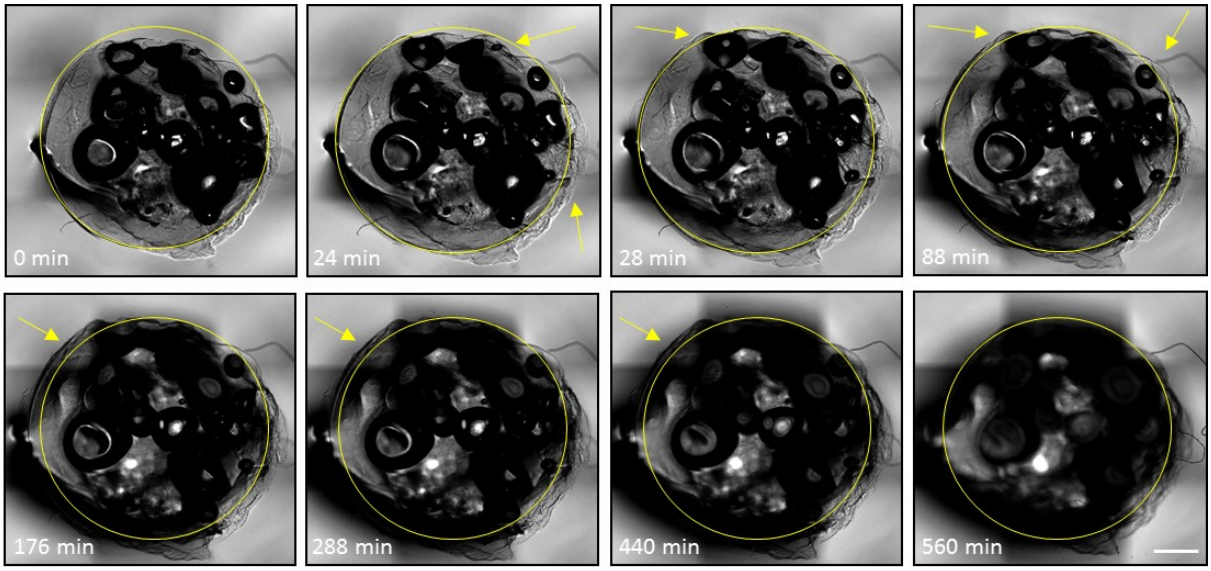

Figure 55 Swelling behavior of HA-DTPH$^{58\%}$-dHA^{+} hydrogel over a total recording time of 14 hours. Depicted are overviews over the full gel (stitched from 12 single images). Swelling and shrinking of the hydrogel are observable, yellow arrows are indicating the change of the hydrogel size upon swelling and shrinking. Scale bar: 50 µm

Imaging the swelling process of **HA-DTPH-dHA^{+}** upon responding to the surrounding pH confirmed successfully the results, described in 3.4.2.1. The hydrogel starts to swell (pH 7) within 24 min until it reaches equilibrium after 288 min. After 440 min it starts to shrink and collapses to the center upon acidifying the surrounding solution (pH 4.7). A number of limitations may influence the results obtained: (1) As anticipated, there were some discrepancies for the equilibrium time, since swell experiments were performed before under shaking and this was not possible while imaging, which had an impact on the diffusion of the solution through the hydrogel and consequently on the swelling process. (2) While the

shrinking process the hydrogel got smaller and the focus of the microscope got lost, which resulted in a blurry image (560 min). (3) The fully swollen state is difficult to image, since it increases in the height. (4) Presented are preliminary images, due to the coronavirus this experiment could not be repeated.

Bibliography

Acid, H. *et al.* (2020) 'Ulva intestinalis Protein Extracts Promote In Vitro Dermal Fibroblasts'.

Ahmed, E. M. (2015) 'Hydrogel : Preparation , characterization , and applications : A review', *Journal of Advanced Research*. Cairo University, 6(2), pp. 105–121. doi: 10.1016/j.jare.2013.07.006.

Alesa, D. *et al.* (2017) 'A review of the designs and prominent biomedical advances of natural and synthetic hydrogel formulations', 88(01), pp. 373–392. doi: 10.1016/j.eurpolymj.2017.01.027.

Allen, E. M. G. and Mieyal, J. J. (2012) 'Protein-Thiol Oxidation and Cell Death : Regulatory Role of Glutaredoxins', 17(12), pp. 1748–1763. doi: 10.1089/ars.2012.4644.

Andrianantoandro, E. *et al.* (2006) 'Synthetic biology : new engineering rules for an emerging discipline', pp. 1–14. doi: 10.1038/msb4100073.

Article, O. (2004) 'Renal hyaluronan accumulation and hyaluronan synthase expression after ischaemia-reperfusion injury in the rat Viktoria Go', 19(4), pp. 823–830. doi: 10.1093/ndt/gfh003.

Ballard, N., Asua, J. M. and Jime, N. (2019) 'Hydrogen Bond-Directed Formation of Sti ff Polymer Films Using Naturally Occurring Polyphenols'. doi: 10.1021/acs.macromol.9b01694.

Barnes, J. M., Przybyla, L. and Weaver, V. M. (2017) 'Tissue mechanics regulate brain development , homeostasis and disease', pp. 71–82. doi: 10.1242/jcs.191742.

Bennett, N. T. and Schultz, G. S. (1993) 'Growth factors and wound healing: Part II. Role in normal and chronic wound healing.', *American journal of surgery*, 166(1), pp. 74–81. doi: 10.1016/S0002-9610(05)80589-6.

Bergen, L. A. H. Van, Roos, G. and Proft, F. De (2014) 'From Thiol to Sulfonic Acid: Modeling the Oxidation Pathway of Protein Thiols by Hydrogen Peroxide'. doi: 10.1021/jp5018339.

Berger, J. *et al.* (2004) 'Structure and interactions in covalently and ionically crosslinked chitosan hydrogels for biomedical applications', *European Journal of Pharmaceutics and Biopharmaceutics*, 57(1), pp. 19–34. doi: 10.1016/S0939-6411(03)00161-9.

Bernkop-schnu, A. (2005) 'Thiomers : A new generation of mucoadhesive polymers B', 57, pp. 1569–1582. doi: 10.1016/j.addr.2005.07.002.

Bi, F. *et al.* (2010) 'Physicochemical characterization and ionic studies of sodium alginate from Sargassum terrarium (brown algae)', 9104. doi: 10.1080/00319100600745198.

Breakspear, S., Noecker, B. and Popescu, C. (2019) 'Relevance and Evaluation of Hydrogen and Disul fi de Bond Contribution to the Mechanics of Hard α - Keratin Fibers'. doi: 10.1021/acs.jpcb.9b01690.

Bro, E., Friedl, P. and Za, K. S. (1998) 'Cell Migration Strategies in 3-D Extracellular Matrix : Differences in Morphology , Cell Matrix Interactions , and Integrin Function', 378(96), pp. 369–378.

Budday, S. *et al.* (2016) 'HHS Public Access', pp. 318–330. doi: 10.1016/j.jmbbm.2015.02.024.Mechanical.

Buenger, D., Topuz, F. and Groll, J. (2012) 'Progress in Polymer Science Hydrogels in sensing applications', *Progress in Polymer Science*. Elsevier Ltd, 37(12), pp. 1678–1719. doi: 10.1016/j.progpolymsci.2012.09.001.

Buhren, B. A. *et al.* (2016) 'Hyaluronidase : from clinical applications to molecular and cellular mechanisms', *European Journal of Medical Research*. BioMed Central, pp. 1–7. doi: 10.1186/s40001-016-0201-5.

Cao, Y. *et al.* (2019) 'Journal of Colloid and Interface Science Tunable keratin hydrogel based on disulfide shuffling strategy for drug delivery and tissue engineering', *Journal of Colloid And Interface Science*. Elsevier Inc., 544, pp. 121–129. doi: 10.1016/j.jcis.2019.02.049.

Cha, C. *et al.* (2011) 'Acta Biomaterialia Tuning the dependency between stiffness and permeability of a cell encapsulating hydrogel with hydrophilic pendant chains', *Acta Biomaterialia*. Acta Materialia Inc., 7(10), pp. 3719–3728. doi: 10.1016/j.actbio.2011.06.017.

Chaicharoenaudomrung, N., Kunhorm, P. and Noisa, P. (2019) 'Author contributions ':, 11(12), pp. 1065–1084. doi: 10.4252/wjsc.v11.i12.1065.

Chase, F. (1999) 'Hyaluronan forms specific stable tertiary structures in aqueous solution : A 13 C NMR study', 96(April), pp. 4850–4855.

Chen, S. and Zommorodi, M. (2004) 'Hydrogel modified uptake of salt ions and calcium in Populus euphratica under saline conditions', pp. 175–183. doi: 10.1007/s00468-003-0267-x.

Chen, X. and Thibeault, S. L. (2010) 'Biocompatibility of a synthetic extracellular matrix on immortalized vocal fold fibroblasts in 3-D culture', *Acta Biomaterialia*, 6(8), pp. 2940–2948. doi: 10.1016/j.actbio.2010.01.032.

Cotts, S. (2016) 'Fundamentals of Polymer Rheology Rheology : An Introduction = Viscosity = Modulus Shear Flow in Parallel Plates', pp. 1–25.

Coulocheri, S. A. *et al.* (2007) 'Hydrogen bonds in protein e DNA complexes : Where geometry meets plasticity', 89, pp. 1291–1303. doi: 10.1016/j.biochi.2007.07.020.

Cowman, M. K. *et al.* (2005) 'Extended , Relaxed , and Condensed Conformations of Hyaluronan Observed by Atomic Force Microscopy', 88(January), pp. 590–602. doi: 10.1529/biophysj.104.049361.

Cox, T. R. and Erler, J. T. (2011) 'Remodeling and homeostasis of the extracellular matrix : implications for fibrotic diseases and cancer', 178, pp. 165–178. doi: 10.1242/dmm.004077.

Cyphert, J. M., Trempus, C. S. and Garantziotis, S. (2015) 'Size Matters : Molecular Weight Specificity of Hyaluronan Effects in Cell Biology'. Hindawi Publishing Corporation, 2015. doi: 10.1155/2015/563818.

Daniel, E. (2013) 'Materials Chemistry B', 1(31). doi: 10.1039/c3tb20193g.

Desiraju, G. R. (2011) 'Reflections on the Hydrogen Bond in Crystal Engineering', pp. 896–898. doi: 10.1021/cg200100m.

Donald, J. E., Kulp, D. W. and Degrado, W. F. (2012) 'NIH Public Access', 79(3), pp. 898–915. doi: 10.1002/prot.22927.Salt.

Drury, J. L. and Mooney, D. J. (2003) 'Hydrogels for tissue engineering : scaffold design variables and applications', 24, pp. 4337–4351. doi: 10.1016/S0142-9612(03)00340-5.

Dv, F. (no date) 'Viscoelasticity and dynamic mechanical testing', (1), pp. 1–7.

Ellman, G. L. (1958) 'A colorimetric method for determining low concentrations of mercaptans', *Archives of Biochemistry and Biophysics*, 74(2), pp. 443–450. doi: 10.1016/0003-9861(58)90014-6.

Engler, A. J. *et al.* (2006) 'Matrix Elasticity Directs Stem Cell Lineage Specification', pp. 677–689. doi: 10.1016/j.cell.2006.06.044.

Fajardo, A. R. *et al.* (2013) 'Reactive & Functional Polymers Dual-network hydrogels based on chemically and physically crosslinked chitosan / chondroitin sulfate', 73, pp. 1662–1671. doi: 10.1016/j.reactfunctpolym.2013.10.003.

Fallacara, A. (2018) 'Hyaluronic Acid in the Third Millennium'. doi: 10.3390/polym10070701.

Fernández-pérez, J. (2019) 'The impact of decellularization methods on extracellular matrix derived hydrogels', pp. 1–12.

Ferreira, L., Vidal, M. M. and Gil, M. H. (2000) 'Evaluation of poly (2-hydroxyethyl methacrylate) gels as drug delivery systems at different pH values', 194, pp. 169–180.

Gao, S. *et al.* (2018) 'Effects of high-concentration salt solutions and pH on swelling behavior of physically and chemically cross-linked hybrid hydrophobic association hydrogels with good mechanical strength', 4468. doi: 10.1080/1539445X.2018.1489844.

Ghobril, C. and Grinstaff, M. W. (2015) 'Chem Soc Rev The chemistry and engineering of polymeric hydrogel adhesives for wound closure : a tutorial'. Royal Society of Chemistry, pp. 1820–1835. doi: 10.1039/c4cs00332b.

Gil, E. S. and Hudson, S. M. (2004) 'Stimuli-reponsive polymers and their bioconjugates', 29, pp. 1173–1222. doi: 10.1016/j.progpolymsci.2004.08.003.

Gospodarowicz, D., Greenburg, G. and Birdwell, C. R. (1978) 'Determination of Cellular Shape by the Extracellular Matrix and Its Correlation with the Control of Cellular Growth1', (November), pp. 4155–4171.

Gregoritza, M., Goepferich, A. M. and Brandl, F. P. (2016) 'Polyanions effectively prevent protein conjugation and activity loss during hydrogel cross-linking', *Journal of Controlled Release*. Elsevier B.V., 238, pp. 92–102. doi: 10.1016/j.jconrel.2016.07.030.

Gritsch, L., Motta, F. L. and Natta, C. G. (2015) 'iMedPub Journals History and Applications of Hydrogels', pp. 1–23.

Gun, V. M., Savina, I. N. and Mikhalovsky, S. V (2017) 'Properties of Water Bound in Hydrogels'. doi: 10.3390/gels3040037.

Gupta, S. K., Mishra, N. C. and Dhasmana, A. (2018) 'Erratum to : Decellularization Methods for Scaffold Fabrication', (January), p. 7651. doi: 10.1007/7651.

Gyarmati, B., Némethy, Á. and Szilágyi, A. (2013) 'Reversible disulphide formation in polymer networks : A versatile functional group from synthesis to applications', 49, pp. 1268–1286. doi: 10.1016/j.eurpolymj.2013.03.001.

Haworth, N. L., George, J. E. G. R. A. and Wouters, M. A. (2010) 'Evaluating the stability of disulfide bridges in proteins : a torsional potential energy surface for diethyl disulfide', 33(July 2007), pp. 475–485. doi: 10.1080/08927020701361876.

Haxaire, K. *et al.* (2000) 'Conformational behavior of hyaluronan in relation to its physical properties as probed by molecular modeling', 10(6), pp. 587–594.

Highley, C. B., Prestwich, G. D. and Burdick, J. A. (2016) 'ScienceDirect Recent advances in hyaluronic acid hydrogels for biomedical applications', *Current Opinion in Biotechnology*. Elsevier Ltd, 40, pp. 35–40. doi: 10.1016/j.copbio.2016.02.008.

Hinderer, S., Lee, S. and Schenke-layland, K. (2016) 'ECM and ECM-like materials — Biomaterials for applications in regenerative medicine and cancer therapy ☆', *Advanced Drug Delivery Reviews*. The Authors, 97, pp. 260–269. doi: 10.1016/j.addr.2015.11.019.

Hobert, E. M. *et al.* (2014) 'chemistry and biology', 53(8), pp. 567–576. doi: 10.1002/ijch.201300063.Effective.

Horkay, F., Tasaki, I. and Basser, P. J. (2000) 'Osmotic Swelling of Polyacrylate Hydrogels in Physiological Salt Solutions', pp. 84–90. doi: 10.1021/bm9905031.

Hornof, M. D., Kast, C. E. and Bernkop-schnu, A. (2003) 'In vitro evaluation of the viscoelastic properties of chitosan – thioglycolic acid conjugates', 55, pp. 185–190. doi: 10.1016/S0939-6411(02)00162-5.

Hu, W., Wang, Z. and Xiao, Y. (2019) 'Biomaterials Science Advances in crosslinking strategies of biomedical hydrogels'. Royal Society of Chemistry, pp. 843–855. doi: 10.1039/c8bm01246f.

Hu, X. *et al.* (2015) 'Weak Hydrogen Bonding Enables Hard , Strong , Tough , and Elastic Hydrogels', pp. 6899–6905. doi: 10.1002/adma.201503724.

Huang, Y. *et al.* (2019) 'Gamma-Irradiation-Prepared Low Molecular Weight Hyaluronic Acid Promotes Skin Wound Healing', pp. 1–12. doi: 10.3390/polym11071214.

Hunt, N. C. and Grover, L. M. (2010) 'Cell encapsulation using biopolymer gels for regenerative medicine', pp. 733–742. doi: 10.1007/s10529-010-0221-0.

Hydrogels, H. A. *et al.* (2005) 'Hydroxamic Acid-Containing Hydrogels for Nonabsorbed Iron Chelation Therapy: Synthesis, Characterization, and Biological Evaluation', 1, pp. 2946–2953. doi: 10.1021/bm050036p.

Hydrogels, H. H. *et al.* (2016) 'Charged Triazole Cross-Linkers for Hyaluronan-Based Hybrid Hydrogels', pp. 1–11. doi: 10.3390/ma9100810.

Hyponatremia, P. O. F. (2007) 'Tumor-Related Hyponatremia', 5(4), pp. 228–237. doi: 10.3121/cmr.2007.762.

Itano, N. *et al.* (1999) 'Three Isoforms of Mammalian Hyaluronan Synthases Have Distinct Enzymatic Properties *', 274(35), pp. 25085–25092.

Javed, R. *et al.* (2018) 'RSC Advances Uptake of heavy metal ions from aqueous media by hydrogels and their conversion to nanoparticles for generation of a catalyst system : two-fold application study †'. Royal Society of Chemistry, pp. 14787–14797. doi: 10.1039/c8ra00578h.

Jelesarov, I. and Karshikoff, A. (no date) *Defining the Role of Salt Bridges in Protein Stability*. doi: 10.1007/978-1-59745-367-7.

Karimi, A. R. *et al.* (2018) 'International Journal of Biological Macromolecules amine : Swelling and drug delivery', *International Journal of Biological Macromolecules*. Elsevier B.V., 118, pp. 1863–1870. doi: 10.1016/j.ijbiomac.2018.07.037.

Kato, N., Yamanobe, S. and Takahashi, F. (1997) 'Property of magneto-driven poly (N-isopropylacrylamide) gel containing y-Fe-O , in NaCI solution as a chemomechanical device', *Materials Science & Engineering C*. Elsevier Science S.A., 5(2), pp. 141–147. doi: 10.1016/S0928-4931(97)00030-1.

Khoo, K. K. and Norton, R. S. (2012) 'Role of Disulfide Bonds in Peptide and Protein Conformation', 5.

Kim, J. *et al.* (2012) 'Effect of pH on Swelling Property of Hyaluronic Acid Hydrogels for Smart Drug Delivery Systems', 21(4), pp. 256–262.

Kim, S. J., Lee, K. J. and Kim, S. I. (2004) 'Swelling Behavior of Polyelectrolyte Complex Hydrogels Composed of Chitosan and Hyaluronic Acid', (August 2003). doi: 10.1002/app.20560.

Kim, Y. and Kumar, S. (2014) 'CD44-Mediated Adhesion to Hyaluronic Acid Contributes to Mechanosensing and Invasive Motility', pp. 1–15. doi: 10.1158/1541-7786.MCR-13-0629.

Kouvidi, K. *et al.* (2011) 'Role of Receptor for Hyaluronic Acid-mediated Motility (RHAMM) in Low Molecular Weight Hyaluronan (LMWHA) - mediated Fibrosarcoma Cell Adhesion □', 286(44), pp. 38509–38520. doi: 10.1074/jbc.M111.275875.

Koziolek, M. *et al.* (2015) 'Investigation of pH and Temperature Profiles in the GI Tract of Fasted Human Subjects Using the Intellicap R System', pp. 2855–2863. doi: 10.1002/jps.24274.

Krog, M. and Version, D. (2010) *Rheology of Cross-linked Polymer Networks*.

Kuhn, Z. W. (1949) 'Br ves c o m m u n i c a t i o n s - Kurze M i t t e i l u n g e n Brevi c o m u n i c a z i o n i - Brief Reports', V, pp. 318–319.

Kujawa, P. *et al.* (2005) 'Effect of Molecular Weight on the Exponential Growth and Morphology of Hyaluronan / Chitosan Multilayers : A Surface Plasmon Resonance Spectroscopy and Atomic Force Microscopy Investigation', (4), pp. 9224–9234. doi: 10.1021/ja044385n.

Kumar, P. and Honnegowda, T. M. (2015) 'Effect of limited access dressing on surface pH of chronic wounds', pp. 257–260. doi: 10.4103/2347-9264.165449.

Kuo, J., Swann, D. A. and Prestwich, G. D. (1991) 'Chemical Modification of Hyaluronic Acid by Carbodiimides', pp. 232–241. doi: 10.1021/bc00010a007.

Lee, J. *et al.* (2017) 'HHS Public Access', 3(5), pp. 447–451. doi: 10.1039/x0xx00x.

Lele, A. K. (2017) 'RSC Advances solutions of patchy polymers †'. Royal Society of Chemistry, pp. 5101–5110. doi: 10.1039/c6ra27030a.

Li, J. and Mooney, D. J. (2018) 'Designing hydrogels for controlled drug delivery', 1(12), pp. 1–38. doi: 10.1038/natrevmats.2016.71.Designing.

Lin, Y. *et al.* (2005) 'Physically crosslinked alginate / N , O-carboxymethyl chitosan hydrogels with calcium for oral delivery of protein drugs', 26, pp. 2105–2113. doi: 10.1016/j.biomaterials.2004.06.011.

Liu, L. *et al.* (2011) 'Microbial production of hyaluronic acid : current state , challenges , and perspectives', pp. 1–9.

Liu, Y., Shu, X. Z. and Prestwich, G. D. (2005) 'Biocompatibility and stability of disulfide-crosslinked hyaluronan films', *Biomaterials*, 26(23), pp. 4737–4746. doi: 10.1016/j.biomaterials.2005.01.003.

Loebel, C. *et al.* (2015) 'Precise tailoring of tyramine-based hyaluronan hydrogel properties using DMTMM conjugation', *Carbohydrate Polymers*. Elsevier Ltd., 115, pp. 325–333. doi: 10.1016/j.carbpol.2014.08.097.

Lu, P., Weaver, V. M. and Werb, Z. (2012) 'The extracellular matrix : A dynamic niche in cancer progression', 196(4), pp. 395–406. doi: 10.1083/jcb.201102147.

Maitra, J. and Shukla, V. K. (2014) 'Cross-linking in Hydrogels - A Review', 4(2), pp. 25–31. doi: 10.5923/j.ajps.20140402.01.

Majumder, S. and Liu, A. P. (2018) 'Bottom-up synthetic biology : modular design for making artificial platelets Bottom-up synthetic biology : modular design for making artificial platelets'. IOP Publishing.

Maleki, A. and Nystro, B. (2008) 'Effect of pH on the Behavior of Hyaluronic Acid in Dilute and Semidilute Aqueous Solutions', pp. 131–140. doi: 10.1002/masy.200851418.

Manuscript, A. (2011) 'NIH Public Access', 39(9), pp. 3528–3540. doi: 10.1039/b919449p.Rheological.

Manuscript, A. (2012) 'NIH Public Access', 22(5), pp. 655–660. doi: 10.1016/j.copbio.2011.01.003.Bioconjugation.

Manuscript, A. (2013a) 'molecule pulling experiments', 134(2), pp. 301–314. doi: 10.1021/ja206557y.Effects.

Manuscript, A. (2013b) 'NIH Public Access', 25(3), pp. 741–746. doi: 10.1021/tx200540z.Molecular.

Manuscript, A. (2013c) 'The gastrointestinal mucus system in health and disease', 10(6), pp. 352–361. doi: 10.1038/nrgastro.2013.35.The.

Manuscript, A. (2014) 'NIH Public Access', 126(4), pp. 1172–1180. doi: 10.1097/PRS.0b013e3181eae781.Scarless.

Manuscript, A. (2015) 'NIH Public Access', 10(4), pp. 1558–1570. doi: 10.1016/j.actbio.2013.12.019.Hyaluronan.

Manuscript, A. and Stimuli, M. E. (2016) 'NIH Public Access', 36(3), pp. 332–338. doi: 10.1002/marc.201400586.Chitosan-PEG.

Mao, A. S. and Mooney, D. J. (2015) 'Regenerative medicine: Current therapies and future directions', *Proceedings of the National Academy of Sciences*, 112(47), pp. 14452–14459. doi: 10.1073/pnas.1508520112.

Mendichi, R. *et al.* (2006) 'Degradative Action of Reactive Oxygen Species on Hyaluronan', pp. 659–668. doi: 10.1021/bm050867v.

Mero, A. and Campisi, M. (2014) 'Hyaluronic Acid Bioconjugates for the Delivery of Bioactive Molecules', pp. 346–369. doi: 10.3390/polym6020346.

Middelkoop, E. and Ulrich, M. M. W. (2010) 'Comparison between human fetal and adult skin', pp. 47–55. doi: 10.1007/s00403-009-0989-8.

Misra, S. and Ghatak, S. (2015) 'Interactions between hyaluronan and its receptors (CD44 , RHAMM) regulate the activities of', 6(May). doi: 10.3389/fimmu.2015.00201.

Mitteilungen, K. and Reports, B. (1994) 'R a p i d S w e l l i n g and D e s w e l l i n g of R e v e r s i b l e Gels of P o l y m e r i c A c i d s by I o n i z a t i o n (A synthetic "Contractile System")', 432(1947), pp. 319–320.

Miwa, Y. *et al.* (no date) 'ultrastretchability in a single elastomer', *Communications Chemistry*. Springer US, (2018), pp. 1–8. doi: 10.1038/s42004-017-0004-9.

Mondal, S., Das, S. and Nandi, A. K. (2020) 'A review on recent advances in polymer and peptide hydrogels'. Royal Society of Chemistry, pp. 1404–1454. doi: 10.1039/c9sm02127b.

Mseka, T., Bamburg, J. R. and Cramer, L. P. (2007) 'ADF / cofilin family proteins control formation of oriented actin-filament bundles in the cell body to trigger fibroblast polarization', pp. 4332–4344. doi: 10.1242/jcs.017640.

Nakamoto, H. and Bardwell, J. C. A. (2004) 'Catalysis of disulfide bond formation and isomerization in the Escherichia coli periplasm', 1694, pp. 111–119. doi: 10.1016/j.bbamcr.2004.02.012.

Napier, M. A. and Hadler, N. M. (1978) 'Effect of calcium on structure and function of a hyaluronic acid matrix : Carbon-13 nuclear magnetic resonance analysis and the diffusional behavior of small solutes', 75(5), pp. 2261–2265.

Nicodemus, G. D., Bryant, S. J. and Ph, D. (2008) 'Cell Encapsulation in Biodegradable Hydrogels for Tissue Engineering Applications', 14(2). doi: 10.1089/ten.teb.2007.0332.

Noda, S. *et al.* (2008) 'ARTICLE IN PRESS Molecular structures of gellan gum imaged with atomic force microscopy in relation to the rheological behavior in aqueous systems . 1 . Gellan gum with various acyl contents in the presence and absence of potassium', 22, pp. 1148–1159. doi: 10.1016/j.foodhyd.2007.06.007.

Of, R., In, T. and Stress, O. (2019) 'HHS Public Access', pp. 133–139. doi: 10.1016/j.cotox.2018.03.005.ROLE.

Online, V. A. *et al.* (2016) 'Diffusion of macromolecules in a polymer hydrogel : from microscopic to macroscopic', pp. 12860–12876. doi: 10.1039/C5CP07781H.

Ourjavadi, B. A. P., Urdtabar, Ã. M. K. and Hasemzadeh, H. G. (2008) 'Salt- and pH-Resisting Collagen-based Highly Porous Hydrogel', 40(2), pp. 94–103. doi: 10.1295/polymj.PJ2007042.

Panagopoulou, A., Molina, J. V. and Kyritsis, A. (2013) 'Glass Transition and Water Dynamics in Hyaluronic Acid Hydrogels'. doi: 10.1007/s11483-013-9295-2.

Paoli, P. *et al.* (2001) 'Hydrogen Peroxide Triggers the Formation of a Disulfide Dimer of Muscle Acylphosphatase and Modifies Some Functional Properties of the Enzyme *', 276(45), pp. 41862–41869. doi: 10.1074/jbc.M106886200.

Papakonstantinou, E., Roth, M. and Karakiulakis, G. (2012) 'A key molecule in skin aging Hyaluronic acid', (December), pp. 253–258.

Parhi, R. (2017) 'Cross-Linked Hydrogel for Pharmaceutical Applications : A Review', *Tabriz University of Medical Sciences*, 7(4), pp. 515–530. doi: 10.15171/apb.2017.064.

'Part I General Introduction' (no date).

Peppas, N. A. *et al.* (2000) 'Hydrogels in pharmaceutical formulations', *European Journal of Pharmaceutics and Biopharmaceutics*, 50(1), pp. 27–46. doi: 10.1016/S0939-6411(00)00090-4.

Phys, J. C. and Grest, G. S. (2016) 'Communication : Polymer entanglement dynamics : Role of attractive interactions Communication : Polymer entanglement dynamics : Role', 141101(August). doi: 10.1063/1.4964617.

Pomin, V. H. and Mulloy, B. (2018) 'Glycosaminoglycans and Proteoglycans with with', pp. 1–9. doi: 10.3390/ph11010027.

Pylaeva, S., Brehm, M. and Sebastiani, D. (2018) 'Salt Bridge in Aqueous Solution : Strong Structural Motifs but Weak Enthalpic Effect', *Scientific Reports*. Springer US, (August), pp. 1–7. doi: 10.1038/s41598-018-31935-z.

Qiu, Y. and Park, K. (2001) 'Environment-sensitive hydrogels for drug delivery', 53, pp. 321–339.

Reactions, F. G., Chemistry, C. C. and Decade, F. (2011) 'Toward a Few Good Reactions : Celebrating Click Chemistry s First Decade', pp. 2568–2569. doi: 10.1002/asia.201100755.

Rehor, A. *et al.* (2008) 'Functionalization of polysulfide nanoparticles and their performance as circulating carriers', 29, pp. 1958–1966. doi: 10.1016/j.biomaterials.2007.12.035.

Ren, Z. *et al.* (2015) 'Hydrogen bonded and ionically crosslinked high strength hydrogels exhibiting Ca2+-triggered shape memory properties and volume shrinkage for cell detachment'. Royal Society of Chemistry, pp. 6347–6354. doi: 10.1039/c5tb00781j.

Ribeiro, M. N. *et al.* (2018) 'Physiological and biochemical blood variables of goats subjected to heat stress – a review', *Journal of Applied Animal Research*. Taylor & Francis, 46(1), pp. 1036–1041. doi: 10.1080/09712119.2018.1456439.

Rizwan, M. *et al.* (no date) 'pH Sensitive Hydrogels in Drug Delivery : Brief History , Properties , Swelling , and Release Mechanism , Material Selection and Applications'. doi: 10.3390/polym9040137.

Schueler, O. and Margalit, H. (1995) 'Conservation of Salt Bridges in Protein Families', pp. 125–135.

'sciencedirect-topic-disulfide-bond.pdf' (no date).

'sciencedirect-topic-electrostatic-interaction.pdf' (no date).

Selyanin, M. A., Boykov, P. Y. and Khabarov, V. N. (1934) 'The History of Hyaluronic Acid Research and Initial Use', pp. 1–8.

Sharpe, L. A. *et al.* (2015) 'Therapeutic applications of hydrogels in oral drug delivery', 11(6), pp. 901–915. doi: 10.1517/17425247.2014.902047.Therapeutic.

Shu, X. Z. *et al.* (2002) 'Disulfide cross-linked hyaluronan hydrogels', *Biomacromolecules*, 3(6), pp. 1304–1311. doi: 10.1021/bm025603c.

Sintchak, M. D. (2000) 'Hydroxyl hydrogen conformations in trypsin determined by the neutron diffraction solvent difference map method : Relative importance of steric and electrostatic factors in defining hydrogen-bonding geometries', 87(June 1990), pp. 4468–4472.

Stair-nawy, S., Cso, A. B. and Stern, R. (1999) 'Hyaluronidase Expression in Human Skin Fibroblasts', 273, pp. 268–273.

Symons, M. C. R. *et al.* (2001) 'Hydrogen peroxide : a potent cytotoxic agent effective in causing cellular damage and used in the possible treatment for certain tumours', 57, pp. 56–58. doi: 10.1054/mehy.2000.1406.

Synthases, M. H. (2002) 'Review Article', 1, pp. 195–199. doi: 10.1080/15216540290114478.

Takata, K. *et al.* (2017) 'Analysis of the sol-to-gel transition behavior of temperature-responsive injectable polymer systems by fl uorescence resonance energy transfer'. Nature Publishing Group, 49(9), pp. 677–684. doi: 10.1038/pj.2017.33.

Tan, H. *et al.* (2009) 'Biomaterials Injectable in situ forming biodegradable chitosan – hyaluronic acid based hydrogels for cartilage tissue engineering', *Biomaterials*. Elsevier Ltd, 30(13), pp. 2499–2506. doi: 10.1016/j.biomaterials.2008.12.080.

Tanaka, K., Adachi, S. and Chujo, Y. (2010) 'Side-Chain Effect of Octa-Substituted POSS Fillers on Refraction in Polymer Composites', 48(1), pp. 5712–5717. doi: 10.1002/pola.24370.

Tavianatou, A. G. *et al.* (2019) 'Hyaluronan : molecular size-dependent signaling and biological functions in inflammation and cancer', 286, pp. 2883–2908. doi: 10.1111/febs.14777.

Terazawa, S. *et al.* (2015) 'The decreased secretion of hyaluronan by older human fibroblasts under physiological conditions is mainly associated with the down-regulated expression of hyaluronan synthases but not with the expression levels of hyaluronidases', *Cytotechnology*. Springer Netherlands, 67(4), pp. 609–620. doi: 10.1007/s10616-014-9707-2.

Theocharis, A. D. *et al.* (2016) 'Extracellular matrix structure ☆', *Advanced Drug Delivery Reviews*. Elsevier B.V., 97, pp. 4–27. doi: 10.1016/j.addr.2015.11.001.

Tokita, Y. and Okamoto, A. (1995) 'Hydrolytic degradation of hyaluronic', 48, pp. 269–273.

Traitel, T. and Kost, J. (no date) 'pH-Responsive Hydrogels : Swelling Model', (Figure 1), pp. 29–30.

'US20180015205A1.pdf' (no date).

Velegol, D. and Lanni, F. (2001) 'Cell Traction Forces on Soft Biomaterials . I . Microrheology of Type I Collagen Gels', 81(September), pp. 1786–1792.

Vercruysse, K. P. *et al.* (1997) 'Synthesis and in vitro degradation of new polyvalent hydrazide cross-linked hydrogels of hyaluronic acid', *Bioconjugate Chemistry*, 8(5), pp. 686–694. doi: 10.1021/bc9701095.

Vibert, A., Lopin-Bon, C. and Jacquinet, J. C. (2009) 'From polymer to size-defined oligomers: A step economy process for the efficient and stereocontrolled construction of chondroitin oligosaccharides and biotinylated conjugates thereof: Part 1', *Chemistry - A European Journal*, 15(37), pp. 9561–9578. doi: 10.1002/chem.200900740.

Vogus, D. R. *et al.* (2017) 'A hyaluronic acid conjugate engineered to synergistically and sequentially deliver gemcitabine and doxorubicin to treat triple negative breast cancer', *Journal of Controlled Release*. Elsevier, 267(June), pp. 191–202. doi: 10.1016/j.jconrel.2017.08.016.

Wang, K. *et al.* (2012) 'RSC Advances Preparation and characterization of pH-sensitive hydrogel for drug delivery system', pp. 7772–7780. doi: 10.1039/c2ra20989f.

Weaver, V. M. *et al.* (2009) 'NIH Public Access', 2(3), pp. 205–216.

Wedemeyer, W. J. *et al.* (2000) 'Disulfide Bonds and Protein Folding †', 39(15). doi: 10.1021/bi992922o.

Weigel, P. H. and Deangelis, P. L. (2007) 'Hyaluronan Synthases : A Decade-plus of Novel', 282(51), pp. 36777–36781. doi: 10.1074/jbc.R700036200.

Weigel, P. H., Hascall, V. C. and Tammi, M. (1997) 'Hyaluronan Synthases *', (23), pp. 13997–14001.

Weinfurtner, D. (2018) ‘Analysis of Disulfide Bond Formation in Therapeutic Proteins’. The Royal Society of Chemistry, (9).

West, D. C. *et al.* (1997) ‘Fibrotic Healing of Adult and Late Gestation Fetal Wounds Correlates with Increased Hyaluronidase Activity and Removal of Hyaluronan’, 29(I), pp. 201–210.

Whittemore, E. R. (1995) ‘PEROXIDE-INDUCED CELL DEATH IN PRIMARY NEURONAL CULTURE’, 61(4).

Wirsch, A., Cisl, W. P. and Wirsch, A. (2014) ‘Analysis of a Top-Down Bottom-Up Data Analysis Framework and Software Architecture Design Analysis of a Top - Down Bottom - up Data Analysis Framework and Software Architecture Design’, (May).

Wolny, P. M. *et al.* (2010) ‘Analysis of CD44-Hyaluronan Interactions in an Artificial INSIGHTS INTO THE DISTINCT BINDING PROPERTIES OF HIGH AND LOW MOLECULAR’, 285(39), pp. 30170–30180. doi: 10.1074/jbc.M110.137562.

Wu, T. *et al.* (2015) ‘The lubrication effect of hyaluronic acid and chondroitin sulfate on the natural temporomandibular cartilage under torsional fretting wear’, (February 2014), pp. 29–44. doi: 10.1002/ls.

Xu, H. and Matysiak, S. (2017) ‘network structure †’. Royal Society of Chemistry, pp. 7373–7376. doi: 10.1039/c7cc01826f.

Xu, Z. and Bratlie, K. M. (2018) ‘Click Chemistry and Material Selection for in Situ Fabrication of Hydrogels in Tissue Engineering Applications’. doi: 10.1021/acsbiomaterials.8b00230.

Zhang, H., Zhang, F. and Wu, J. (2013) ‘Reactive & Functional Polymers Physically crosslinked hydrogels from polysaccharides prepared by freeze – thaw technique’, *Reactive and Functional Polymers*. Elsevier Ltd, 73(7), pp. 923–928. doi: 10.1016/j.reactfunctpolym.2012.12.014.

Zhang, L. *et al.* (2012) ‘Synthesis and characterization of a degradable composite agarose / HA hydrogel’, *Carbohydrate Polymers*. Elsevier Ltd., 88(4), pp. 1445–1452. doi: 10.1016/j.carbpol.2012.02.050.

Zheng, X. *et al.* (2003) 'Disulfide-crosslinked hyaluronan-gelatin hydrogel films : a covalent mimic of the extracellular matrix for in vitro cell growth', 24, pp. 3825–3834. doi: 10.1016/S0142-9612(03)00267-9.

List of Figures

List of Tables